Fakultät für Medizin

Klinik und Poliklinik für Innere Medizin II

Elucidating the role of oxidative signaling and antimicrobial proteins in the context of pancreatic ductal adenocarcinoma (PDAC)

Sankaranarayanan Ramasubramanian

Vollständiger Abdruck der von der Fakultät für Medizin der Technischen Universität München zur Erlangung des akademischen Grades eines

Doctor of Philosophy (Ph.D.)

genehmigten Dissertation.

Vorsitzender: Priv.-Doz. Dr. Christian Sorg

Betreuer: Prof. Dr. Roland M. Schmid

Prüfer der Dissertation:

1. Prof. Dr. Martin Klingenspor

2. Priv.-Doz. Dr. Günter Schneider

Die Dissertation wurde am 30.09.2020 bei der Fakultät für Medizin der Technischen Universität München eingereicht und durch die Fakultät für Medizin am 07.12.2020 angenommen.

TABLE OF CONTENTS

LIST OF ABBREVIATIONS

PDAC	pancreatic ductal adenocarcinoma
ROS	reactive oxygen species
ADM	acinar-to-ductal metaplasia
PanIN	pancreatic intraepithelial neoplasia
IPMN	intraductal papillary mucinous neoplasm
MCN	mucinous cystic neoplasm
SOD	superoxide dismutase
MnTBAP	Mn(III)tetrakis (4-benzoic acid) porphyrin
OCR	oxygen consumption rate
ECAR	extracellular acidification rate
CCCP	carbonyl cyanide *m*-chlorophenyl hydrazone
AMP	adenosine monophosphate
ATP	adenosine triphosphate
AMPKa	AMP-activated protein kinase alpha
pAMPKa	phospho-AMPKa
TGFa	transforming growth factor alpha
ERK	extracellular receptor kinase
c-Myc	myelocytomatosis oncogene
BrdU	5-Bromo-2-deoxyuridine
H_2O_2	hydrogen peroxide
CRISPR	clustered regularly interspaced short palindromic repeats
Cas	CRISPR-associated protein
ETC	electron transport chain
OXPHOS	oxidative phosphorylation
TCA	tricarboxylic acid cycle
SDH	succinate dehydrogenase
GLUT1	glucose transporter 1
Reg	regenerating islet-derived protein
PAP	pancreatitis-associated protein
IHC	immunohistochemistry
H&E	hemalaun & eosin
WT	wild-type
2-DG	2-deoxy-d-glucose
Rot/AA	Rotenone/Antimycin A
PCR	polymerase chain reaction
FFPE	formalin-fixed, paraffin-embedded
WST-1	2-(4-Iodophenyl)-3-(4-nitrophenyl)-5-(2,4-disulfophenyl)-2H-tetrazolium, monosodium salt
BSA	bovine serum albumin
$O_2^{\bullet-}$	superoxide
Trx	Thioredoxin
TrxR	Thioredoxin reductase

ABSTRACT

Pancreatic ductal adenocarcinoma (PDAC) is one of the leading causes of cancer-related mortalities, which show very poor prognosis due to delayed diagnosis and insensitivity to current treatment strategies. There is a desperate need for extensive research into factors influencing PDAC initiation and biology of PDAC-derived cancer cell lines. Oxidative signaling and pancreatitis have been implicated to play critical roles in determining the tumourigenicity of PDAC.

Oxidative signaling (also referred to as ROS signaling) has been shown to exhibit conflicting roles in pancreatic ductal adenocarcinoma (PDAC) development. The role of ROS as pro-tumour or anti-tumour depends on the balance between the antioxidant enzymes and ROS levels. Antioxidant enzymes are responsible for maintaining cellular redox homeostasis. Manganese superoxide dismutase (SOD2: protein / *Sod2*: gene), an enzyme found in the mitochondrial matrix, protects mitochondria from oxidative damage due to ROS. *Sod2* has been shown to have a dichotomous role in cancer. In this thesis, we report that *Sod2* deficienct cancer cells favour mitochondrial bioenergetics by increasing their reliance on mitochondrial oxidative phosphorylation. However, chronic *Sod2* deficiency results in dysfunctional mitochondria causing a switch to reliance on glycolysis. Taken together, we present a comparative study of 2 types of *Sod2* deficient cancer cell line systems (acute and chronic *Sod2* deficiency) to illuminate the dynamicity of oxidative signaling in modulating PDAC cancer cell line bioenergetics.

Reg3b belongs to regenerating family of proteins, which are shown to have anti-inflammatory properties and bactericidal functions in the intestine. Reg3b levels were found to be elevated in pancreatic tissue and serum from patients with pancreatitis, a risk factor for PDAC. Hence, the other name for Reg3b is pancreatitis-associated protein 1 (PAP1). There are studies which claim that *Reg3b* is essential for the development of PDAC mediated by oncogenic $Kras^{G12D}$, while there are also studies

that have shown that deficiency of *Reg3* genes facilitate bacterial translocation from the gut and thus inducing an inflammatory environment in other organs (such as the liver). In our study, we present evidence to support the significance of antimicrobial Reg3b in protecting $Kras^{G12D}$ pancreas from PDAC initiation. To this end, we study the role of *Reg3b* in pancreatic cancer development using a mouse model with whole body deletion of *Reg3b* and pancreas-specific activation of $Kras^{G12D}$.

At an early timepoint of 12 weeks, mice lacking *Reg3b* show an increase in metaplastic lesions (acinar to ductal metaplasia (ADM), metaplastic tubular complexes) in the pancreas. *Reg3b* knockout pancreata show increased signs of inflammation, marked by an increased expression of macrophage marker F4/80. Interestingly, mRNA levels of all the other *Reg3* family genes are downregulated in response to *Reg3b* deletion. Considering the importance of *Reg* genes in maintaining the integrity of intestinal membrane, this systemic *Reg* family downregulation could be an indication of the loss of gut membrane integrity and point towards the translocation of microbes to the pancreas and hence, resulting in an inflammatory environment in the pancreas favouring PDAC development. We validated the presence of microbes in pancreas using 16S rRNA sequencing. Taken together, the present thesis suggests that the antimicrobial role of Reg3b in the intestine could influence pancreatic cancer initiation.

ZUSAMMENFASSUNG

Das duktale Adenokarzinom des Pankreas (PDAC) ist eine der häufigsten krebsassoziierten Todesursachen. Aufgrund der oft erst spät im Krankheitsverlauf gestellten Diagnose und der unzureichenden Sensitivität gegenüber den aktuell verfügbaren Therapiestrategien, ist die Prognose für Patienten sehr schlecht. Die derzeitige Situation verdeutlicht die dringende Notwendigkeit sowohl Einflussfaktoren für die Entstehung des PDAC aufzuklären als auch die Biologie von Krebszelllinien, die aus PDAC isoliert wurden, zu untersuchen. Aus vorhergehenden Arbeiten konnte bereits gezeigt werden, dass oxidativer Stress und eine zugrunde liegende Pankreatitis mit einer verstärkten Kanzerogenität des PDAC korrelieren.

Reaktive Sauerstoffspezies (ROS) spielen als Signalmoleküle bekannterweise widersprüchliche Rollen in der Entwicklung des PDAC. Welche Rolle reaktive Sauerstoffe in der Karzinogenese einnehmen ist abhängig von der Balance zwischen Antioxidantien, die für die Aufrechterhaltung der zellulären Redox-Homöostase verantwortlich sind, und dem ROS-Spiegel. Das Enzym Mangan-Superoxiddismutase (SOD2: Protein / *Sod2*: Gen) liegt in der Matrix von Mitochondrien vor und schützt diese vor oxidativem Stress. Das Gen *Sod2* hat funktional nachweislich kontroverse Eigenschaften in der Krebsentwicklung. In dieser Arbeit zeigen wir, dass ein *Sod2*-Mangel die mitochondriale Energiegewinnung durch eine Zunahme der oxidativen Phosphorylierung begünstigt. Ein chronischer *Sod2*-Mangel hingegen führt zur Dysfunktion der Mitochondrien was zu einem Wechsel in der Energiegewinnung hin zur Glykolyse führt. Unter anderem stellt diese Arbeit eine Vergleichsstudie zwischen zwei verschiedenen *Sod2*-defizienten Krebszelllinien (akuter und chronischer *Sod2*-Mangel) dar, um die Dynamik oxidativer Signale bei der Modulierung der Energiegewinnung in PDAC-Krebszelllinien zu beleuchten.

Reg3b gehört zu den intestinalen antibakteriellen Proteinen (regenerating islet-derived 3 beta), die nachweislich über antiinflammatorische Eigenschaften

bakterizide Funktionen im Darm verfügen. Da in Patienten mit Pankreatitis, einem Risikofaktor für die Entwicklung von PDAC, erhöhte Reg3b-Spiegel in Pankreasbiopsien und im Serum gemessen werden können, lautet eine weitere Bezeichnung für Reg3b auch Pankreatitis-assoziiertes Protein 1 (PAP1). Einige Studien schreiben Reg3b sogar eine essentielle Rolle in der Entwicklung des $Kras^{G12D}$-vermittelten PDAC zu, während andere zeigen, dass ein Mangel an *Reg3*-Genen eine Translokation von Darmbakterien in Organe (z.B. die Leber) erleichtert und so einen entzündlichen Hintergrund in verschiedenen Organen begünstigt. In dieser Arbeit zeigen wir Daten, die die Signifikanz von antimikrobiellem Reg3b beim Schutz eines $Kras^{G12D}$-Pankreas vor der Entwicklung eines PDAC unterstützen.

Die Rolle von *Reg3b* bei der Pankreaskarzinogenese wurde mit Hilfe eines Mausmodells untersucht, das über einen globalen *Reg3b*-Knockout und pankreasspezifisch aktiviertes $Kras^{G12D/+}$ verfügt. Schon in 12 Wochen alten Tieren mit *Reg3b*-Verlust ist eine Zunahme an metaplastischen Veränderungen (azinoduktale Metaplasie (ADM), metaplastische tubuläre Komplexe) im Pankreas nachweisbar. *Reg3b*-Knockout-Tiere weisen in ihrem Pankreas erhöhte Expression von F4/80-Antigen auf, was als Entzündungsmarker auf die Anwesenheit von Makrophagen hindeutet. Interessanterweise sind die mRNA-Level aller anderen Mitglieder der *Reg3*-Familie als Antwort auf den *Reg3b*-Verlust herunterreguliert. Zieht man die Relevanz der *Reg*-Gene für die Aufrechterhaltung der Membranintegrität des Darms in Betracht, könnte diese systemische Herabregulierung der Reg-Familie einen Indikator für den Verlust der Darmmembranintegrität darstellen und hinweisend sein für eine Translokation von Darmmikroben ins Pankreas, die letztendlich eine entzündliche Umgebung des Pankreas und damit die Entwicklung eines pankreatischen Adenokarzinoms begünstigt. Die Validierung der Präsenz von Darmmikroben in der Bauchspeicheldrüse erfolgte durch 16S rRNA-Sequenzierung von Kot- und Pankreasproben. Die vorliegende Arbeit zeigt, dass die antimikrobielle Funktion des Reg3b im Darm die Entstehung des Pankreaskarzinoms beeinflusst.

I. INTRODUCTION

I.1. PANCREATIC PATHOLOGY

I.1.1. STRUCTURE AND FUNCTION OF THE PANCREAS

The pancreas is located in the upper abdominal region where exposure to physical trauma is minimal. This location also makes the accessibility to the organ difficult during physical examination procedures. Hence, pancreatic diseases that do not cause pain or discomfort can progress without being detected easily. The pancreas is divided into three functional segments: the head (duodenal end); the body; and the tail (splenic end). The pancreas is specialised to produce and secrete several enzymes and hormones. Majority of the pancreas is composed of cellular units called acinar cells, which are involved in secreting enzymes (such as lipases, proteases, amylases, and nucleases) into the intestine through pancreatic ducts. These acinar cells and the ductal system form the exocrine pancreas. About 1-2 % of the pancreas is made of a specialised unit of cells called islets. The islets are involved in secreting hormones like insulin, glucagon, and somatostatin [1].

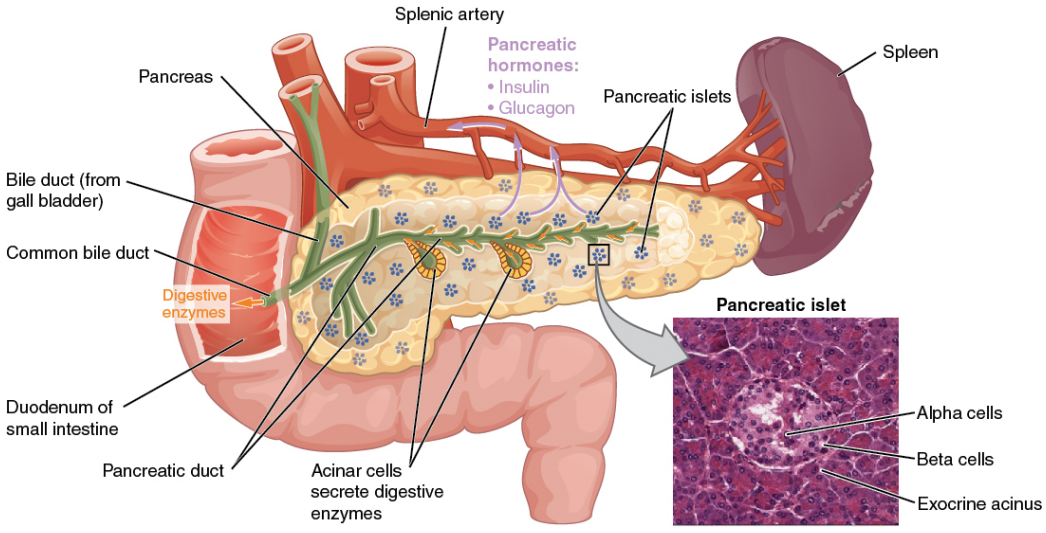

Figure I.1: Pancreas anatomy and function. The exocrine system of pancreas includes the acinar cells which secrete digestive enzymes via the pancreatic duct system into the intestine and the endocrine system comprise of the islet cells, which release hormones into the

bloodstream directly. The image is adapted and modified from an OpenStax College resource [2].

The exocrine functionality of the pancreas is orchestrated by the acinar lobules (groups of acinar cells). These acini produce a range of enzymes and store them as granules, usually as latent pro-enzymes. These include lipases, proteases (such as trypsin, chymotrypsin, elastases, aminopeptidases, carboxypeptidases, etc.), amylases, and nucleases. After a meal, acinar cells secrete these enzymes toward the centre of the acinar lobules and then they reach the pancreatic duct system and finally entering the duodenum. Once they reach the duodenum, these inactive pro-enzymes are activated by the enteral kinases, which then mediates the digestion process [3,4].

Pancreatic islets contain four types of cells: alpha cells (produces glucagon); beta cells (produces insulin); delta cells (produces somatostatin); and pancreatic polypeptide cells (PP cells, produce pancreatic polypeptide hormone). Glucagon is released upon low blood glucose levels and plays a crucial role in regulating blood glucose levels. Insulin is released upon high glucose levels sensed in blood and brings the blood glucose levels down to normal levels. Somatostatin also plays a crucial role in regulating blood glucose levels, as it functions as an inhibitor of both glucagon and insulin. Pancreatic polypeptide hormone secreted by the PP cells has been shown to have roles in regulating both the exocrine and endocrine secretions of the pancreas [2].

In addition to the above-mentioned cell types, there is another cell type in the pancreas called as the stellate cells. These have a fibroblast-like appearance and lie silently beside the vasculature, acinar and ductal structures. These cells are activated and start proliferating during inflammatory conditions like pancreatitis and start producing collagen type I. This is the reason behind fibrosis observed during pancreatic cancer and pancreatitis [4].

I.2. Pancreatic diseases

The most common diseases that arise out of pancreas are diabetes, pancreatitis, and pancreatic cancer. However, defective organogenesis can also result in a variety of other pancreatic disorders.

I.2.1. Diabetes (also called Diabetes Mellitus)

Diabetes refers to a set of metabolic diseases manifested in the form of high levels of glucose in the blood (hyperglycaemia). This condition is often a result of defects associated with insulin secretion, action, or both. This is either caused by the destruction of beta cells of the pancreas resulting in deficiency in insulin production or other conditions that result in insensitivity to insulin function resulting in hyperglycaemia. Sustained or chronic hyperglycaemia can result in damage and failure of other organs like the kidneys, eyes, nerves, heart, and blood vessels [5].

I.2.2. Pancreatitis

Pancreatitis refers to a pathological condition characterised by the inflammation of the pancreas. Histopathological features of this disease include swelling and damage to the cytosolic organelles of acinar cells of the pancreas resulting in exocrine insufficiency with chronic disease. Pancreatitis has been broadly classified into acute and chronic pancreatitis based on deliberations from specialist groups (surgeons, histopathological experts) in the field. Acute pancreatitis is defined as an acute condition accompanied by elevated levels of pancreatic enzymes in blood and/or urine caused due to inflammation of the pancreas. Chronic pancreatitis refers to the long-term and continuing inflammatory state of the pancreas. Morphological alterations caused by chronic pancreatitis are irreversible and is often accompanied by partial or total loss of pancreatic exocrine function. The most noted morphological changes seen with chronic pancreatitis include inflammatory infiltrates, fibrosis, and lobular necrosis [6].

I.2.3. PANCREATIC CANCER

Pancreatic cancer is a disease that arises due to neoplastic transformation of cells in the pancreatic tissue. These neoplastic cells multiply abnormally and eventually acquire the ability to invade other organs and to metastasize. There are several types of pancreatic cancer classified based on the cellular origin. However, the term “pancreatic cancer” generally refers to the most common type of cancer arising from pancreas called pancreatic ductal adenocarcinoma (PDAC). PDAC accounts for majority (~90%) of the cases having a cancer arising out of the pancreas [7]. PDAC is a cancer of the exocrine compartment of the pancreas and is characterised by a very poor prognosis. PDAC is one of the deadliest malignancies of all solid cancers with a very low median survival and 5-year survival rate. Research from the past two decades have now elucidated that PDAC comprises and originates out of germ line and acquired somatic mutations. *KRAS*, *p16*, *TP53*, and *SMAD4* are the most common genes found to be altered, with *KRAS* being recognised as the critical driver and the most frequently mutated oncogene in PDAC [9,10]. These mutations are additionally aided by other genomic alterations that regulate cell cycle, invasion, and metastases [8].

I.3. PDAC CARCINOGENESIS

Experimental models from genetically engineered mice have shown that pancreatic cancer (PDAC) does not arise *de novo* and have established the contribution from genetic alterations (*KRAS*, *p16*, *TP53*, and *SMAD4*) contributing to carcinogenesis [8]. PDAC development has been shown to be a process of multi-step carcinogenesis involving accumulating mutations. Activating *KRAS* mutations has been found in all PDAC patients from this study [9] and these mutations have been shown to increase in frequency with disease progression [8,9]. Other studies have also shown that *KRAS* mutations are the first set of genetic alterations observed in the progression series of PDAC [10]. *KRAS* gene belongs to the RAS family of guanosine triphosphate (GTP)-binding proteins, which are involved in regulating plethora of cellular functions like survival, proliferation, motility, cytoskeletal remodelling, and invasion which are crucial for cancer development and maintenance [8,11]. Activating

mutations of *KRAS* gene includes a point mutation in codon 12 of the gene and interestingly, these mutations have been found on pancreatic lesions that are considered to be precursor lesions that have the potential to evolve into PDAC with the help of other accumulating alterations (silencing mutations) to tumour suppressor genes like *p16* and *TP53* [12,13]. These findings emphasise the importance of understanding the precursor lesions that contribute to pancreatic cancer development.

Precursor lesions of PDAC are non-invasive lesions that have the potential to evolve into an aggressive form of ductal adenocarcinoma with the help of accumulating genetic, cellular, and molecular alterations. Categories of lesions classified as PDAC precursors include: Pancreatic Intraepithelial Neoplasia (PanIN), Intraductal Papillary Mucinous Neoplasm (IPMN), and Mucinous Cystic Neoplasm (MCN) [14]. PanINs are microscopic intraductal lesions comprising of mucinous cells displaying varying degrees of dysplasia and are further classified into low-grade PanINs (PanIN-1 and PanIN-2) and high-grade PanIN (PanIN-3) based on the severity of dysplastic features (presence of mitotic figures, loss of polarity, and complex architecture) [15,16]. IPMNs are defined as intraductal non-infiltrating lesions comprising of mucinous cells that have papillary architecture. IPMNs are also classified into low-grade and high-grade in a similar fashion to PanINs based on the degree of dysplasia. MCNs are lesions that have columnar cells accompanied by the presence of mucin in the luminal part of the cells and the common histopathological features of MCNs include multi-layer stratification and enlarged nuclei [14]. Molecular characterisation of PanIN lesions have shown that low-grade PanINs harbor *KRAS* mutations and high-grade PanINs display mutations to the tumour suppressor genes (*p16* and *TP53*) [17,18]. IPMNs show mutations to *GNAS* and *KRAS* genes and interestingly, high-grade IPMNs also show silencing of tumour suppressor genes similar to the situation observed with high-grade PanINs [19]. PanINs arise due to transdifferentiation of acinar cells and IPMNs develop from ductal cells, this indicates the presence of two unrelated pathways (one from acinar cells and another from ductal cells) leading to PDAC development. This also explains how biologically different lesions like PanINs and IPMNs can contribute to an overt ductal adenocarcinoma [20,21]. Considering the cancer-developing potential PanIN lesions

hold, transdifferentiation of acinar cells is also considered to be a critical step in PDAC carcinogenesis. The process of acinar-to-ductal metaplasia (ADM) is defined by transdifferentiation of acinar cells into a ductal-like phenotype. Hence, factors that trigger ADM can induce a suitable environment for oncogene driven PDAC development [22]. Thus, factors influencing ADM also becomes important in the context of studying PDAC development.

I.4. Factors influencing PDAC development, maintenance, and biology

Chronic pancreatitis, especially the hereditary forms, are risk factors in PDAC formation. Other risk factors for PDAC include diabetes, infectious diseases, and obesity. These non-hereditary risk factors have been linked to acquired habits that modulate oxidative signaling and inflammatory signaling pathways that increase the risk of PDAC [23,24,25,26]. This puts oxidative stress and antioxidant compounds crucial in the context of PDAC research. Oxidative stress is a result of excessive production and accumulation of free radicals such as reactive oxygen species (ROS).

I.4.1. Oxidative signaling

Oxidative signaling refers to oxidative stress-mediated signaling. Oxidative stress is a result of elevated intracellular levels of reactive oxygen species (ROS). ROS refers to chemical species generated due to incomplete reduction of oxygen and these ROS molecules have the capacity to have damaging effects on proteins, DNA, and lipids. There is a growing body of evidence that puts ROS as signaling molecules [29,30,31]. Despite the extensive evidence that exists for ROS signaling, there is still a lot of scrutiny whether to include ROS as signaling molecules. This arises from the apparent indiscriminate nature of ROS molecules, as opposed to the specificity required to act as a signaling molecule. The ability of ROS in targeting specific atoms of proteins is considered to be strong evidence of its signaling capacity. ROS molecules perform specific molecular recognition at the level of atoms, and not at the macromolecular level [32]. The collective term ROS includes molecules such as superoxide anion ($O_2^{\cdot-}$), hydroxyl radical ($HO^{\cdot}$), and hydrogen peroxide (H_2O_2). The

signaling specificity of ROS molecules is demonstrated by the ability of superoxide and hydrogen peroxide to react with specific biological targets. Hydrogen peroxide specifically targets cysteine residues [33]. Superoxide has high atomic reactivity with iron-sulfur [FeS] clusters. This specificity of superoxide towards FeS clusters stems from the charged nature of superoxide and a consequence of high electrostatic attraction [34]. This signaling ability of ROS molecules display diverse functional and physiological consequences involved in regulating disease conditions such as inflammation, aging, cancer development, and maintenance [35].

I.4.1.1. ANTIOXIDANT SYSTEMS

Considering the above findings that elaborate on the signaling capacity and damaging effects of ROS-mediated oxidative stress, the basis for scavenging ROS becomes crucial in the context of cellular homeostasis. Antioxidants within cells are responsible for scavenging ROS and hence, inhibiting harmful effects of excessive ROS production. This emphasises the importance of balance between ROS levels and antioxidant systems in maintaining redox homeostasis [36]. Antioxidants, as the name suggests, are responsible for thwarting free radicals and neutralising oxidants. Endogenous antioxidants are broadly categorised into 3 groups: (1) enzymatic antioxidants like superoxide dismutases (SODs), catalase (CAT), thioredoxin (Trx), and glutathione peroxidase (GPx); (2) lipophilic radical antioxidants such as ubiquinol, carotenoid, and tocopherol; (3) hydrophilic antioxidants such as flavonoids, glutathione, ascorbate, and urate. Small molecules obtained through diet also contribute to ROS defense as exogenous antioxidants such as vitamins, minerals, phenolic acids, phenolics, and carotenoids [37,38]. The enzymatic antioxidants are reported to have more effective defense against oxidative damage due to the ability of decomposing ROS [39]. Hence, this set of enzymatic antioxidants (SOD, CAT, GPx and TrX) is considered crucial in the context of disease states such as inflammation, cancer development, and maintenance. SOD catalyses the conversion of superoxide into oxygen and hydrogen peroxide. CAT is then involved in decomposing hydrogen peroxide into molecular oxygen and water. SODs are classified into: cytosolic SOD (SOD1 or CuZn-SOD), mitochondrial SOD (SOD2 or Mn-SOD), and extracellular SOD (SOD3). SOD is the first line of defense in scavenging oxygen-derived free radicals and is activated immediately in conditions

inducing oxidative stress [39,40,41]. GPx uses glutathione as a reductant in catalysing organic hydroperoxides or hydrogen peroxide into corresponding alcohols or water, respectively [42]. The GPx family comprises of 3 evolutionary groups: GPx1/GPx2, GPx3/GPx5/GPx6, and GPx4/GPx7/GPx8. GPx1 is present ubiquitously in the cytoplasm and mitochondria, GPx2 is present in the nucleus and cytoplasm, GPx3 is in the plasma, and GPx4 is shown to protect membranes from oxidative stress and is membrane-bound [43,44,45]. The Trx antioxidant system comprises of NADPH, thioredoxin reductase (TrxR), and thioredoxin (Trx). Trx and TrxR are the dimeric enzyme system involved in catalysing NADPH-dependent reduction of the active-site disulfide in oxidized Trx (Trx-S_2) to give a dithiol in reduced Trx (Trx-$(SH)_2$) [46,47,48].

I.4.1.2. MITOCHONDRIAL SOD2 AND PDAC

Considering that mitochondria are involved in regulating both energy metabolism and cell death functions, implicating mitochondrial activity in cancer development and maintenance becomes inevitable. It is now well established that mitochondria are the primary source of cellular ROS and mitochondrial ROS participate in a diverse range of signaling networks to influence cancer biology [49,50]. Mitochondria-derived superoxide is the primary oxidant responsible for oxidative stress related damaging effects that modulate cellular physiology. The superoxide produced through mitochondria is detoxified to hydrogen peroxide by mitochondrial matrix localised superoxide dismutase (SOD2) enzyme. This association between superoxide and its scavenger SOD2 emphasises the importance of antioxidant SOD2 in the context of cancer [51,52,53]. It has been previously reported that SOD2 expression is decreased in human pancreatic cancer cell lines and enforcing SOD2 activity causes a decrease in growth rate of these cancer cell lines [54]. SOD2 overexpression in human pancreatic cancer cells is shown to suppress the malignancy of these cancer cells [55]. These findings indicate that SOD2 mediated superoxide scavenging might have a protective function against pancreatic cancer development and maintenance. Contrary to the previous findings indicating a protective function of SOD2 in the context of pancreatic cancer, redox-based treatments for pancreatic cancer, which work through induction of ROS, are associated with increased expression and activity of SOD2. This increased expression of SOD2 is associated with resistance to radio-

chemotherapy treatment strategies [56,57,58]. A previous study from our laboratory has shown that *Sod2* deficient oncogenic pancreas containing mice have very low tumour incidence and hence, indicating SOD2 activity might be indispensable for pancreatic cancer development [77]. These contrasting findings regarding the role of SOD2 in pancreatic cancer indicates the need for more research into SOD2, which would help in unravelling details about the complex nature of oxidative signaling.

I.4.2. Pancreatitis and PDAC

Chronic pancreatitis is a progressive inflammatory disease characterised by permanent functional and morphological alterations. In humans, it is reported to be a major risk factor in the development of pancreatic cancer (PDAC) [59]. Genetically modified mouse models harbouring an active *KRAS* oncogene have been used to successfully reproduce human ADM, PanIN, and PDAC. Using a mouse model that allows controlled temporal expression of *KRAS* oncogene in acinar cells, it has been shown that adult mice do not form neoplastic lesions unless accompanied by chronic pancreatitis [60]. In another study using mouse models, it has been shown that pancreatitis-induced inflammation contributes to pancreatic cancer development by inhibiting oncogene-induced senescence [61]. These findings illustrate the significance of research into pancreatitis and regulators of pancreatitis to better understand pancreatic cancer (PDAC) development.

I.4.2.1. Regenerating family of proteins

The regenerating (Reg) family of proteins includes C-type lectin-like proteins discovered during pancreatitis and pancreatic islet regeneration. The first Reg protein was discovered in pancreatic stones and was also named as lithostathine referring to its supposed role as an inhibitor of pancreatic cancer stone formation. This protein was re-discovered subsequently in regenerating rat islets and the name "regenerating protein" was given based on this [62,63,64]. Reg proteins/genes were categorised into 4 groups based on the homology of their DNA sequences and protein structures: (a) Type 1 includes the mouse Reg1, human Reg1a and Reg1b, rat Reg1, (b) Type 2 includes only the mouse and hamster Reg2, (c) Type 3 contains mouse Reg3a, Reg3b, Reg3g, Reg3d, rat Reg3, rat PAP, rat PAPIII, and human

PAP [66,67,68,69]. A new Reg family protein recently discovered was human REG4, which shares great similarity to both PAP and REG1 [70].

Reg family proteins are detected in several organs under normal and disease states. In the pancreas, Reg proteins have been reported during disease states such as pancreatitis and pancreatic cancer. Reg proteins have also been reported to be involved in the regulation of acinar and islet cell transdifferentiation and proliferation [71,72,73]. Reg proteins in the intestine have been shown to control bacterial levels owing to their antimicrobial activity mediated by their capacity to bind to the peptidoglycan moieties of bacteria and induce damage to the cell wall of bacteria [74,75]. This shows the importance of Reg proteins in maintaining intestinal microbiota and hence, gut homeostasis.

II. Materials and Methods

II.1. Standard chemicals

Chemicals	Article Number	Company
PBS Dulbecco	L182-50	Merck
Nonidet P 40 Substitute	74385-1L	Sigma-Aldrich
D-Mannitol	M4125-100G	Sigma-Aldrich
Ethanol, absolute	1.00983.1000	Merck
Ethylenediaminetetraacetic acid (EDTA)	E6511-100G	Sigma-Aldrich
Glycine	50046-1KG	Sigma-Aldrich
Isopropanol	109634	Merck
Magnesium Chloride	M8266-100G	Sigma-Aldrich
Methanol	8045	J. T. Baker
Dimethyl Sulfoxide (DMSO)	472301-100mL	Honeywell
Bovine Serum Albumin (BSA)	A4503-100G	Sigma-Aldrich
Sodium dodecyl sulfate (SDS)	A7249, 1000	AppliChem
Skim Milk Powder	70166-500G	Sigma-Aldrich
Sodium Chloride (NaCl)	71376-5KG	Sigma-Aldrich
Sodium Deoxycholate	D6750-500G	Sigma-Aldrich
Sodium Hydroxide (NaOH)	6771.1	Roth
Sucrose	S0389-500G	Sigma-Aldrich
Tris	5429.2	Roth
Tris-HCl	9090.3	Roth
Triton X 100	T9284-100ML	Sigma-Aldrich
WZB117	S7927-50MG	Selleck chemicals
MnTBAP chloride	SC-221954	Santa Cruz
Sterile DPBS	14200075	Gibco™
Trypsin-EDTA (0.05%), phenol red	25300054	Gibco™

II.2. Cell culture-based methods

II.2.1. Equipment and Supplies

All cancer cell lines, and acinar explants were handled in a Herasafe class II Hera Safe biological safety cabinet (ThemoFisher) and incubated in a humidified HeracellTM 240 incubator (ThemoFisher) at 37°C and 5% CO_2. To prevent contamination, sterilized deionized water used in the incubator and supplemented with Incuwater-CleanTM (A5219, 0100, Applichem). The incubator was cleaned with Incubator-CleanTM BC (A5230, 1000, Applichem) every month. Plasma treated cell culture plates and vented cap flasks were purchased from Corning. Sterile, single packed pipettes were ordered from Greiner Bio-One. For pipetting volumes of less than 1 ml, SafeSeal-Tips® professional (Biozym) were used. For separation of supernatants and cell pellets, autoclaved single-use glass Pasteur pipettes and appropriate centrifuges (depending on rotor capacity and rotation speed) were used. For 1.5/2 ml volume, microcentrifuge was used (5417R, fixed-angle rotor, Eppendorf®). For 15/50 ml volume, benchtop centrifuge was used (5702R, fixed-angle rotor, Eppendorf®).

II.2.2. Culture of PDAC (murine) Cell Lines

Cancer cell lines isolated from cancer tissue (PDAC) were removed from liquid nitrogen storage and thawed using a 37°C water bath and then suspended into a pre-warmed standard culture medium (DMEM, 41965-062, Gibco) and then transferred to an appropriate cell culture flask/dish and cultivated in the cell culture incubator. Medium was removed and replaced with fresh medium after 24 h. After attaining confluence, cells were split according to their respective proliferation capacity.

II.2.3. Treatment of PDAC (murine) Cell Lines

Cancer cells were used for experiments only after at least two passages/splits. For treatments, cells were seeded into appropriate cell culture dishes and allowed to attach overnight. The next day, standard medium was replaced with a fresh and sterile medium containing the reagents of interest depending on the aim of the

experiment and plates were again returned to the incubator for cultivation in case of a time-course experiment or for measuring data at different time points.

Glucose medium (Basal):

- 10 % v/v FCS (10499-044, Life Technologies)
- 1 % v/v MEM-NEAA (11140-068, Life Technologies)
- 1 % Pen/Strep (15140-163, Life Technologies)
  Added to 25 mM glucose containing DMEM (41965-062, Gibco)

Galactose medium:

- 10 mM Galactose (G5388, Sigma)
- 10 % v/v FCS (10499-044, Life Technologies)
- 1 % v/v MEM-NEAA (11140-068, Life Technologies)
- 1 % Pen/Strep (15140-163, Life Technologies)
  Added to glucose-free DMEM (11966-025, Gibco)

II.2.4. Cell Proliferation assay

CyQuant cell proliferation assay kit (C7026, ThemoFisher) was used to determine the cell number based on DNA content and hence, cell proliferation rates at 0 h, 24 h, 48 h, and 72 h time-points. Reagents used were supplied with the kit and they were:

- CyQuant GR dye (Component A)

- Cell lysis buffer (Component B)

Cancer cell lines were seeded in black/clear bottom 96 well plates at a density of 2000 cells/well and allowed to attach the overnight. Cell lines were seeded in multiple plates at the same density (2000 cells/well) to measure cell proliferation rates from 0 h to 72 h. The cell lines were maintained in basal culture conditions until the cells attached to the wells and this denotes 0 h time point. Other time-points (24 h, 48 h, and 72 h) were estimated relative to the start of treatments or different culture

conditions (0 h). For every time point attained, corresponding plates had their medium removed and the plates were frozen at -80 °C for a few hours to 3 days. Reagent mixture of components A and B done as mentioned in the kit manual. Frozen plates were thawed to room temperature and the reagent mixture added to the wells of the plates and fluorescence measurements were for ~480 nm excitation and ~520 nm emission maxima. 24 h, 48 h, and 72 h sample fluorescence measurements were normalised to 0 h sample fluorescence to determine the proliferation rates of cancer cell lines.

II.2.5. CRISPR/CAS9 TECHNOLOGY

Targeted deletion of *Sod2* in cancer cell lines was achieved using the double nicking approach of the CRISPR/Cas9 technology. Guide RNA (gRNA) oligos targeting two different sites of *Sod2* gene (Sod2 A and Sod2 B) were annealed to pX462 plasmid (containing the D10A variant of Cas9 nickase).

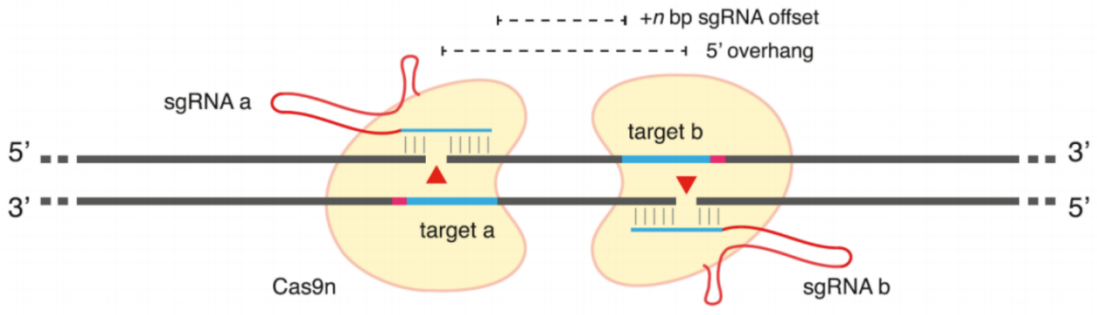

Figure II.1. CRISPR/Cas9 technology. General scheme depicting CRISPR/Cas9 approach used to generate in vitro *Sod2* deficient cell lines (CKΔSOD). Image taken from [27].

Cancer cell lines were transfected with the plasmids containing the gRNAs (jetPRIME DNA and siRNA transfection reagent, Polyplus). Transfection protocol was performed as mention in the kit manual. At 24 h post transfection, the transfection medium was discarded, and the cells were replaced with selection medium (3 µg/ml puromycin).

The cells were kept in selection medium for 48 to 72 h until only successfully transfected cells survive the selection medium. Once successful transfection was confirmed, individual clones were generated. To this end, 400 cells were seeded in 10 cm dishes and cultured in 10 ml puromycin medium with a concentration of 3 µg/ml. After the cells grow into colonies, individual clones were picked and transferred to a 96-well plate with 100 µl puromycin medium with a concentration of 3 µg/ml. The clones were then transferred into a 12-well plate until they attained confluency. The clones were then transferred to 6-well plates and finally, 10 cm dishes for RNA and protein isolation and for freezing the clones. Sequences used for gRNA design and oligo annealing are as follows:

Oligos	(5' -> 3')
Sod2_cc_A_upper	CAC CGA GCC CGC GGC ACC GGC CAC A
Sod2_cc_A_lower	AAA CTG TGG CCG GTG CCG CGG GCT C
Sod2_cc_B_upper	CAC CGG CCT TAC GAC TAT GGC GCG C
Sod2_cc_B_lower	AAA CGC GCG CCA TAG TCG TAA GGC C

II.2.6. Mitochondrial Enrichment and SOD2 activity assay

Mitochondrial enrichment from murine pancreatic cancer cell lines was preformed using a protocol modified from an established protocol for cultured fibroblasts [28]. Cancer cell lines were seeded in 150 mm culture dishes and maintained at 37 °C, 5% CO_2 until 80-90% confluency, to have at least 5 x 10^6 to 10^7 cells to yield sufficient enriched mitochondria. Once 80-90% confluency is attained, the cells were washed with 10 mL DPBS (Gibco) and then the cells were detached from the dishes using 10 mL 0.05 % Trypsin-EDTA (Gibco), by incubating the cells for 5 min at 37 °C, 5 % CO2. Then the detached cells in suspension were neutralised with 10 ml of standard medium (DMEM) and then the cells were spun down at 3000 g, 4 °C for 10 min. The supernatant was discarded, and the cell pellet was resuspended in 1 ml DMEM. 10 µL of the cell suspension was mixed with 10 µL of Trypan Blue (ThermoFisher) for cell counting, to check for enough input cells for mitochondrial enrichment, using Countess II Automated Cell Counter (ThermoFisher). Cell suspension was made up to 10 ml with standard medium and centrifuged at 3000 g, 4 °C for 10 min. The supernatant was discarded, and the cell pellet resuspended in 1 ml cold DPBS.

Followed by centrifugation at 600 g, 4 °C for 10 min. The supernatant was discarded again, and the pellet was resuspended in 500 µL cold IB_c buffer. Cell suspension was then transferred a Tissue Grinder Potter-Elvehjem (15 ml capacity), , the suspension was churned for about 100 turns with a PTFE pestle, and then the cell suspension was spun down at 600 g, 4 °C for 10 min. Then the supernatant was collected and spun down at 7000 g, 4 °C for 10 min. This was followed by discarding the supernatant and resuspending the cell pellet in 200 µL IB_c buffer and then spun down at 7000 g, 4 °C for 10 min. As a final step for enrichment of mitochondria, 50 µL of supernatant were removed and the mitochondria-containing pellet re-suspended in the remaining volume (150 µL) of IB_c buffer. To make sure the functionality of mitochondria is not disturbed, enriched mitochondria was immediately used for SOD activity assay after the enrichment procedure. SOD activity was determined using the SOD Determination kit (19160, Sigma-Aldrich). SOD activity measured on enriched mitochondrial samples gives us a measure of SOD2 activity (As SOD2 is exclusively localised on the mitochondrial matrix). This kit allows SOD activity determination by using the water soluble tetrazolium salt (WST-1), which produces a formazan dye upon reduction with a superoxide anion. The rate of the reduction with oxygen has a linear relation to the xanthine oxidase activity, and is inhibited by SOD. SOD activity is measured colorimetrically as % superoxide inhibition activity. The absorbance at 440 nm is directly proportional to the amount of superoxide anion present in the samples and the SOD activity as an inhibition activity is quantified by measuring the decrease in the colored product at 440 nm. Measured SOD activity was then normalised to the mitochondrial protein concentration, measured using the Pierce® BCA Protein Assay Kit (#23225, ThemoFisher). The SOD activity is then depicted relative to control ($Kras^{G12D}$) cancer cell lines and expressed as U/mg protein, where U represents amount of SOD that inhibits the rate of formazan dye formation.

II.2.7. SEAHORSE ANALYSIS

OCR and ECAR measurements were performed using the XF96 Extracellular Flux analyzer (Seahorse Bioscience) as described previously [65]. Cancer cell lines were plated at 7000 cells/well on XF96 plate (Seahorse Bioscience) and incubated for 24 h in a humidified 37 °C incubator with 5% CO_2 (Glucose medium). The same cancer cell lines were plated in duplicate in in 96-well plates (353072, Falcon) to estimate the

protein concentration using Pierce™ BCA Protein Assay Kit (23227, ThermoFisher Scientific). The medium was then replaced with XF Assay medium (pH 7.4, Seahorse Bioscience) supplemented with 25 mM glucose, 1 mM sodium pyruvate. Cells were then placed in a CO_2 –free incubator for 1 h at 37 °C. The OCR and ECAR values were normalised in each well using the protein concentrations.

Various respiratory parameters and ATP turnover were calculated as follows: Firstly, baseline OCR was measured and from which basal respiration was calculated as the difference between baseline OCR and non-mitochondrial respiration. Next, complex V (ATP synthase) inhibitor oligomycin was added and the resulting OCR was used to obtain ATP-linked respiration as the difference between baseline OCR and oligomycin rate. Next CCCP, an uncoupler, was added to boost ETC to function at maximal capacity and this was used to derive maximum respiration by subtracting non-mitochondrial respiration from CCCP rate. Then, antimycin A and rotenone (complex III and complex I inhibitors) were added to shut down ETC and revealing non-mitochondrial respiration.

ATP from mitochondria/OXPHOS was calculated by multiplying P/O ratio (2.75) and the OCR rate that drives mitochondrial ATP synthesis (calculated as difference between basal respiration and oligomycin rate). ECAR data was used to derive ATP from glycolysis (calculated as the difference between basal ECAR and 2-DG rate).

II.2.8. Electron microscopy

Cells were fixed with 2.5% glutaraldehyde (Science Services GmbH), postfixed with 1% osmium tetroxide, dehydrated with aceton and were embedded in epoxy resin. Sixty-nanometer sections were cut using the Reichert-Jung Ultracut E microtome (now Leica Biosystems). Ultrathin sections were negative-stained with Uranyless (Science Services) and lead citrate. Images were acquired using a Jeol 1200 EXII electron microscope (Akishima, Tokyo, Japan) equipped with a KeenViewII digital camera (Olympus, Hamburg, Germany) and processed with the iTEM software package (anlySISFive; Olympus).

II.3. Protein-based Methods

II.3.1. Protein purification from PDAC Cell lines

Cancer cell lines plated were in 10 cm cell culture dish and were washed with ice-cold PBS (2x) and lysed on ice with 1 ml of ice-cold Supplemented RIPA buffer for 5 min. The cells start detaching and then they were thoroughly detached with a Cell Scraper S (99002, TPP) and the contents of each dish were transferred each to 1.5 ml Eppendorf tubes.

After the lysis with Supplemented RIPA buffer, lysates were centrifuged at 20,000 rcf at 4 °C for 15 min to sediment the cellular debris. Supernatants, containing the purified protein samples, were then transferred to sterile 1.5 ml Eppendorf tubes, and continued to be kept on ice if meant for immediate use. For long-term storage, lysates were snap frozen and stored in liquid nitrogen.

RIPA buffer: 50 mM TRIS-HCl (stock solution: 1 M, pH 7.5)
150 mM NaCl (stock solution: 5 M)
1 % (v/v) NP-40
0.5 % (w/v) sodium deoxycholate
0.1 % (w/v) SDS
in deionized water. Kept refrigerated at 4 °C.

Supplemented RIPA buffer:
1 Tablet of 25x Complete Protease Inhibitor Cocktail Tablets (04693132001, Roche Diagnostics) in 2ml aqua water

1 Tablet of 10x PhosSTOP Phosphatase Inhibitor Cocktail Tablets (04906837001, Roche Diagnostics) in 1ml aqua water.

Both the tablets (dissolved in aqua water) were then added to RIPA buffer at a dilution of 25x for complete protease inhibitor cocktail and 10x for PhosSTOP phosphatase inhibitor cocktail.

II.3.2. WESTERN BLOTTING

Western blotting procedure was used to determine the expression level differences of several proteins of interest using appropriate antibodies mentioned below. Prior to starting the Western blot, Pierce® BCA Protein Assay Kit (#23225, ThemoFisher) to obtain the protein concentrations. Protein samples were diluted with water (5 µl protein samples + 20 µl water) and Standards from the BCA protein assay kit was diluted with lysis (RIPA) buffer (20 µl standards + 5 µl RIPA buffer). For every protein sample to be used for Western blot analysis, lysates were adjusted to equal concentrations with supplemented RIPA buffer. After which, 1/5 volume of 6x SDS sample buffer was added to each sample and samples were denatured for 5 min at 95 °C in a Thermomixer® compact (Eppendorf).

SDS-polyacrylamide gel electrophoreses (SDS-PAGE) and protein transfer (wet transfer) was performed using the mini-PROTEAN Tetra Cell system (Bio-Rad). Percentage of polyacrylamide chosen based on the target protein size. Equal amounts of protein lysates were loaded into the pockets of each gel. The Fermentas Spectra™ Multicolor Broad Range Protein Ladder (11862124, ThemoFisher) was used as a marker for size reference. Gels were run first at 80 V until the protein ladder and dye reached the stacking/separation gel border and at 200 V for the rest of the gel length.

After SDS-PAGE, proteins were transferred onto a Protran BA83 or BA85 Nitrocellulose Blotting Membrane (10402495, GE Healthcare) or PVDF (10600030, GE Healthcare) depending on the target protein size for 120 min at 100 V. If PVDF membrane is being used, the membranes were activated with methanol by soaking in 100% methanol for 30 seconds. The membranes were later washed briefly in TBS-T and blocked in 5 % (w/v) blocking agent (milk or BSA depending on the primary antibody used) in TBS-T for one hour at room temperature. Subsequently, membranes were incubated in target protein specific primary antibody diluted in blocking solution as specified by manufacturer's instructions and incubated at 4 °C or in a cold room overnight on a shaker.

The following day, membranes were washed once for 15 min and three times for 5 min with TBS-T. Membranes were then incubated in a 1:5000 dilution of secondary antibody matching the organism that the respective primary antibody was made in, anti-rabbit, anti-mouse, or anti-rat (NA934-1ML, NA931-1ML, or NA935, GE Healthcare). Then the membranes were washed again once for 15 min and three times for 5 min in TBS-T. Horseradish peroxidase-conjugated secondary antibodies were detected on Gel doc (CHEMIDOC XRS+, Bio-Rad) with Amersham ECL Western Blotting Detection Reagent (RPN2106, GE Healthcare).

Target protein (Primary Antibody)	**Order Number, Brand/Company**	**Target Protein Size**	**Blocking Agent**	**Primary Antibody Dilution**	**Secondary Antibody**
Erk1/2	sc-93 and -154, Santa Cruz	42 and 44 KD	5 % Milk-TBST	1:2000	anti-rabbit
Sod2	ADI-SOD-111-F, ENZO	25 KD	5 % Milk-TBST	1:1000	anti-rabbit
AMPK	#2532, Cell Signaling	62 KD	5 % Milk-TBST	1:1000	anti-rabbit
pAMPKa	#2535, Cell Signaling	62 KD	5 % BSA-TBST	1:1000	anti-rabbit
HIF1a	sc-10790, Santa Cruz	132 KD	5 % Milk-TBST	1:1000	anti-rabbit
c-Myc	ab32072, abcam	57 KD	5 % Milk-TBST	1:1000	anti-rabbit
OXPHOS complexes (Antibody cocktail)	ab110413, abcam	CI- 20 kD CII- 30KD CIII- 48 KD CIV- 40 KD CV- 55 KD	5 % Milk-TBST	1:250	anti-mouse

II.3.3. OXPHOS COMPLEXES EXPRESSION

Western Blotting technique was used to visualise the expression levels of the complexes of electron transport chain involved in oxidative phosphorylation. During

this procedure, whole cell lysates from cancer cell lines were denatured with 6x SDS and the samples were not heated, as OXPHOS complexes are sensitive to heating. Samples were then fractionated by SDS-PAGE and then transferred to a polyvinylidene difluoride membrane by performing a wet transfer. This was followed by blocking the membrane with incubation with 5% non-fat dry milk in TBS-T for 1 hour. The membrane was then incubated with the antibody cocktail (ab110413; 1:250 dilution in 1% nonfat dry milk in PBS) targeting one subunit from each of the 5 complexes (Complex I- NDUFB8 subunit; Complex II- SDHB subunit; Complex III- UQCRC2 subunit; Complex IV- MTCO1 subunit; Complex V- ATP5A subunit). This incubation with the antibody was at 4 °C for 12 hours. Membranes were then washed 4 times with TBS-T and then incubated with a 1:5000 dilution of horseradish peroxidase-conjugated anti-mouse for 2 hours. Blots were then developed to visualise the expression levels of complexes with the ECL detection system (Amersham Biosciences) as per the manufacturer's instructions.

II.4. RNA-BASED METHODS

II.4.1. RNA ISOLATION

RNA isolation from murine pancreas was performed with 200 µl of RLT buffer-shredded tissue (see II.6.3) using Maxwell® 16 LEV simplyRNA Tissue Kit (AS1280, Promega) and Maxwell® 16 Instrument (Promega) as per the manufacturer's instructions. This was followed by eluting the samples in 30 µl PCR-grade water. RNA concentration and quality was determined using a NanoDrop 2000 (ThemoFisher). Isolated RNA was stored at -80 °C until used for Reverse Transcription-Polymerase Chain Reaction (RT-PCR).

II.4.2. REVERSE TRANSCRIPTION-POLYMERASE CHAIN REACTION (RT-PCR)

Reverse transcription of RNA involves cDNA synthesis, and this was started by mixing 1 / 24 vol of Random Primers (C118A, Promega), 1 / 12 vol of 10 mM dNTP Mix (18427-013, Invitrogen™) and 1 µg RNA of acceptable quality ($A_{260/280}$ = 2.0 ± 0.2 and $A_{260/230}$ = 2.2 ± 0.3), heated to 65 °C for 5 min and put on ice. 1 / 5 vol of First Strand Buffer (of SuperScript II Reverse Transcipase system; 18064-014,

Invitrogen™) and 0.1 M DTT (Y00147, Invitrogen™) was added and solution was mixed at 25 °C for 2 min. Then, 1/25 vol of SuperScript II Enzyme was added, and reaction was started with 25 °C for 10min, 42 °C for 50 min and 70 °C for 15 min (all in a Mastercycler, Eppendorf). This was followed by a quantitative PCR (qPCR) to determine RNA expression. The qPCR was performed using the LightCycler® 480 SYBR Green I Master (04887352001, Roche Diagnostics) in a PCR plates containing 2.5 pmol of forward and reverse primers. To which, 2.5 µl of a 1:40 dilution of cDNA was added. LightCycler® 480 (Roche Diagnostics) was used for the reaction and data acquisition. Primers were designed and then ordered from Eurofins Genomics as lyophilised oligonucleotides, suspended at 100 µM in 1 x TE buffer according to the manufacturer's instructions and stored at -20 °C freezer. PCR program used is as follows:

- Denaturation (95 °C, 10 min)
- 45 cycles of denaturation (95 °C, 20 sec)
- annealing (52 °C, 30 sec)
- elongation and acquisition (72 °C, 25 sec)

Followed by a melt analysis consisting of 65 to 97 °C temperature gradient at a ramp rate of 0.11 °C/s with acquisition every 5 °C. Melt curves were obtained to confirm quality of primers, thus showing one specific PCR product. Primer sequences used are reported below.

Target gene	Primer Sequence
Cyclophilin A	1. 5'-ATGGTCAACCCCACCGTG-3' 2. 5'-TTCTGCTGTCTTTGGAACTTTGTC-3'
Reg1	1. 5'-GCAACTTTGTGGCCTCTCTG -3' 2. 5'-CCAGTTGCCCAGGATTTGTAG -3'
Reg2	1. 5'-CTTATGCCTGATGTTCCTGTCA -3' 2. 5'-CCAGGTCAAACGGTCTTCAATT -3'
Reg3a	1. 5'-TGGGCTCCATGATCCAACAA -3' 2. 5'-ACCACGGTTGACAGTAGAGG -3'

Reg3b	1. 5'-CTCTCCTGCCTGATGCTCTT-3' 2. 5'-GTAGGAGCCATAAGCCCTGGG -3'
Reg3g	1. 5'-TCCCTGTCCTCCATGATCAAAA -3' 2. 5'-CATCCACCTCTGTTGGGTTCA -3'
Reg3d	1. 5'-ACAGTTTGACCACATTCCCA -3' 2. 5'-GCAACACAGTAGCATCCAGG -3'
Reg4	1. 5'-GACAAAGAGTGAAGCCAGGC -3' 2. 5'-CCACACAGGCAGGTTTCTCT -3'

Quantification was done relative to *Cyclophilin A* mRNA expression using the LightCycler® 480 software (version 1.5.0.39, Roche Diagnostics) as 2nd Derivative Max type analysis with an All-To-Mean pairing rule.

II.5. DNA-BASED METHODS

II.5.1. DNA ISOLATION

Extraction of high-quality DNA from murine pancreas was performed using the DNeasy® Blood & Tissue Kit (69504, Qiagen) with RNaseA digestion according to the manufacturer's instructions and stored at -20 °C in a laboratory freezer until analysis. For genotyping of the genetically engineered mice, crude DNA was extracted from tail biopsies or punched out ear tissue samples. 200 µl of DirectPCR-Tail Lysis Reagent (31-102-T, Peqlab) supplemented with 10 µl of Proteinase K (03115828001, Roche Diagnostics) was used to perform DNA extraction. The samples were then incubated at 55 °C in a Thermomixer® compact (Eppendorf) for at least 6 hours and subsequent incubation at 85 °C for 45 min. The samples were then stored at 4 °C.

II.5.2. POLYMERASE CHAIN REACTION (PCR)

PCR was predominantly performed to determine the genotype of the genetically modified mice. For the PCR reaction, the ReadyMixTM REDTaq® or ReadyMixTM

GREENTaq® PCR Reaction Mix with MgCl2 (R2648, Sigma) was used according to the manufacturer's protocol in a 12 µl-reaction volume containing 5 pmol of both forward and reverse primers. Followed by addition of 0.5 µl of tail or ear clip DNA. Primers were obtained from Eurofins Genomics as High Purity Salt Free (HPSF) purified lyophilized oligonucleotides, suspended at 100 mM in 1 x TE buffer according to the manufacturer's instructions and stored at -20 °C. Further primer dilutions were done in PCR-grade water. PCRs were performed either in a T100TM Thermal Cycler (Biorad). An annealing temperature of 58 °C was used and elongation time was 1 min for amplicons smaller than 1 kilobase and 1.5 min for amplicons larger than 1 kilobase. All primer sequences and amplicon sizes can be found in the table below.

Target	**Primer Sequences**	**Amplicon Size**
Cre	1. 5'-ACCAGCCAGCTATCAACTCG-3' 2. 5'-TTACATTGGTCCAGCCACC-3' 3. 5'-CTAGGCCACAGAATTGAAAGATCT-3' 4. 5'-GTAGGTGGAAATTCTAGCATCATCC-3'	324 bp (all), 199 bp (Cre)
Ptf1a-Creex1	1. 5'-GTCCAATTTACTGACCGTACACCAA-3' 2. 5'-CCTCGAAGGCGTCGTTGATGGACTGCA-3'	1155 bp
Sod2fl	1. 5'-GAGGGGCATCTAGTGGAGAA-3' 2. 5'-CCAGATCTGCAATTTCCAAAA-3'	180 bp (wt, *Sod2*Δ/Δ) 250 bp (*Sod2*fl)
Kras$^{G12D/+}$	1. 5'-CACCAGCTTCGGCTCCTATT-3' 2. 5'-AGCTAATGGCTCTCAAAGGAATGTA-3' 3. 5'-CCATGGCTTGAGTAAGTCTGC-3'	180 bp (wt) 280 bp (*Kras*$^{G12D/+}$)
Reg3b_genot	1. 5'-GTCCTCCATGGTGAAGAGAAC-3' 2. 5'-ATTCCCATCCACCTCCATTG-3'	700 bp (wt)
Reg3b_neo	1. 5'-AGAGGCTATTCGGCTATGACT-3' 2. 5'-CCTGATCGACAAGACCGGCTT-3'	700 bp, 400 bp (Reg3b+/-) 400 bp (Reg3b-/-)

II.5.3. Agarose Gel Electrophoresis

PCR products were detected by ethidium bromide-based agarose gel electrophoresis using the Sub-Cell® horizontal electrophoresis system (Bio-Rad). Agarose gels were prepared at 2 % (w/v) in 1 x TAE buffer and contained 5 µg/ml ethidium bromide (2218.2, Carl Roth). For each sample, 10 µl of PCR product was loaded into the gel pockets. DNA Ladder-Mix (25-2040, VWR) was used as a marker according to the manufacturer's instructions. Gels were run at constant voltages (100-180 V depending on gel length) until fragment sizes were clearly distinguishable and photographed with a Gel Doc^{TM} XR system (Bio-Rad) and the Quantity One software (version 4.5.2 (Basic), Bio-Rad).

TAE buffer composition
- 40 mM TRIS
- 2 mM Titriplex® III
- 20 mM acetic acid, glacial
- in deionized water. Stored at room temperature.

II.6. Mice

II.6.1. Mouse strains and husbandry

Reg3b deleted (whole body deletion) mouse strain has been previously described [76] and was backcrossed to a C57BL/6J background. Age-matched littermates with no *Kras*$^{G12D/+}$ mutation and no Reg3b deletion were used as wild-type (WT) controls. The following genotypes and abbreviations were used:

Ptf1a-Cre^{ex1}; Kras$^{G12D/+}$; Reg3b-/-	*Kras$^{G12D/+}$; Reg3bΔ/Δ (or) Kras$^{G12D/+}$; Reg3b-/- (CKReg3b)*
Ptf1a-Cre^{ex1}; Kras$^{G12D/+}$	*Kras$^{G12D/+}$ (CK)*
Reg3b-/-	*Reg3bΔ/Δ (or) Reg3b-/-*

All mice were kept at the animal facilities of the Klinikum rechts der Isar University Hospital of the Technische Universität München (TUM) under specific pathogen free (SPF) conditions according to the recommendations of the Federation of European Laboratory Animal Science Associations (FELASA). Sentinel mice were examined for hygiene monitoring every three months. The animals were housed in groups of up to six in Sealsafe NEXT Green Line cages (#1145T, Scanbur) at 20 to 24 °C, 50 to 60 % humidity, and a 12 h/12 h light/dark cycle. Sterile filtered water was given *ad libitum*. All mice were kept on a standard diet (#Forti, Altromin Spezialfutter). Breedings were started at six weeks for male and eight weeks for female mice. Mice were weaned and ear marked with an ear puncher at three weeks of age. Genotyping of these punched out ear biopsies was performed as described in II.5.1, II.5.2, and II.5.3. All animal experiments were conducted in accordance with German Federal Animal Protection Laws and approved by the Institutional Animal Care and Use Committee of the Technische Universität München, Munich, Germany.

II.6.2. Mouse-derived acinar explants

Murine primary acini were explanted from 4-week-old mice. Mice were anesthetized with isoflurane (798-932, cp-pharma) and sacrificed by exsanguination of the heart. Then, the pancreas was quickly harvested and transferred to a sterile cell culture dish containing sterile PBS. In the biological safety cabinet, the pancreas was washed two more times with sterile PBS and transferred to another sterile cell culture dish containing 5 ml of sterile filtered (0.2 µm) Solution 2. Solution 2 was collected with a sterile syringe and injected into the pancreas with a sterile needle (Sterican® Gr. 1, 4657519, B. Braun). This step was repeated one more time, thereafter, the pancreas was cut into small pieces using sterile surgical scissors and pipetted up and down for one time. Then, the suspension was incubated in the cell culture incubator. After 10 min of incubation, the tissue suspension together with 10 ml of Solution 1, which was used to flush the petri dish, was transferred to a sterile 50 ml-Falcon tube and spun down. The supernatant was removed, and the pellet suspended in 5 ml of fresh Solution 2. Then, the suspension was transferred to a sterile cell culture dish and incubated for another 10 min in the cell culture incubator. Followed by passing the suspension through a 100 µm nylon mesh (08-771-19, Corning) into another sterile 50 ml-Falcon tube. The nylon mesh was flushed with 10 ml of Solution 1, which was

also collected in the Falcon tube. Followed by another centrifugation (300 rcf and 18 °C for 5 min), the supernatant was removed, and the pellet was washed with 19 ml of Solution 1 and centrifuged again at 300 rcf and 18 °C for 5 min. The supernatant was removed, and the cells were suspended in 2 ml of acinar cell medium supplemented with 30 % (v/v) fetal bovine serum (FBS; 10499044, Life Technologies). The suspension was transferred to a sterile cell culture dish and placed in the cell culture incubator for recovery. In the meantime, the culture plates were coated with collagen solution 1 and allowed to solidify in the cell culture incubator for 20 min. After 30-60 min of recovery, the cell suspension was transferred to a sterile 15 ml-Falcon tube, centrifuged, and the supernatant was removed. Then, the cell pellet was suspended in 1-2 ml of acinar cell medium (depending on the pellet size), mixed with collagen solution 2, plated into collagen-coated culture plates and placed in the cell culture incubator for 30 min for solidification. Thereafter, the acinar cell suspension/collagen solution 2 mixture was covered with another layer of collagen solution 1 and placed again in the cell culture incubator for another 30 min to allow solidification. Finally, the collagen disks were covered with sterile filtered (0.2 µm) acinar cell medium and cultivated under standard cell culture conditions. Medium was replaced with fresh media after 24 h.

All centrifugation steps were performed at 300 rcf and 18 °C for 5 min.

PBS: 14190-169, Life Technologies.

Solution 1:

- 0.1 % (w/v) BSA (A4503-100G, Sigma-Aldrich)
- 0.02 % (w/v) Trypsin Inhibitor (from soybean; T9008-5ML, Sigma-Aldrich) in McCoy's 5A Medium (M8403, Sigma-Aldrich). Prepared freshly.

Solution 2:

- 1.2 mg/ml Collagenase from *Clostridium histolyticum*, Type VIII (C2139-100MG, Sigma-Aldrich) in Solution 1. Prepared freshly.

Acinar cell medium:

- 0.1 % (w/v) BSA (A4503-100G, Sigma-Aldrich)
- 0.1 % (v/v) FBS (10499-044, Life Technologies)
- 0.01 % (w/v) Trypsin Inhibitor (from soybean; T9008-5ML, Sigma-Aldrich)
- 1 x Insulin-Trans-Sel-G (41400045, Life Technologies)
- 50 µg/ml Bovine Pituitary Extract (13022814, Life Technologies)
- 10 mM HEPES (15630-080, Life Technologies)
- 0.26 % (w/v) $NaHCO_3$ (1.06329.0500, Merck)
  in Waymouth's MB 752/1 Medium (31220023, Life Technologies). Prepared freshly.

Collagen solution 1:

- 2.5 mg/ml Rat Tail Collagen Type I (354236, Corning)
- 0.01 % (w/v) NaOH in PBS. Prepared freshly.

Collagen solution 2:

- 2.5 mg/ml Rat Tail Collagen Type I (354236, Corning
- 0.01 % (w/v) NaOH in acinar cell medium minus volume of cell suspension. Prepared freshly.

Acinar-to-ductal transdifferentiation (in vitro ADM) rates of wild-type (WT) and *Reg3b-/-* acini were quantified after 3 days of culture. Wells were examined in an inverted light microscope. Transdifferentiated and total acinar colonies were quantified in at least three high power fields of vision for each well. Transdifferentiation rates expressed as ratio of number of transdifferentiated colonies to acinar colonies.

II.6.3. Tissue Harvesting and Preparation of Formalin-Fixed, Paraffin-Embedded (FFPE) Tissue Blocks

Mice were considered for analysis at indicated time points (4 weeks for acinar explants, or at 12 weeks) or if terminally ill. On the day of the analysis, mice were injected intraperitoneally at 10 µl/g body weight with 5-Bromo-2-deoxyuridine (BrdU) working solution. 2 h after BrdU injection, mice were anesthetized with isoflurane (798-932, cp-pharma) and sacrificed by cervical dislocation. The pancreas was quickly resected, transferred to a sterile petri dish. Small pieces of the organ were taken for RNA, and protein isolation from at least two distinctive sites. Protein samples were snap-frozen in liquid nitrogen. RNA samples were suspended in RLT Lysis buffer (1015762, Qiagen) supplemented with 10 % (v/v) 2-Mercaptoethanol (4227.3, Carl Roth), blended with a SilentCrusher M (Heidolph) until crushed completely and then snap-frozen in liquid nitrogen. Protein samples were stored in liquid nitrogen and RNA samples at -80 °C. Small sections of the lung, liver, the upper duodenum, and the spleen were resected and, together with the remaining pancreatic tissue, fixed in 4 % (w/v) paraformaldehyde at 4 °C overnight. The following day, the organs were dehydrated with increasing concentrations of ethanol, xylol and paraffin in a S300 tissue processing unit (Leica). Finally, organs were embedded in liquid paraffin and stored at room temperature.

4 % paraformaldehyde:

- 16 % (w/v) paraformaldehyde solution (#15710, EMS) diluted in PBS. Prepared freshly.

BrdU stock solution:

- 50 mg/µl BrdU (B5002-5G, Sigma-Aldrich) dissolved in deionized water by alkalization with 10 M sodium hydroxide (NaOH). Stored in single-use aliquots at -20 °C.

BrdU working solution:

- 1:10 dilution of BrdU stock solution in sterile 0.9 % (w/v) sodium chloride (NaCl; 6697366.00.00, B. Braun). Stored at -20 °C.

II.6.4. Hemalaun & Eosin (H&E) Staining

For obtaining information about histological features of pancreas using H&E staining, 2 µm paraffin sections were cut from the FFPE tissue blocks on a MICROM HM 355S microtome (ThermoFisher) and mounted on SUPERFROST® PLUS microscope slides (ThermoFisher). After air-drying overnight at room temperature, slides were used for the staining protocol as described below. First, paraffin sections were deparaffinized by incubation in Roti-Histol (6640.4, Carl Roth) twice for 5 min each. Then, the slides were rehydrated in decreasing concentrations of ethanol in demineralized water, namely, 100 %, 96 %; 70 %, and 0 % (v/v), twice for 3 min per concentration. Subsequently, basophilic tissue structures were stained in Mayer's hemalaun solution (1.09249.2500, Merck) for 3 min and washed under running tap water for 10 min. Acidophilic tissue structures were then counterstained in eosin (2C-140, Waldeck) for 3.5 min. After staining, slides were dehydrated by incubation in 96 % (v/v) ethanol and isopropanol for 25 sec each. Finally, slides were cleared in Roti-Histol (6640.4, Carl Roth) twice for 5 min each, mounted in pertex embedding medium (41-4012-00, Medite) and sheeted with coverslips (MENZEL-Gläser, e.g. BB024032A1, ThermoFisher). Slides were scanned at the core facility of animal pathology of Zentrum der Präklinischen Forschung, TU München, by the laboratory of Katja Steiger. The scanned slides were uploaded to aperio imagescope (pathology slide viewing software) and the scanned slides were used for quantification of ADM, PanIN1, PanIN2, and PanIN3 lesions.

II.6.5. Immunohistochemistry

For detection of infiltrating macrophages in the pancreas, paraffin tissue slides were subjected to immunohistochemistry. Incubation steps were performed in a humidified chamber with the tissue slides containing tissues encircled with an ImmEdge pen (H-4000, Vector). Firstly, paraffin slides were deparaffinized and rehydrated as described for H&E staining (II.6.4). This was followed by antigen unmasking using

proteinase K solution for 3 min (100 µl 1x proteinase K (111 µl + 5 ml TE-Buffer) + 1.9 ml TE-Buffer pH 8). This was then followed by washing the slides three times with deionized water. Thereafter, endogenous peroxidases were blocked using the peroxidase blocking solution (3% H_2O_2 in distilled water) for 1 h at room temperature. This was followed by 3 rounds of washing (1x distilled water and 2x PBS). This was followed by the blocking step to prevent any unspecific antibody binding and this was achieved using incubating the tissue sections in the blocking solution (PBS + 4 drops of streptavidin for every 1 ml PBS + 5% rabbit serum) for 1 hour at room temperature. This was followed by primary antibody incubation overnight at 4 ºC to detect F4/80 expression (MF48000, 1:100 in diluent, Invitrogen) in the tissue sections. The diluent used for the primary antibody dilution is 4 drops of Biotin in 1 ml PBS + 5% rabbit serum. This was followed by washing with PBS and then the primary antibody was detected by incubation in a 1:500 solution of the respective secondary antibody (anti rat in rabbit) diluted in blocking solution. This was followed by signal amplification with the Vectastain ABC Kit (PK- 6100, Vector) according to the manufacturer's protocol. Slides were then washed three times in deionized water. Next, signal was detected with the DAB Peroxidase Substrate Kit (SK-4100, Vector; brown color) for 1 to 4 min at room temperature according to the manufacturer's protocol and slides were washed for 5 min in deionized water. Tissues were then counterstained by quickly dipping slides into hematoxylin solution (1.05175.2500, Merck) and subsequent washing under running tap water for 10 min. Finally, slides were dehydrated, cleared and mounted.

II.6.6. Microbiome analysis using 16S rRNA sequencing

Pancreas tissue samples and faecal pellets were collected from 4 animals from each of the 4 groups: *Wild type* (WT), *Reg3b*$^{\Delta/\Delta}$, *Kras*$^{G12D/+}$ (CK), and *Kras*$^{G12D/+}$*; Reg3b*$^{\Delta/\Delta}$ (CKReg3b). Faecal pellets and pancreas tissue samples were snap frozen in liquid nitrogen and stored at -80 °C until DNA purification using phenol-chloroform extraction with mechanical disruption (bead-beating) as described previously [135] and this was followed by purifications on columns (OneStep-96 PCR Inhibitor Removal Kit, Zymo Research, Irvine, CA). 16S rRNA gene amplicons spanning the V4 – V5 hypervariable region were sequenced using a MiSeq system (Illumina, San

Diego, CA) as described previously [135]. Sequence data were compiled and processed using mother, then screened and filtered for quality. Operational taxonomic units (OTUs) were clustered at 97 % sequence similarity using NCBI blastn classifier and the alignment hit with the highest score. To correct for very rare OTUs to avoid bias lin downstream statistical analyses, OTUs with less than 10 counts in less than 5 % of all samples were excluded. Alpha diversity was then calculated on the basis of species richness represented as observed_species.

II.6.7. IMAGE ACQUISITION AND ANALYSIS

Bright field images were captured using an Axio Imager A1 microscope (Carl Zeiss). Objectives used were 5x, 10x, and 20x EC Plan-Neofluar (420330-9900, 420340-9900, or 420350-9900, Carl Zeiss). Whole slides were scanned with Aperio ScanScope CS2 slide scanning device.

II.7. STATISTICAL ANALYSIS

Statistical analysis was performed using the GraphPad Prism version 6. Paired t-test was used for comparison between control cell lines and corresponding CRISPR/Cas knockout cell lines. Unpaired t-test was used for comparison between control group and genetically engineered knockout group. Data are expressed as mean ± SEM (Standard error of the mean). Statistical significance was considered when the p-value was less than 0.05.

III. Results

III.1. Role of Sod2 in modulating PDAC biology, and maintenance

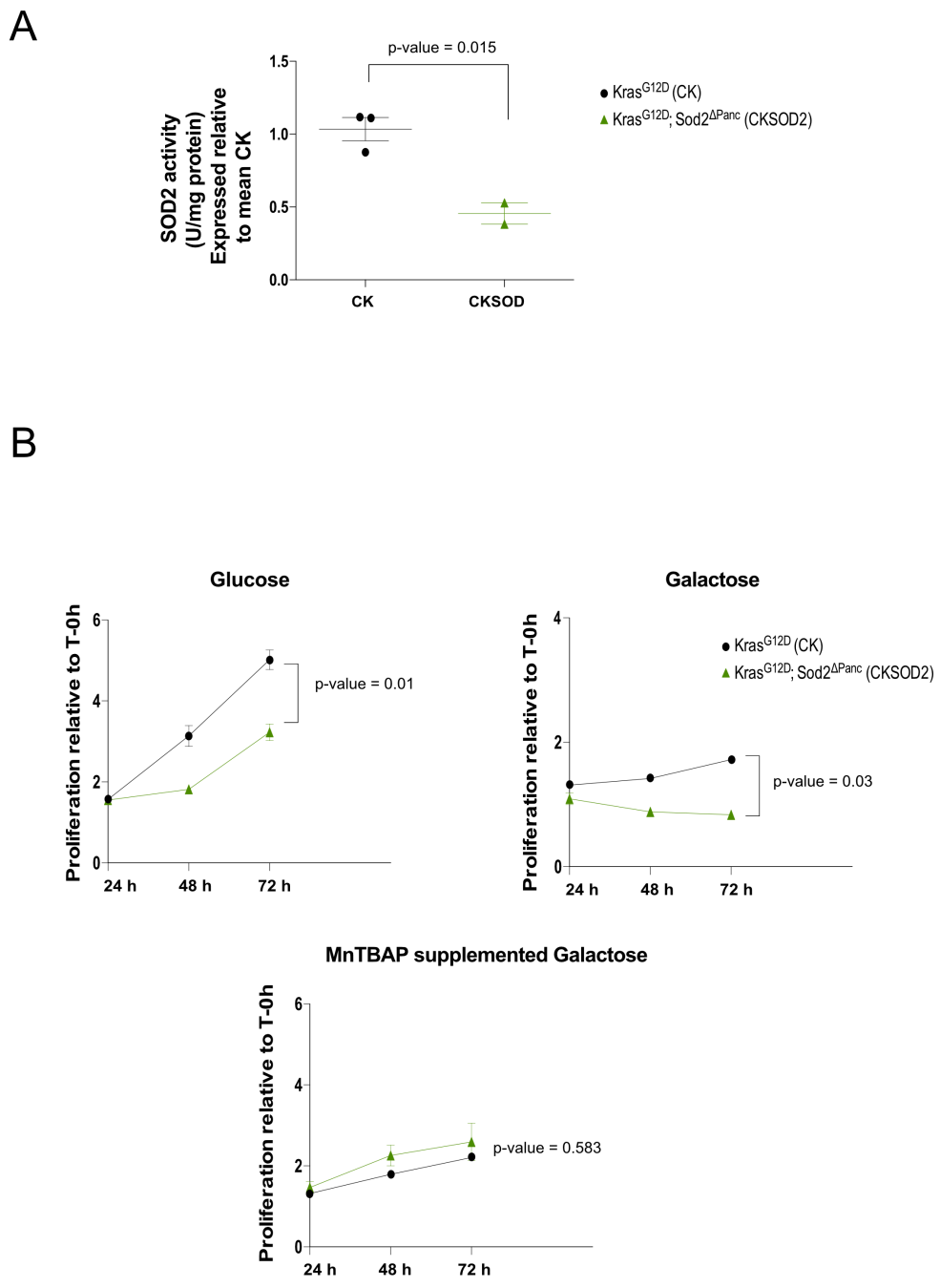

Figure III.1: Characterization of *Sod2* deficient tumour cell lines and biological differences upon acute (*in vitro*, B) and chronic (*in vivo*, A) *Sod2* deficiency. (A) Mitochondrial SOD2 activity (for 3 CK and 2 CKSOD2 cancer cell lines) normalised to mitochondrial protein amounts and expressed relative to control (CK) activity. **(B)** Proliferation differences between 3 CK and 2 CKSOD2 cancer cell lines in basal (standard glucose)

medium, galactose (glucose-free) medium and MnTBAP (100 µM) supplemented galactose medium.

C

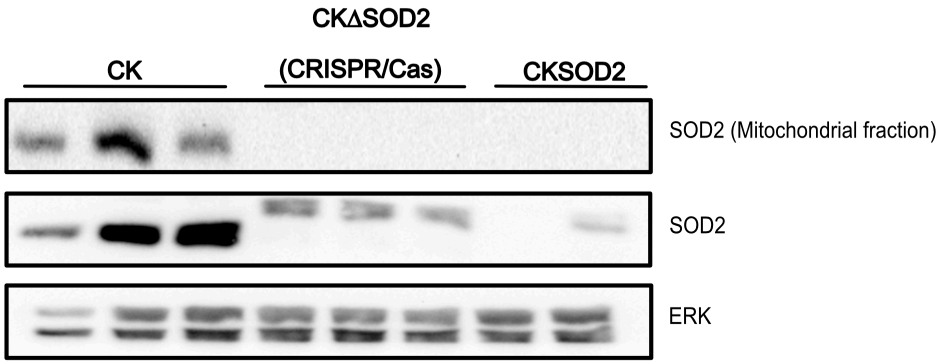

D

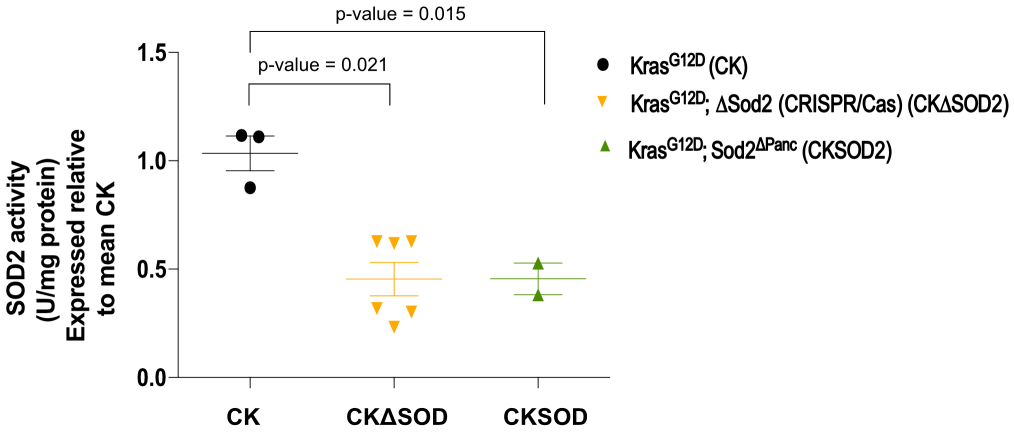

Figure III.1: Characterization of *Sod2* deficient tumour cell lines and biological differences upon acute (*in vitro*) and chronic (*in vivo*) *Sod2* deficiency. (C) Expression levels of SOD2, and ERK-1/2 were determined by western blotting for protein lysates from 3 CK, 3 CKΔSOD2 and 2 CKSOD2 cancer cell lines. **(D)** Mitochondrial SOD2 activity (for 3 CK, 6 CKΔSOD2, and 2 CKSOD2 cancer cell lines) normalized to mitochondrial protein amounts and expressed relative to control (CK) activity.

Kras^{G12D} (CK) and *Kras*^{G12D}*; Sod2*$^{\Delta Panc}$ (CKSOD2) cancer cell lines were isolated from PDAC mouse models generated previously by Christin Ruoff in our laboratory. *Kras*^{G12D}*; Sod2*$^{\Delta Panc}$ (CKSOD2) mice exhibit a lower tumour incidence relative to *Kras*^{G12D} (CK) mice. Thus, only 2 CKSOD cancer cell lines could be isolated from *in vivo Sod2* deficient (*Kras*^{G12D}*; Sod2*$^{\Delta Panc}$ (CKSOD2)) mice [77]. Mitochondria were enriched from *Kras*^{G12D} (CK) and *Kras*^{G12D}*; Sod2*$^{\Delta Panc}$ (CKSOD2) cancer cell lines to determine functional SOD2 (enzymatic) activity. Loss of functional SOD2 confirmed with SOD2 activity assay (Figure III.1.A). Proliferative potential of SOD2 deficient cancer cell lines is decreased (relative to CK cancer cell lines) in both basal (glucose-rich) and galactose (glucose-free) conditions. Additionally, SOD2 deficient cancer cells show vulnerability and struggle to survive in galactose culture. This survival struggle in galactose of CKSOD2 cancer cell lines is rescued when cultured in the presence of a SOD mimetic (MnTBAP) in galactose. (Figure III.1.B).

In vitro deletion of *Sod2* generated from CK cancer cell lines using CRISPR/Cas9 technology involving a double nickase approach. 3 CK cancer cell lines served as a parent to generate corresponding *Sod2* deficient clones (*Kras*^{G12D}*;* Δ*Sod2*/CKΔSOD2). Loss of SOD2 expression was confirmed by western blotting (Figure III.1.C) and functional loss of SOD2 was validated using the SOD2 activity assay (Figure III.1.D). Proliferative potential of acute/ *in vitro Sod2* deficient (CKΔSOD2) cancer cell lines (relative to CK cancer cell lines) was observed to be decreased but not to the extent observed with chronic/ *in vivo Sod2* deficient (CKSOD2) cancer cell lines. CKΔSOD2 cancer cell lines also do not display impaired survival in galactose as observed with CKSOD2 cancer cell lines (Figure III.1.E). Proliferation differences between CK, CKΔSOD, and CKSOD2 under basal and galactose culture conditions and the effect of SOD mimetic (MnTBAP) in rescuing CKSOD2 cancer cell lines can be well-appreciated from the proliferation data at 72h time-point (Figure III.1.F).

Sod2 deletion (both acute and chronic) resulted in a significant increase in phosphorylation of AMPK (Phosphorylation site: Thr^{172}) (Figure III.2.A, Figure III.2.B).

Additionally, it can be observed that the AMPK phosphorylation is unaffected by external addition of H_2O_2, at least these amounts of H_2O_2 treatment does not seem to influence AMPK phosphorylation in these cancer cell lines (Figure III.2.C) and the phosphorylation levels are decreased after a 24-hour treatment with SOD mimetic MnTBAP (Figure III.2.D).

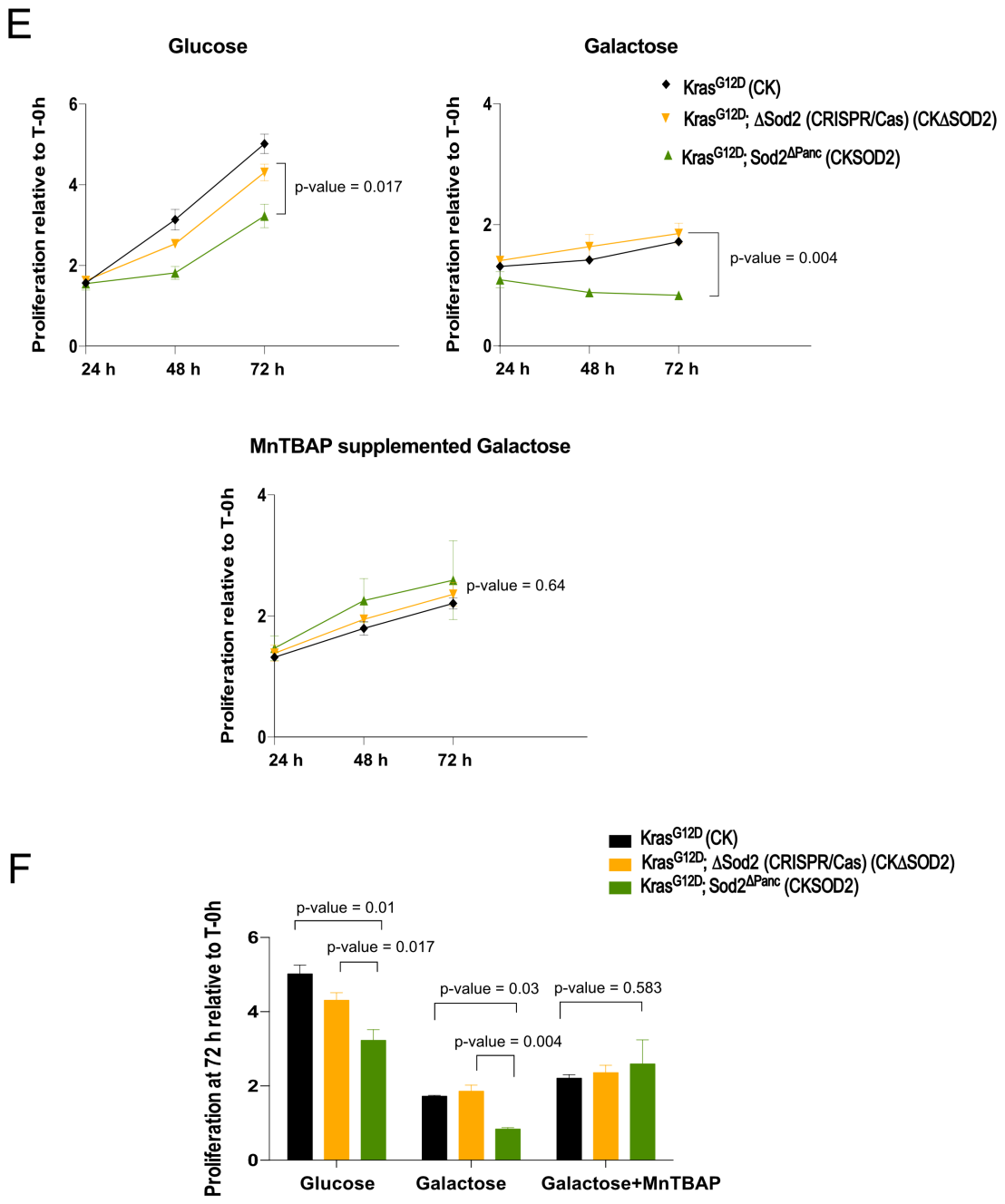

Figure III.1: Characterization of *Sod2* deficient tumour cell lines and biological differences upon acute (*in vitro*) and chronic (*in vivo*) *Sod2* deficiency. (E) Proliferation (relative to T-0h) of 3 CK, 3 CKΔSOD2, and 2 CKSOD2 cancer cell lines in basal (standard glucose) medium, galactose (glucose-free) medium and MnTBAP (100 µM) supplemented galactose medium **(F)** Proliferation rate at 72 hours under the three different conditions. Data are given as means ± standard error of the mean (SEM) (n=3). Statistical analysis performed using unpaired, two-tailed student's *t*-test.

A

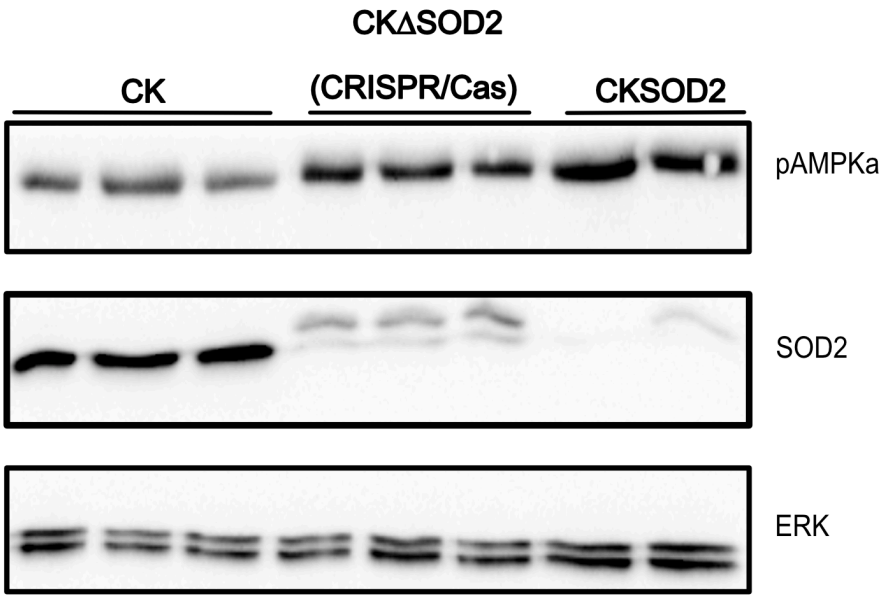

B

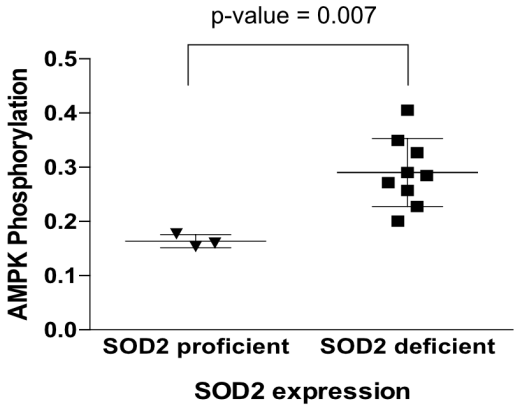

Figure III.2: *Sod2* deficiency results in AMPK activation and unaffected by external addition of H_2O_2. (A) Expression levels of pAMPKa, SOD2, and ERK-1/2 were determined by western blotting for CK, CKΔSOD2 and CKSOD2 cancer cell lines. **(B)** Quantification of AMPK phosphorylation/activation relative to ERK-1/2 expression. Data are given as means ± standard error of the mean (SEM) (n=3). Statistical analysis performed using unpaired, two-tailed student's *t*-test.

C

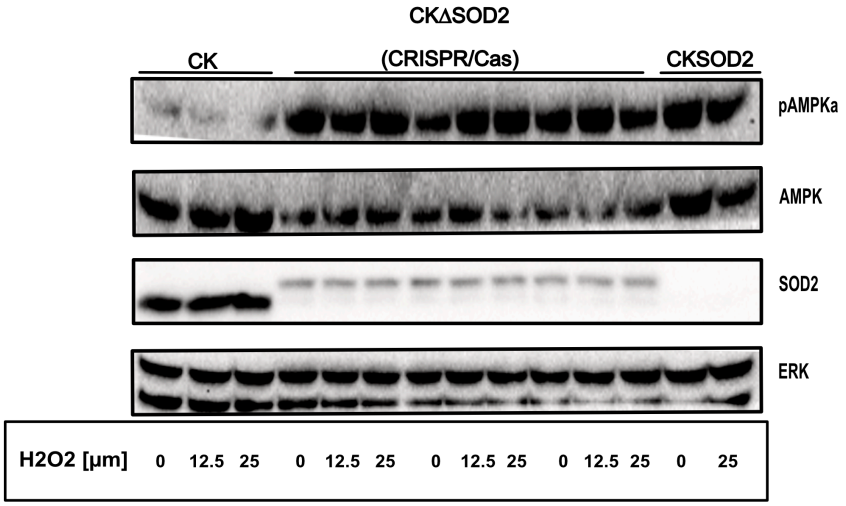

D

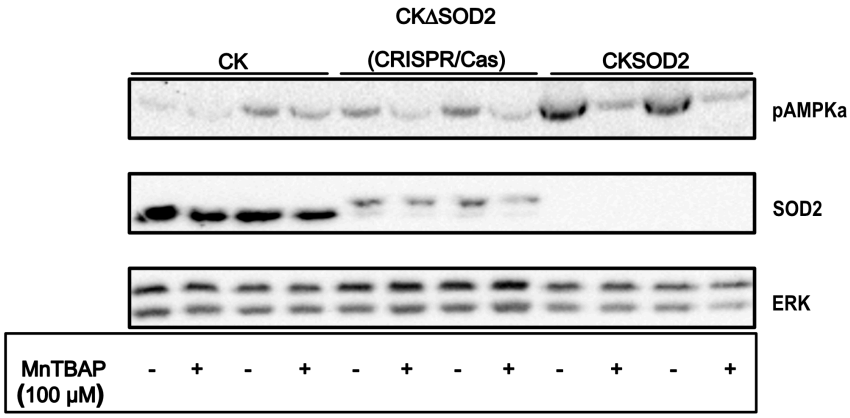

Figure III.2: *Sod2* deficiency results in AMPK activation and unaffected by external addition of H_2O_2. (C) CK, CKΔSOD2, and CKSOD2 cancer cell lines were treated with 0 µM, 12.5 µM and 25 µM (as indicated in the figure) H_2O_2 for 6 hours. Expression levels of ERK-1/2, SOD2, pAMPKa and AMPK were determined using Western blotting. **(D)** CK, CKΔSOD2 and CKSOD2 cancer cell lines were treated with 100 µM MnTBAP for 24 hours. Expression levels of pAMPKa, HIF1a, ERK-1/2 and SOD2 were determined using Western blotting technique.

The observation that the cellular energy sensor AMPK being activated (phosphorylated) in *Sod2* deficient cells led us to investigate the effect of *Sod2* deletion on cellular respiration. To this end, we performed seahorse analysis which gives us a measure of the respiratory profile for CK, CKΔSOD2 (acute/ *in vitro Sod2* deletion), and CKSOD2 (chronic/ *in vivo Sod2* deletion) cancer cell lines, determined using the oxygen consumption rate (OCR) and extracellular acidification rate (ECAR). Oligomycin treatment of cancer cell lines was done to estimate oxygen consumption linked to oxidative phosphorylation-mediated ATP production. Treatments with Carbonyl cyanide-m-chlorophenyl hydrazone (CCCP) was done to induce uncoupling by collapsing the inner mitochondrial membrane gradient resulting in electron transport chain (ETC) to be functioning at maximal capacity. This was followed by treatments with inhibitors of complex III (Antimycin A/AA), and complex I (Rotenone/Rot) to arrest electron transport chain (ETC) function and hence, estimate oxygen consumption linked to non-mitochondrial respiration. XF-96 Seahorse analyzer monitors both the oxygen concentration with a sensor (yielding OCR) and also the pH of the media (yielding ECAR). It can be observed that the basal OCR is increased with *Sod2* deficiency, significantly with chronic/ *in vivo* Sod2 deficient (CKSOD2) cancer cell lines. CCCP did not stimulate the OCR of CKSOD2 cancer cell lines but CKΔSOD2 and CK cancer cell lines increased their oxygen consumption upon CCCP. Hence, indicating a respiratory reserve capacity impairment with CKSOD2 cancer cell lines. It can also be seen that CKSOD2 cancer cell lines have their basal OCR as its maximum oxygen consumption. Acute/ *in vitro Sod2* deficient (CKΔSOD2) cancer cell lines show an increased basal oxygen consumption (relative to CK cancer cell lines) and also comfortably increase their oxygen consumption upon uncoupling (CCCP), indicating a comfortable switch to oxidative phosphorylation while the same is not seen with chronic/ *in vivo* Sod2 deficient cancer cell lines (CKSOD2) (Figure III.3.A). A significant increase in ECAR rates can be observed with chronic *Sod2* (CKSOD2) deficient cancer cell lines. Indicating an increase in glycolysis with CKSOD2 cancer cell lines (Figure III.3.B).

Several parameters of cellular respiration rates such as basal, maximal, ATP-linked, proton leak-linked, reserve capacity, and % spare respiratory capacity (relative to basal) were calculated from OCR data and expressed for CK, CKΔSOD2, and

CKSOD2 cancer cell lines. Significant increase in basal respiration rates was observed with chronic *Sod2* deficient (CKSOD2) cancer cell lines. Maximal respiration rate is increased with acute *Sod2* deficient (CKΔSOD2) cancer cell lines but not with chronic *Sod2* deficient (CKSOD2) cancer cell lines. In fact, a decrease in maximal respiration rate is observed with CKSOD2 cancer cell lines suggesting that chronic *Sod2* deficient cancer cell lines have their basal respiration as their maximum respiration rate. It can also be observed that proton leak-linked respiration with CKSOD2 cancer cell lines is significantly increased. This phenotype of CKSOD2 cancer cell lines showing an increased basal oxygen consumption and a decrease in oxygen consumption upon stimulating electron transport chain to full potential (with CCCP treatment) correlates to the impaired spare reserve capacity in CKSOD2 cancer cell lines, indicating a possible mitochondrial bioenergetics defect with chronic *Sod2* deficiency (Figure III.3.C).

Total ATP turnover and pathway-specific ATP production (ATP from glycolysis and ATP from oxidative phosphorylation (OXPHOS)) were calculated from the respiratory profile obtained through OCR and ECAR analysis. There appears to be an increase in total ATP production rate with *Sod2* deficient cancer cell lines (CKΔSOD2 and CKSOD2) relative to CK cancer cell lines, although not a statistically significant increase. A significant increase in ATP derived from oxidative phosphorylation is observed with acute/ *in vitro* *Sod2* deficient cancer cell lines (CKΔSOD2), in alignment with the increased maximal respiration rate observed with these cancer cell lines. Another interesting finding is the increased glycolysis-derived ATP observed with chronic *Sod2* deficient cancer cell lines (CKSOD2) and this goes hand in hand with the increased ECAR observed with CKSOD2 cancer cell lines. Ratios of mitochondria/OXPHOS-derived ATP production and glycolysis-derived ATP production show the considerable contribution of glycolysis observed with chronic *Sod2* deficiency and significant contribution of mitochondrial bioenergetics with acute *Sod2* deficiency (Figure III.3.D).

To better understand the increased maximal respiration, and increased mitochondria/OXPHOS-derived ATP production with CKΔSOD2 cancer cell lines

(Figure III.3.C and Figure III.3.D), cancer cell lines were cultivated under basal conditions (glucose medium) in the presence of an inhibitor for glucose transporter 1 (Glut1). This was done to assess the influence of glycolysis inhibition on the proliferation capacity of cancer cell lines (CK, CKΔSOD2, and CKSOD2). In accordance with increased signs of mitochondrial bioenergetics observed with acute *Sod2* deficiency, CKΔSOD2 cancer cell lines show increased tolerance (in comparison to CK and CKSOD2 cancer cell lines) to glycolysis block via Glut1 inhibition. This can be observed as an increased cell growth rate of CKΔSOD2 cancer lines after 72 h of Glut1 inhibitor cultivation. It can also be observed that chronic Sod2 deficient (CKSOD2) cancer cell lines are vulnerable to glycolysis inhibition (Figure III.4.B). Acute/ *in vitro Sod2* deficient (CKΔSOD2) cancer cell lines show an increased c-Myc protein expression and interestingly, c-Myc expression is drastically decreased with chronic/ *in vivo Sod2* deficient (CKSOD2) cancer cell lines (Figure III.4.A).

On consideration of the contrasting parameters of cellular respiration rate observed upon *Sod2* deficiency, protein expression levels of the 5 complexes involved in electron transport chain (ETC) and oxidative phosphorylation (OXPHOS) were determined using the western blotting technique. A severe deficiency in complex II expression observed with chronic *Sod2* deficient (CKSOD2) cancer cell lines observed. Interestingly, this strong decrease of complex II expression did not occur in acute *Sod2* deficient cancer cell lines (CKΔSOD2) (Figure III.5.A). However, the expression levels of other complexes (complex I, III, IV, V) are not overtly altered between the control and knockout cancer cell lines (Figure III.5.A).

To understand if complex II expression decrease is reversible and if only at the protein level, control (CK) and chronic *Sod2* deficient (CKSOD2) cancer cell lines were treated with SOD mimetic (MnTBAP) in a time-course manner (0 h / untreated, 24 h, 48 h, and 72 h). It can be observed that MnTBAP supplementation restores the decreased complex II expression in CKSOD2 cancer cell lines in a time-dependent fashion (Figure III.5.B). Complex II expression restoration upon MnTBAP treatment is quantified relative to loading control expression (ERK) and expressed relative to

control CK cancer cell lines (Figure III.5.C). This suggests that decreased complex II expression is only transient and can be reversed with restoring the functionality of SOD (in scavenging superoxide) by MnTBAP supplementation.

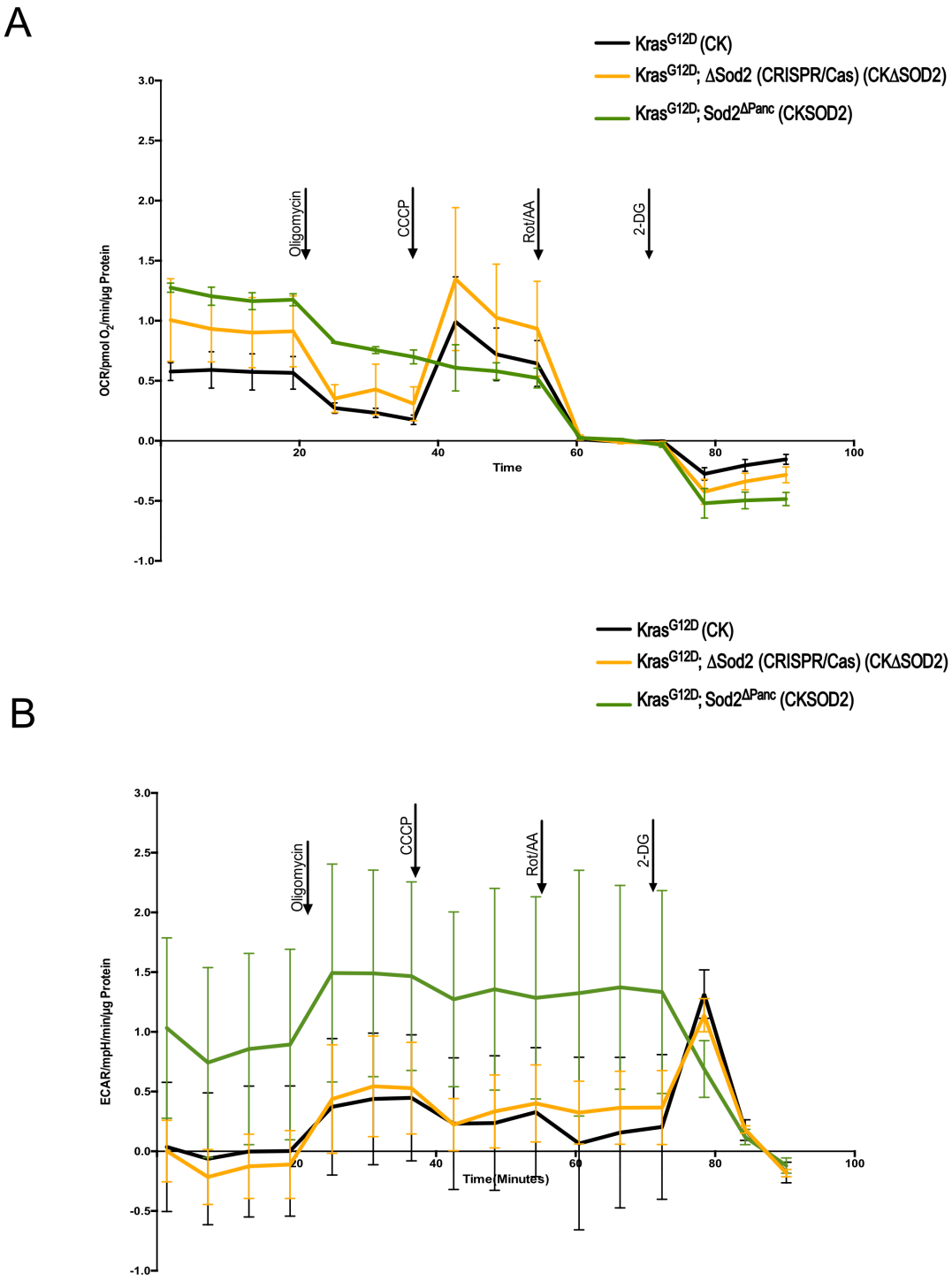

Figure III.3: Respiratory reserve capacity is severely impaired with chronic/ *in vivo* *Sod2* deficiency despite increased basal respiration. (A) Oxygen Consumption Rate

(OCR) determined using XF-96 Seahorse analyzer from CK, CKΔSOD2 and CKSOD2 cancer cell lines. Data shown are OCR ± SEM of biological replicates. **(B)** Extracellular Acidification Rate (ECAR) as a measure of glycolysis determined using XF-96 Seahorse analyzer from CK, CKΔSOD2, and CKSOD2 cancer cell lines. Data shown are OCR ± SEM of biological replicates.

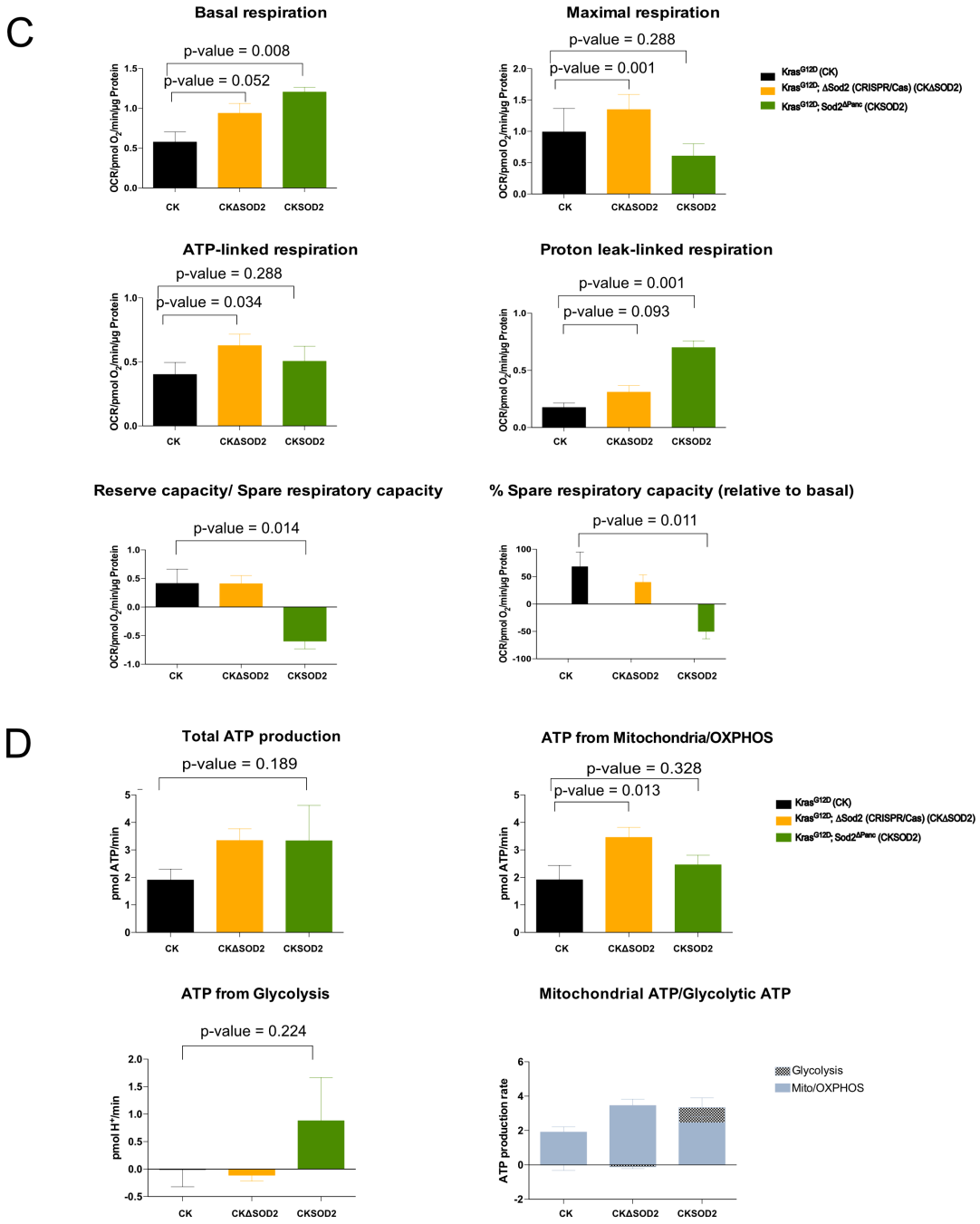

Figure III.3: Respiratory reserve capacity is severely impaired with chronic/ *in vivo* *Sod2* deficiency despite increased basal respiration. (C) Respiratory profile (basal,

maximal, ATP-linked, proton leak-linked, and reserve capacity) of cancer cell lines determined from OCR data. Data shown as means ± standard error of the mean (SEM) of biological replicates. Statistical analysis performed using unpaired, two-tailed student's *t*-test. **(D)** ATP production/turnover (Total ATP turnover, ATP from glycolysis, ATP from OXPHOS) also determined using OCR and ECAR data as mentioned in the materials and methods section (II.2.7).This was used to determine OXPHOS/Glycolysis ATP production rate ratio. Data shown as means ± standard error of the mean (SEM) of biological replicates. Statistical analysis performed using unpaired, two-tailed student's *t*-test.

A

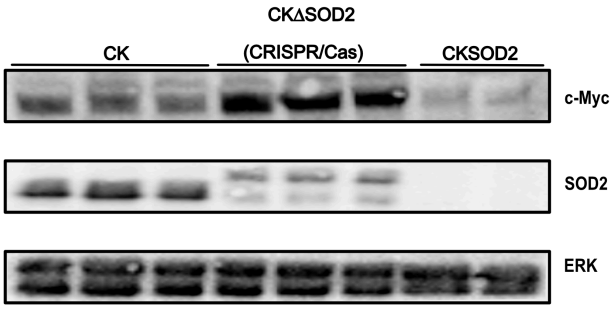

B

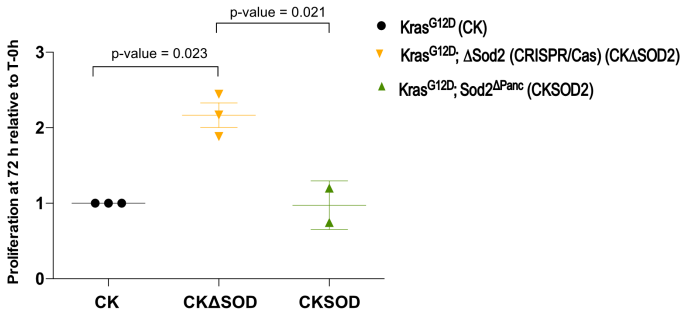

Figure III.4: Different levels of c-Myc expression with acute (*in vitro*) and chronic (*in vivo*) *Sod2* deletion. (A) Expression levels of c-Myc, SOD2, and ERK-1/2 were determined by western blotting for protein lysates from 3 CK, 3 CKΔSOD2, and 2 CKSOD2 cancer cell lines. **(B)** Proliferation rate differences upon pharmacological Glut1 inhibition (30 µM WZB117) at 72h time-point for 3 CK, 3 CKΔSOD2, and 2 CKSOD2 cancer cell lines. Data are given as means ± standard error of the mean (SEM) (n=3). Statistical analysis performed using unpaired, two-tailed student's *t*-test.

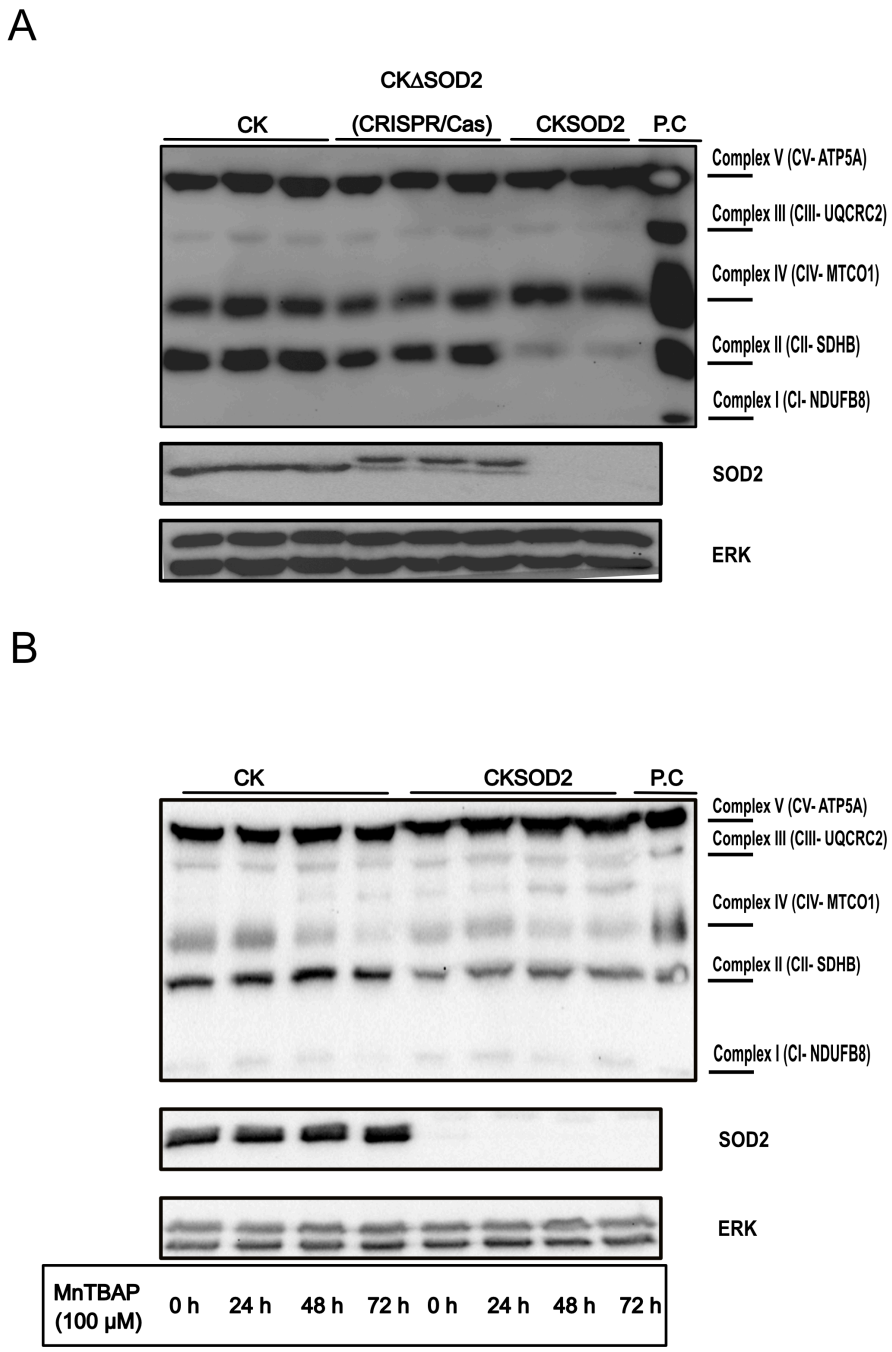

Figure III.5: Loss of Complex II (SDHB) expression with *Sod2* (chronic/ *in vivo*) deletion can be reversed with SOD mimetic MnTBAP. (A) Expression levels of components of the five electron transport chain (ETC) complexes determined by western blotting from protein lysates of 3 CK, 3 CKΔSOD2, and 2 CKSOD2 cancer cell lines. P.C: Positive control (Rat heart mitochondria) **(B)** Representative Western blot depicting the expression levels of components of the five electron transport chain (ETC) complexes determined, after time-course (0 h, 24 h, 48 h, and 72 h) treatment with MnTBAP, by western blotting for protein lysates from 2 CK, and 2 CKSOD2 cancer cell lines. P.C: positive control (rat heart mitochondria).

C

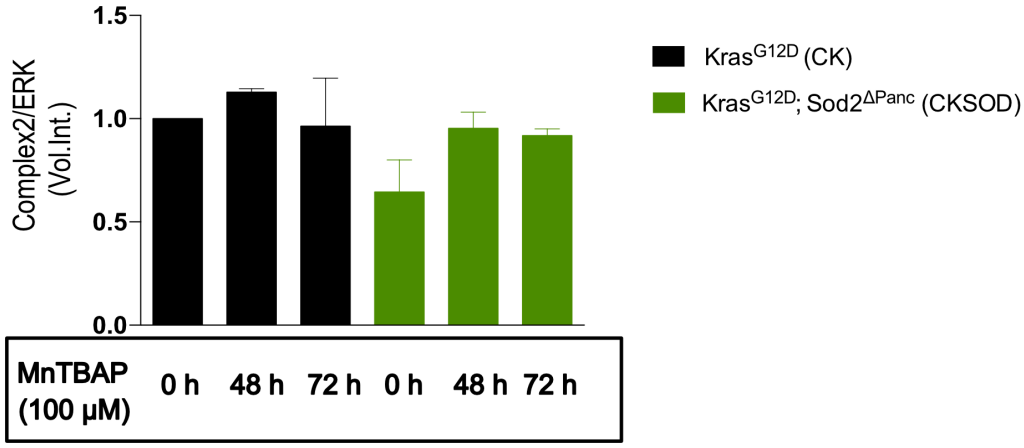

Figure III.5: Loss of complex II (SDHB) expression with *Sod2* (chronic/ *in vivo*) deletion can be reversed with SOD mimetic MnTBAP. (C) Quantification of complex II expression relative to ERK-1/2 expression. Data are given as means ± standard error of the mean (SEM) (n=2).

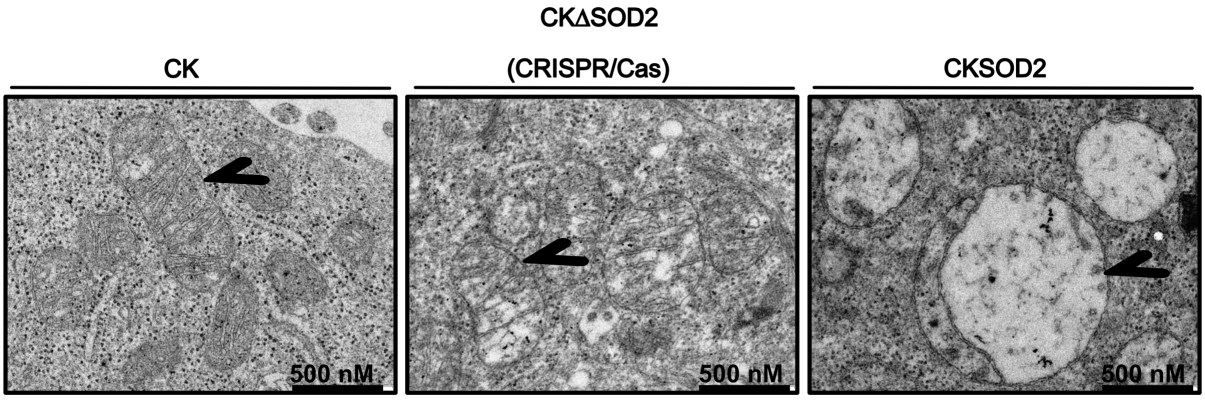

Figure III.6: Mitochondrial morphology after acute (*in vitro*) and chronic (*in vivo*) *Sod2* deletion. Representative images depicting mitochondrial morphology obtained through electron microscopy, from 3 CK, 6 CKΔSOD2, and 2 CKSOD2 cancer cell lines. Arrowheads indicate mitochondrial structures. Images were captured at magnifications of 20,000 fold.

Observations such as loss of complex II expression and galactose survival impaired with chronic *Sod2* deficient cancer cell lines indicate defective mitochondrial functionality. Hence, viewing the morphology of mitochondria in these cancer cell lines could provide direct evidence for proposed dysfunctional mitochondria in chronic *Sod2* deficient cancer cell lines (CKSOD2). To this end, CK, CKΔSOD2, and CKSOD2 cancer cell lines were fixed with glutaraldehyde and submitted for electron microscopy to obtain information about mitochondrial morphology. Mitochondrial structures observed in CK cancer cell lines contain “normal” mitochondrial morphology with clear definition of membrane borders and intact cristae structures. Mitochondrial structures observed with acute *Sod2* deficient cancer cell lines represent slightly swollen mitochondria with partial cristaelysis (loss of cristae structures). However, morphologically still comparable to mitochondria of CK cancer cell lines. Mitochondrial structures in chronic *Sod2* deficient (CKSOD2) cancer cell lines represent the classic swollen mitochondria and total cristaelysis (loss of cristae structures), a compelling proof for structural damage to mitochondria and thus mitochondrial dysfunction (Figure III.6).

III.2. Role of Reg3b in PDAC development

As an initial step to study the role of Reg3b in the context of PDAC development, mice with whole body deletion of *Reg3b (Reg3b*$^{\Delta/\Delta}$ *or Reg3b-/-)* were used (Figure III.7.A). Loss of *Reg3b* confirmed through genotyping PCR and agarose gel electrophoresis (Figure III.7.B). For experiments involving acinar explants and non-oncogenic pancreas, Reg3b-/- (or) Reg3b$^{\Delta/\Delta}$ (whole body deletion of *Reg3b*) mice were used and wild type (WT) littermates were used as controls. To understand the role of *Reg3b* in the context of PDAC development, *Reg3b* deletion was used in combination with an oncogenic pancreas (*Kras*$^{G12D/+}$) resulting in *Kras*$^{G12D/+}$*; Reg3b*$^{\Delta/\Delta}$ (CKReg3b or CKReg3b-/-). The breeding scheme, employed to get CKReg3b (*Kras*$^{G12D/+}$*; Reg3b*$^{\Delta/\Delta}$) mice and control CK (*Kras*$^{G12D/+}$) mice, involves pairing of *Kras*$^{G12D/+}$*; Reg3b*$^{\Delta/\Delta}$ mice with *Reg3b*$^{\Delta/+}$ mice (Figure III.7.C). Loss of *Reg3b* in CKReg3b mice confirmed through RT-PCR, by determining the mRNA expression levels of *Reg3b* (Figure III.7.D).

Acinar cells explanted, from 4-week-old pancreas of *Reg3b*$^{\Delta/\Delta}$ (whole body deletion of Reg3b) mice and wild type (WT) mice, were used for *in vitro* ADM (*in vitro* acinar-to-ductal metaplasia/ ADM) as mentioned in the materials and methods section. This was done to study cell autonomous effects of *Reg3b* deletion on transdifferentiation potential of acinar cells.

A

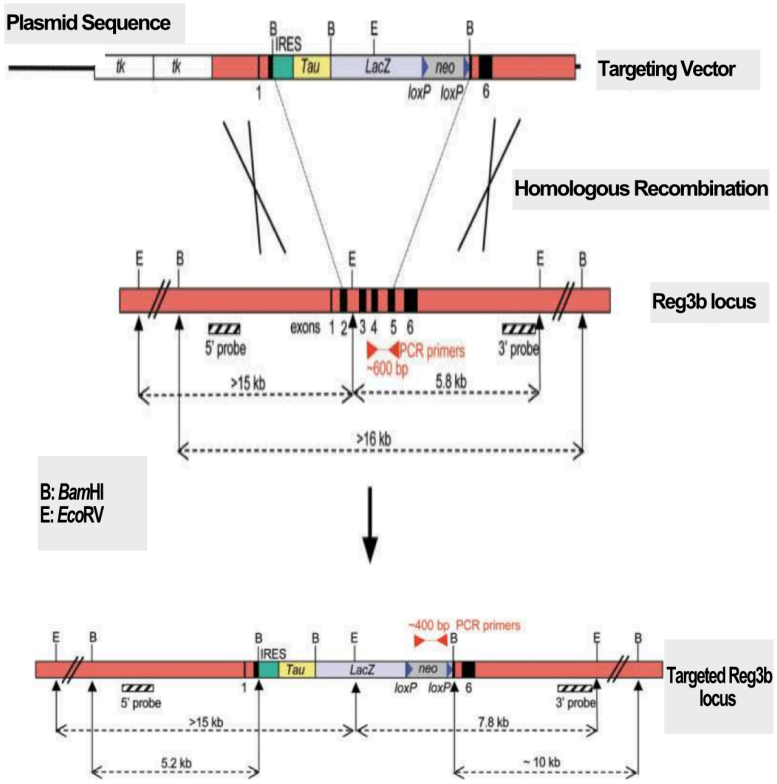

B

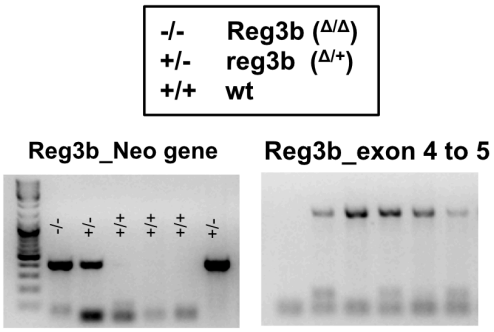

Figure III.7: Mouse model with whole body *Reg3b* deletion and oncogenic (Kras$^{G12D/+}$) pancreas. (A) Graphical representation depicting homologous recombination of targeting construct with the *Reg3b* locus. The vector deletes a region between exons 2 and 5 and is replaced with a reporter cassette, which contains a gene (*neo*) coding for neomycin resistance. Image adapted and modified from [76]. **(B)** Genotyping PCR results confirming the deletion of *Reg3b* (-/-), wild-type (+/+), and heterozygous (+/-) *Reg3b* mice.

C

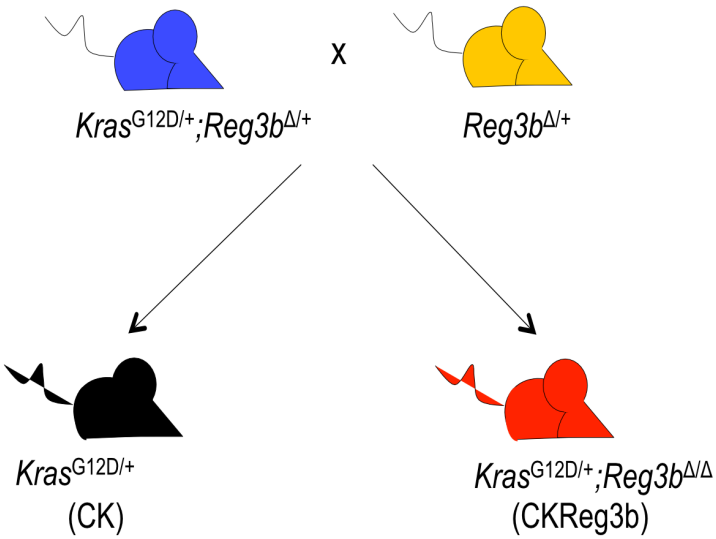

D

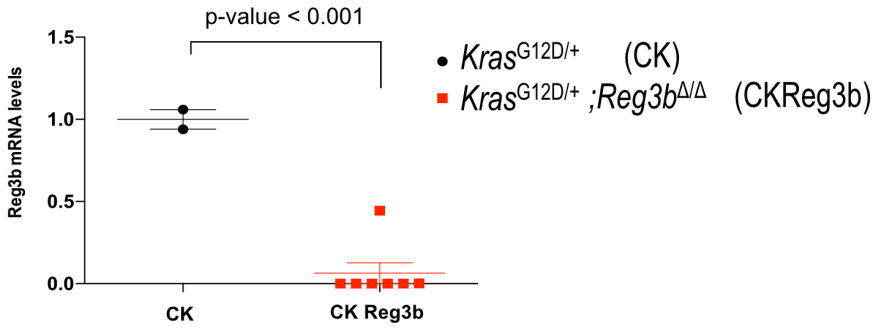

Figure III.7: Mouse model with whole body *Reg3b* deletion and conditional expression of oncogenic (Kras$^{G12D/+}$) in the pancreas. (C) Mating scheme used to generate Kras$^{G12D/+}$ (CK) and Kras$^{G12D/+}$; Reg3b$^{\Delta/\Delta}$ (CKReg3b) mice. **(D)** RT-PCR based validation of *Reg3b* deletion from 12-week-old CK (2) and CKReg3b (7) mice. Data are given as means ± standard error of the mean (SEM). Statistical analysis performed using unpaired, two-tailed student's *t*-test.

A

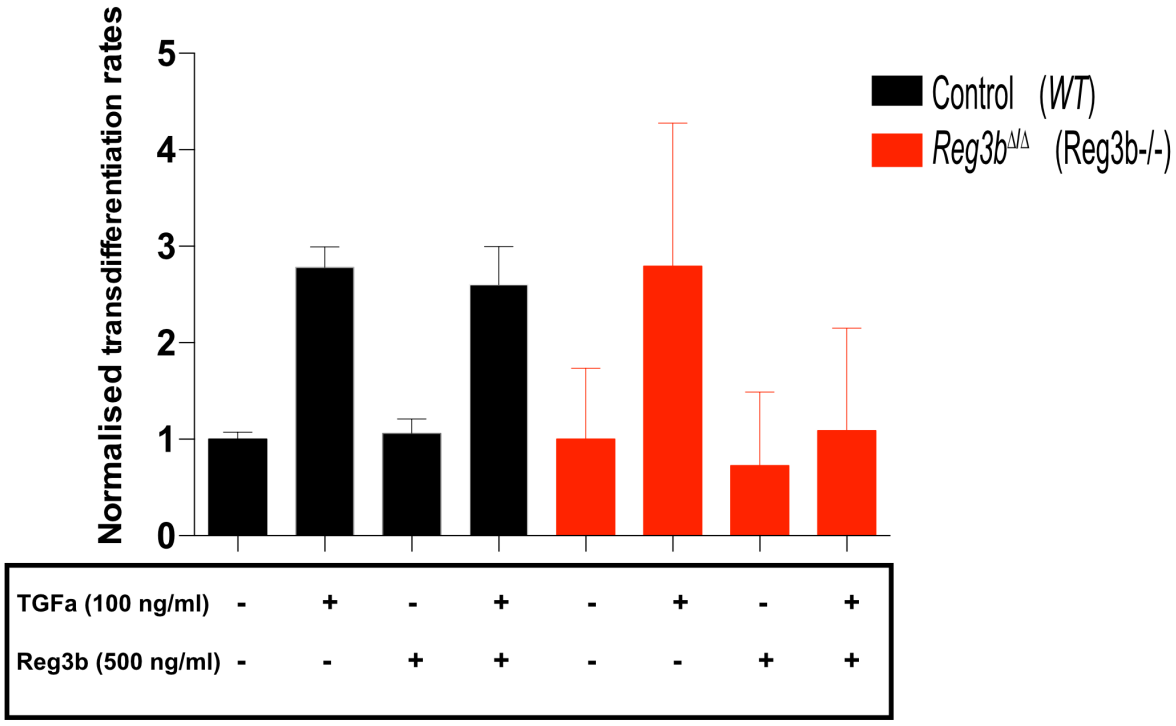

Figure III.8: Increased Acinar-to-Ductal Metaplasia (ADM) observed in 12-week-old pancreas of Reg3b deleted mice despite no differences with *in vitro* ADM from Reg3b deleted acinar explants. (A) Acinar explants from 4-week-old mice (control/wild-type (WT) and *Reg3b* deleted) treated with basal media, TGFα (100 ng/ml), and/or recombinant Reg3b (500 ng/ml). Data for each genotype normalised to respective basal values. Data are given as means ± standard error of the mean (SEM) (n=3-4). Statistical analysis performed using unpaired, two-tailed student's *t*-test.

In vitro stimulation of transdifferentiation of acini into a ductal morphology (*in vitro* ADM) was achieved through treatments with transforming growth factor alpha (TGFα). Wild type (WT) and acini from *Reg3b* deleted mice (Reg3b-/- or Reg3b$^{\Delta/\Delta}$) were also treated with recombinant Reg3b protein to compensate for the loss of Reg3b in Reg3b-/- mice and also to understand the influence of Reg3b in modulating

in vitro ADM under basal (untreated) and TGFα treated conditions. The transdifferentiation rates for the control (Wild-type) and knockout (*Reg3b-/-*) acini were normalised to their respective basal transdifferentiation rates. It can be observed that there is no significant difference in transdifferentiation potential of control and knockout acini under basal conditions and also their transdifferentiaiton rates are comparable upon stimulation with TGFα. Addition of recombinant Reg3b protein does not alter the *in vitro* ADM formation in control acini. In knockout (*Reg3b*$^{\Delta/\Delta}$) acini, addition of recombinant Reg3b protein appears to impede *in vitro* ADM formation, although not statistically significant (Figure III.8.A). It can be safely considered that *Reg3b*$^{\Delta/\Delta}$ acini do not exhibit any cell-autonomous effects in influencing *in vitro* ADM forming capacity.

B

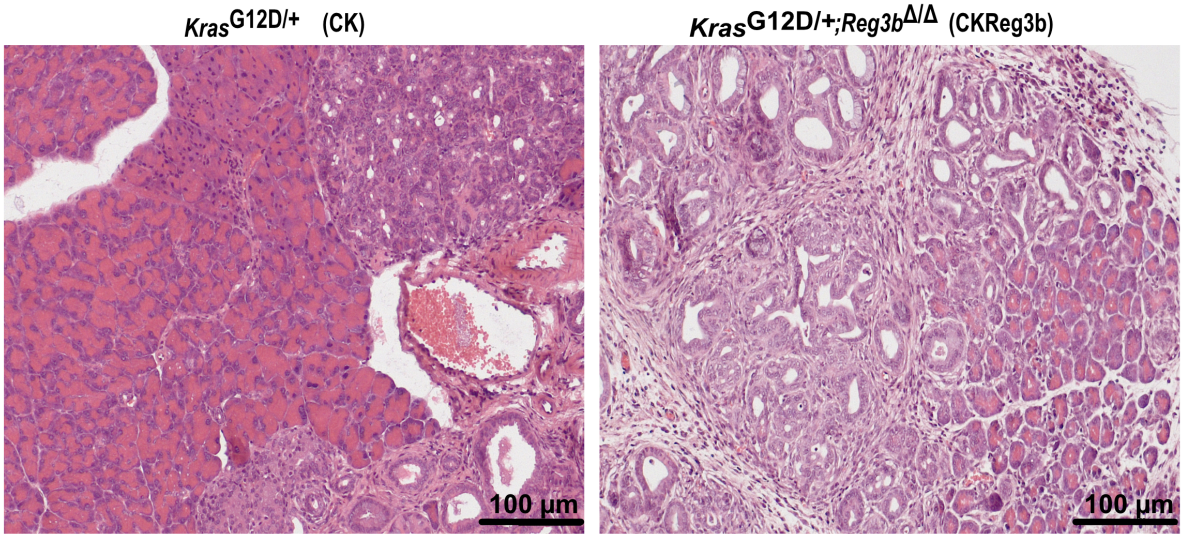

C

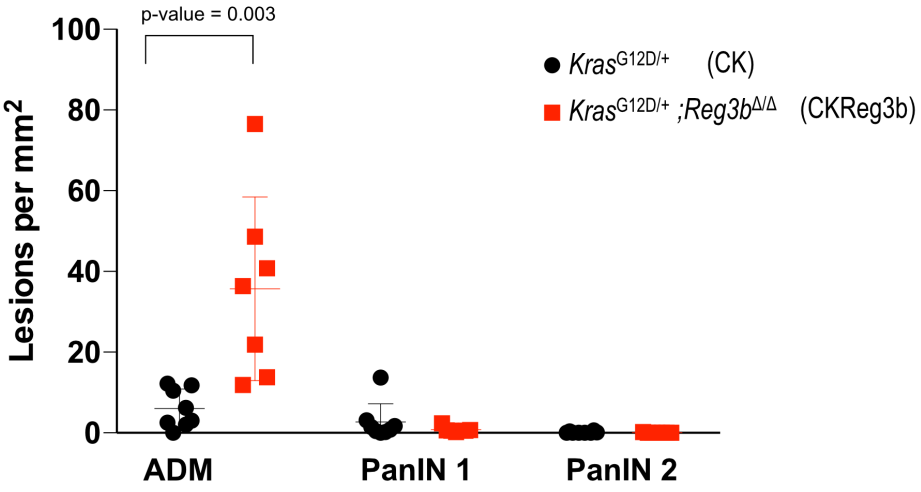

Figure III.8: Increased Acinar-to-Ductal Metaplasia (ADM) observed in 12-week-old pancreas of *Reg3b* deleted mice despite no differences with *in vitro* ADM from *Reg3b* deleted acinar explants. (B) Representative images (H&E staining) of pancreas in $Kras^{G12D/+}$ (CK) and $Kras^{G12D/+}$; $Reg3b^{\Delta/\Delta}$ (CKReg3b) mice at 12 weeks of age. **(C)** Quantification of ADM and PanIN lesions (per mm^2 tissue area). Data shown as means ± standard error of the mean (SEM) (n= 7-8). Statistical analysis performed using unpaired, two-tailed student's *t*-test.

To observe *in vivo* ADM forming potential in *Reg3b* deleted mice, pancreas tissue samples were harvested from $Kras^{G12D/+}$ (CK), and $Kras^{G12D/+}$; $Reg3b^{\Delta/\Delta}$ (CKReg3b) mice when they attained the age of 12 weeks. Hemalaun and Eosin (H&E) staining of the pancreas revealed details about acinar morphology, ductal morphology, and lesions in the pancreas. H&E staining helped in evaluating and quantifying the ADM and PanIN lesions. It can be observed that CKReg3b mice display increased presence of ADM lesions compared to control (CK) pancreas (Figure III.8.B and Figure III.8.C). Contrary to the *in vitro* ADM differences between control (WT) and *Reg3b* deleted acini, *in vivo* ADM was significantly increased with *Reg3b* deleted (CKReg3b) mice. This suggested the influence of non-cell autonomous factors influencing *in vivo* ADM in CKReg3b mice.

To look at the inflammatory state of pancreas in $Kras^{G12D/+}$ (CK), and $Kras^{G12D/+}$; $Reg3b^{\Delta/\Delta}$ (CKReg3b) mice at 12 weeks when they show the presence of ADM, pancreas tissue samples were harvested from mice at the age of 12 weeks and the expression of F4/80 glycoprotein was checked using immunohistochemistry (IHC). F4/80 serves as a marker for macrophage infiltration. For the analysis, 2 control CK mice and 6 knockout (CKReg3b) were used. It can be observed that there are signs of increased presence of macrophage infiltration with CKReg3b pancreas compared to the control CK pancreas (Figure III.8.D and Figure III.8.E).

To observe the effect of *Reg3b* deletion on other *Reg* family genes, twelve-week-old CK and CKReg3b pancreas were used to evaluate mRNA expression levels of Reg family genes including *Reg1*, *Reg2, Reg3a, Reg3d, Reg3g*, and *Reg4*. It can be observed that all Reg family genes, except *Reg1*, display a significantly decreased mRNA expression in CKReg3b pancreas (Figure III.9). This observation suggests the possibility of *Reg3b* as a key regulator of other Reg family genes.

D

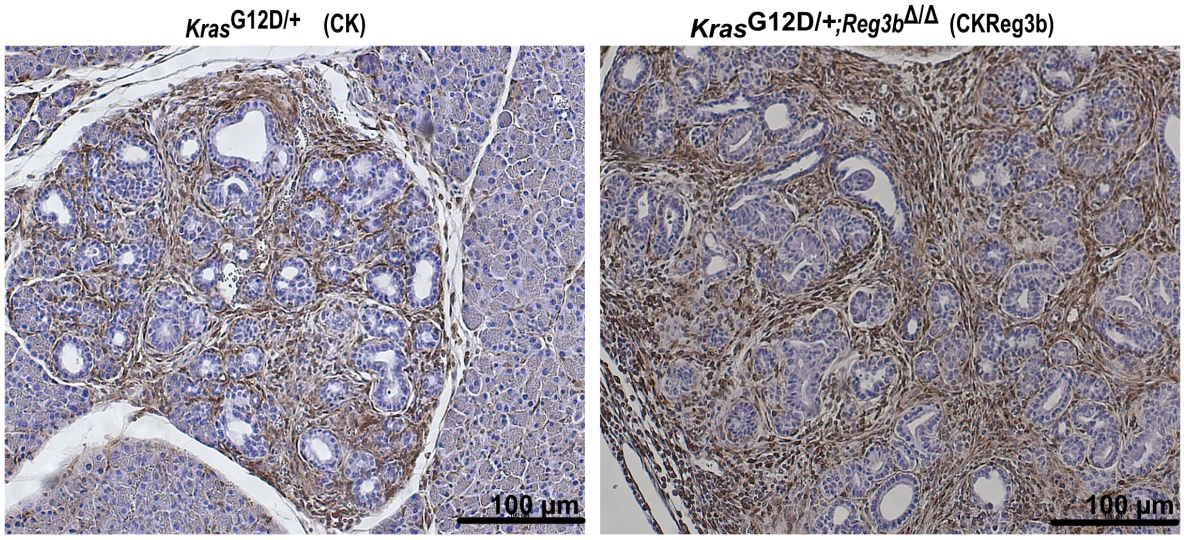

E

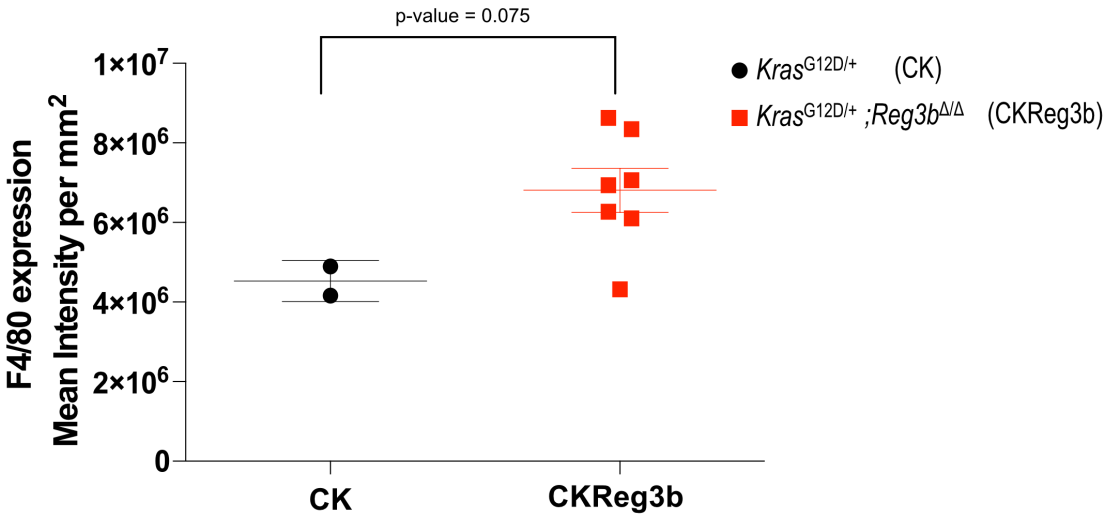

Figure III.8: Increased acinar-to-ductal Metaplasia (ADM) observed in 12-week-old pancreas of Reg3b deleted mice despite no differences with *in vitro* ADM from Reg3b deleted acinar explants. (D) Representative images depicting macrophage infiltration (F4/80 staining) in pancreas of 2 $Kras^{G12D/+}$ (CK) and 6 $Kras^{G12D/+}$; $Reg3b^{\Delta/\Delta}$ (CKReg3b) mice at 12 weeks of age. **(E)** Quantification of F4/80 expression (as mean intensity of expression per mm^2 tissue area). Data are given as means ± standard error of the mean (SEM).

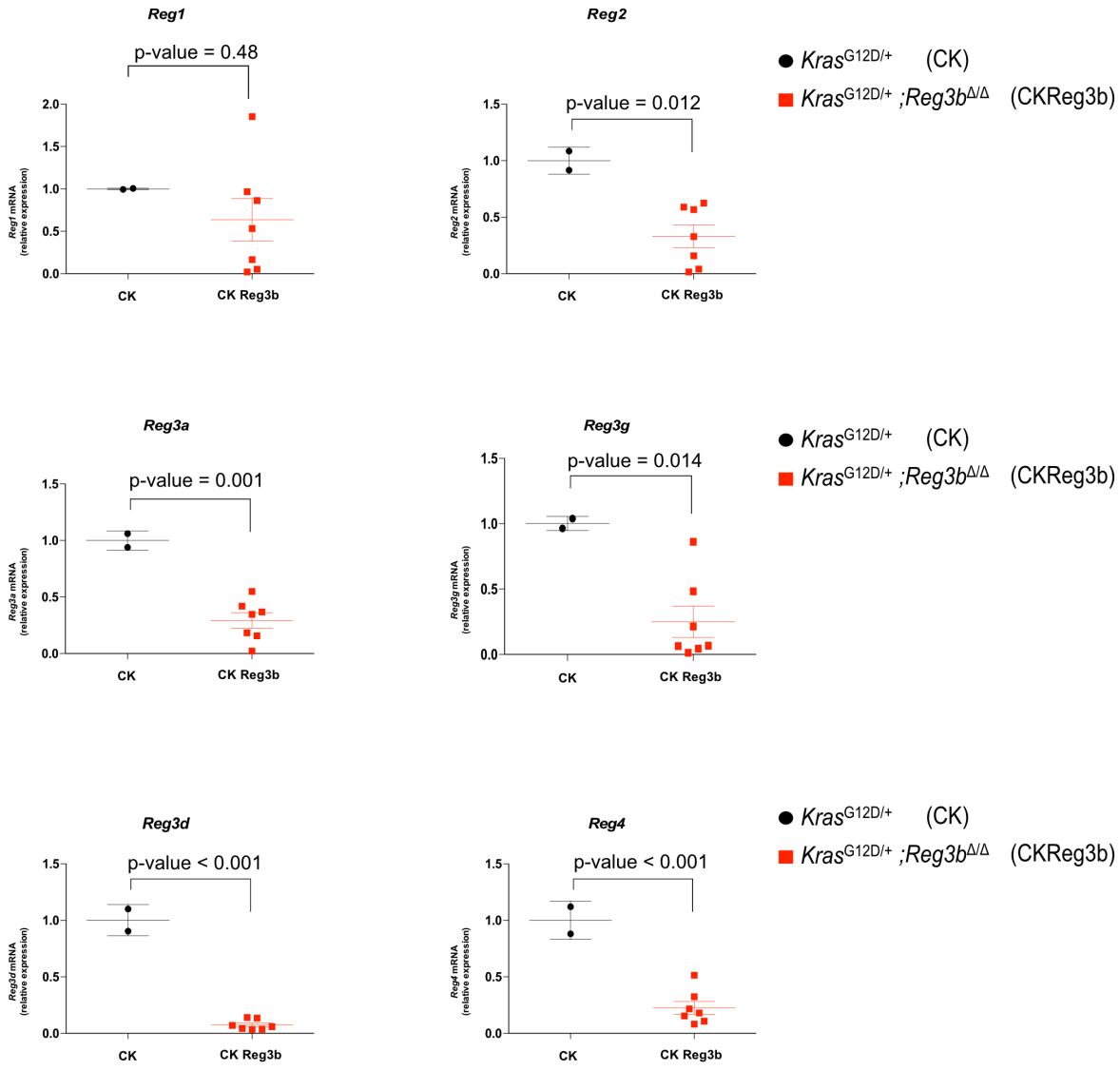

Figure III.9: Overall downregulation of Reg family genes with *Reg3b* deletion. mRNA expression (relative to mean CK) levels of *Reg1, Reg2, Reg3a, Reg3g, Reg3d*, and *Reg4* determined with RT-PCR from pancreas of 2 $Kras^{G12D/+}$ (CK) and 7 $Kras^{G12D/+}$; $Reg3b^{\Delta/\Delta}$ (CKReg3b) mice at 12 weeks of age. Data are given as means ± standard error of the mean (SEM). Statistical analysis performed using unpaired, two-tailed student's *t*-test.

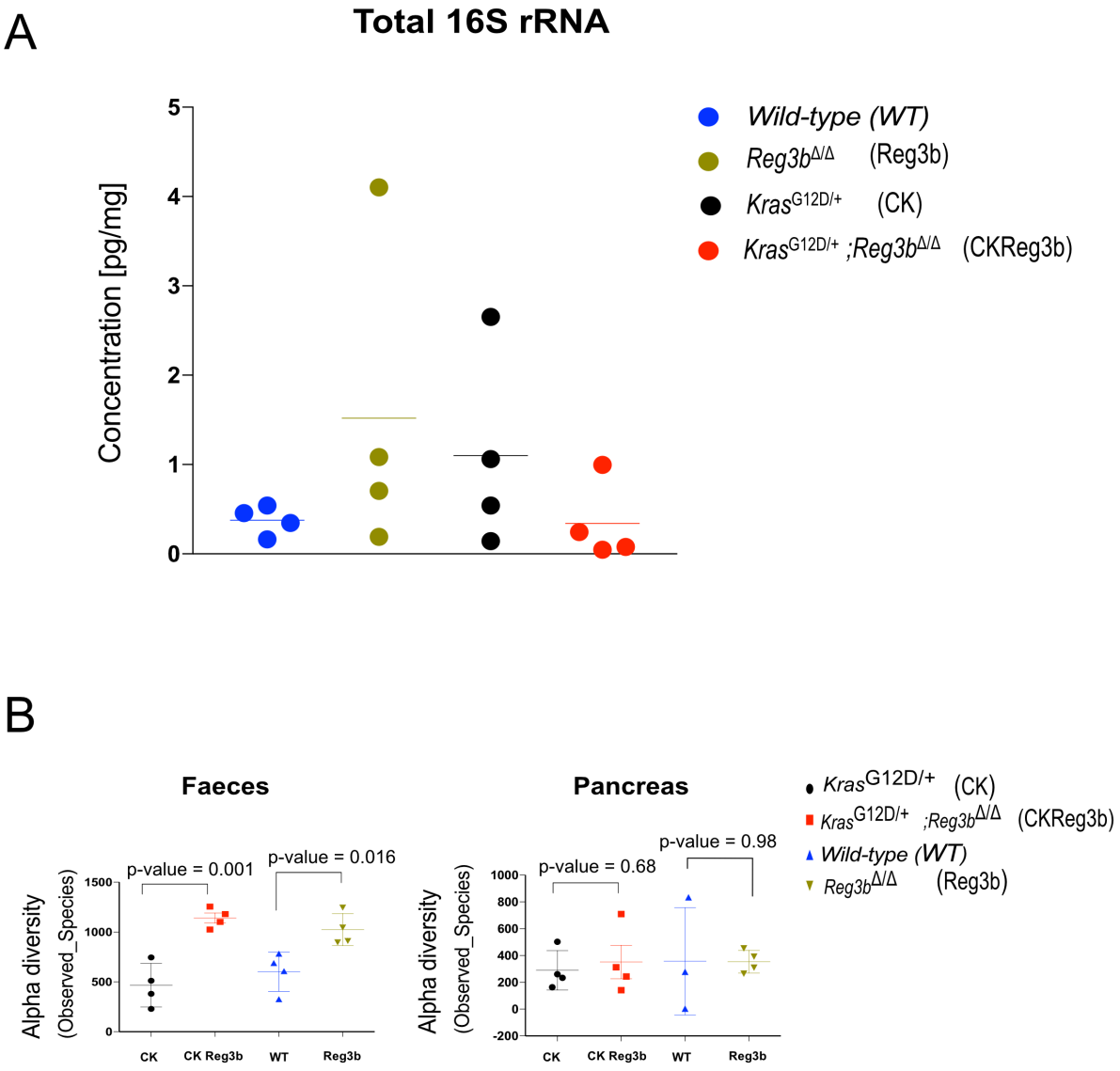

Figure III.10: 16S rRNA sequencing. **(A)** Total 16S load estimated by qPCR in the pancreas of 4 *wild type (WT) (*shown as blue dot*)*, *Reg3b*$^{\Delta/\Delta}$ deleted (Reg3b) (shown as green dot), *Kras*$^{G12D/+}$ (CK), and *Kras*$^{G12D/+}$*; Reg3b*$^{\Delta/\Delta}$ (CKReg3b) mice at 12 weeks of age (reference: E. coli DNA from Zymo Research). **(B)** Alpha diversity, measured by observed species is plotted for faecal and pancreas samples from 4 *wild type (WT)*, *Reg3b*$^{\Delta/\Delta}$ deleted (Reg3b), *Kras*$^{G12D/+}$ (CK), and *Kras*$^{G12D/+}$*; Reg3b*$^{\Delta/\Delta}$ (CKReg3b) mice at 12 weeks of age. Data are given as means ± standard error of the mean (SEM).

Inflammed pancreas and loss of mRNA expression levels of other anti-microbial *Reg* family genes in *Reg3b* deleted mice motivated us to study the microbiome in pancreas and gut from control and *Reg3b* deleted mice. To this end, faecal pellets and pancreas tissue samples were collected from 4 animals from each of the 4 groups: *Wild type* (WT), $Reg3b^{\Delta/\Delta}$, $Kras^{G12D/+}$ (CK), and $Kras^{G12D/+}$; $Reg3b^{\Delta/\Delta}$ (CKReg3b). The samples were submitted for 16S rRNA sequencing to have information about the microbial population in the gut and pancreas of these mice. DNA was isolated from the pancreas tissue samples from the above group of animals and total 16S rRNA measured using a quantitative PCR [reference: E. coli DNA from Zymo Research]. It can be observed that there is a slight increase in total 16S load with $Reg3b^{\Delta/\Delta}$ pancreata in comparison relative to the wild type (WT). However, this pattern of slight increase in total 16S rRNA load with $Reg3b^{\Delta/\Delta}$ pancreata does not hold true for $Kras^{G12D/+}$; $Reg3b^{\Delta/\Delta}$ (CKReg3b) pancreata (Figure III.10.A).

As a measure of diversity of microbial population in the 4 different groups of mice (WT, $Reg3b^{\Delta/\Delta}$, CK, and CKReg3b), “Observed_Species” was used as an estimate of alpha diversity for each of the 4 groups. Alpha diversity was determined for both faecal samples and the pancreas samples from the 4 groups. Alpha diversity of faecal samples indicates that there is a significant increase in alpha diversity (observed_species) for both the *Reg3b* knockout groups ($Reg3b^{\Delta/\Delta}$ and $Kras^{G12D/+}$; $Reg3b^{\Delta/\Delta}$) in comparison to the control groups (*Wild type* and $Kras^{G12D/+}$). However, this significant increase in alpha diversity in faecal samples in *Reg3b* absent mice does not translate at the level of pancreas (Figure III.10.B).

IV. Discussion

IV.1. Studying the role of *Sod2* helps elucidating the significance of oxidative signaling in modulating PDAC biology.

IV.1.1. *In vitro* and *In vivo* deletion of *Sod2* in cancer cell lines to mimic a state of acute and chronic *Sod2* deficiency.

PDAC originating from mice having an oncogenic mutation in the pancreas (*Kras*^{G12D}) and from mice having both an oncogenic mutation and *Sod2* deletion (*Kras*^{G12D}*; Sod2*$^{\Delta Panc}$) were used for isolation of control (CK) and *in vivo Sod2* deficient (CKSOD2) cancer cell lines respectively [77]. CK cancer cell lines served as parental cell lines to generate *in vitro Sod2* deficient cancer cell lines (*Kras*^{G12D}*;* Δ*Sod2*/CKΔSOD2) using CRISPR/Cas9 technology. *In vivo Sod2* deletion represents a state of chronic *Sod2* deficiency, in which carcinogenesis occurred in the absence of *Sod2*. Meanwhile, *in vitro Sod2* deletion represents a state of acute *Sod2* deficiency as carcinogenesis of *Kras*^{G12D} (CK) mice, which, occurred in the presence of *Sod2* and the cells were later deleted for *Sod2* (post cancer development and cell line isolation). As SOD2 localized in the mitochondrial matrix [78], SOD activity assay from enriched mitochondria of cancer cell lines verified the loss of enzymatic activity of SOD2 and thus the functional loss of superoxide scavenging in both acute and chronic *Sod2* deficient cancer cell lines.

IV.1.2. Biological differences upon acute and chronic *Sod2* deficiency in cancer cell lines.

Chronic/*in vivo Sod2* (CKSOD2) deficient cancer cell lines proliferate at a slower rate compared to control (CK) and acute *Sod2* (CKΔSOD) cancer cell lines under basal conditions. No significant proliferation differences observed between CK and CKΔSOD2 cancer cell lines. In galactose (glucose-free) culture conditions, we observed a significant impairment in survival capacity with CKSOD2 cancer cell lines. However, a similar impaired survival in galactose was not observed with CKΔSOD2

cancer cell lines. Considering the impact of galactose culture in favoring mitochondrial energy production [79], we can postulate that the impaired survival capacity of chronic *Sod2* deficient (CKSOD2) cancer cell lines hints to an impaired mitochondrial function. Interestingly, the SOD mimetic (MnTBAP) reverses the impaired survival of CKSOD2 cancer cell lines in galactose. It can be hypothesized that the impaired mitochondrial function seen through impaired galactose survival should be a result of transient alterations incurred because of chronic SOD2 deficiency rather than genomic changes associated with *Sod2* deletion. Also, considering that galactose culture-associated impaired survival being restricted only to chronic *Sod2* deletion and not acute *Sod2* deletion, we hypothesized that alterations responsible for impaired mitochondrial bioenergetics should also be limited only to CKSOD2 cancer cell lines.

IV.1.3. *SOD2* DEFICIENT CANCER CELL LINES DISPLAY INCREASED AMPK ACTIVATION.

AMP-activated protein kinase (AMPK) acts as a sophisticated sensory system for the detection of energetic and oxidative stress [80]. AMPK is a heterotrimeric complex consisting of an alpha-subunit (catalytic) and two other regulatory subunits beta and gamma. The alpha subunit is reported to consist of the kinase domain (residue Thr172), which upon phosphorylation by an upstream kinase results in the activation of AMPK signaling pathway [81]. AMPK signaling is reported to play diverse roles associated with bioenergetics such as regulating glycolysis, oxidative phosphorylation, mitochondrial biogenesis, morphology of mitochondrial network, and mitochondrial quality control [82, 83, 84, 85]. Considering the hypothesis of impaired mitochondrial activity with chronic Sod2 deficient cancer cell lines (CKSOD2), the activation status of AMPK was investigated. Both acute and chronic Sod2 deficient cancer cell lines (CKΔSOD2 and CKSOD2) show increased (relative to CK cancer cell lines (or) *Sod2* proficient cell lines) phosphorylation of AMP-activated protein kinase alpha subunit (AMPKa) at Thr172. This indicates that AMPK activation is one of the immediate effects of *Sod2* absence.

As mentioned earlier about energetic stress and oxidative stress activating AMPK, it has also been shown that mitochondria-derived ROS (H_2O_2 in particular) activates

AMPK [86]. To this end, H_2O_2 was added exogenously to cancer cell lines (CK, CKΔSOD2, and CKSOD2) and then monitored the phosphorylation levels of AMPK. We observed no considerable changes in AMPK activation status upon H_2O_2 treatment in any of the cancer cell lines. To better understand the influence of H_2O_2 on AMPK activation, studying the effect of catalase on AMPK activation would give a clearer picture on the role of H_2O_2 [134]. Hence, the role and presence of H_2O_2 in AMPK activation in *Sod2* deficient cancer cell lines is still yet to be explored thoroughly. As we have observed earlier that SOD mimetic (MnTBAP) rescues the impaired survival in galactose, we then checked if mechanistic and functional complementation of SOD activity with MnTBAP in *Sod2* deficient cancer cell lines influences or reverses AMPK activation. To this end, cancer cell lines (CK, CKΔSOD2, and CKSOD2) were treated with MnTBAP and the expression levels of phosphorylated AMPK in cancer cell lines were determined. This transient complementation of SOD activity by MnTBAP leads to a decrease in AMPK activation. This confirmed that AMPK activation observed is a direct result of loss of superoxide dismutase activity in *Sod2* deficient cancer cell lines.

IV.1.4. Impaired respiratory reserve capacity with chronic *Sod2* deficiency despite increased basal respiration.

Cellular respiratory profiles obtained from seahorse measurements (OCR and ECAR) provide insight into mitochondrial bioenergetics and glycolytic capacity of cells [87]. Here we report a considerable increase in basal oxygen consumption rate observed with *Sod2* deficient cancer cell lines (chronic *Sod2* deficient in particular). However, upon stimulating electron transport chain to function at maximum capacity with an uncoupling agent CCCP, we observe that chronic *Sod2* deficient cancer cell lines (CKSOD2) do not increase their oxygen consumption rate as much as control CK cancer cell lines and acute *Sod2* deficient cancer cell lines (CKΔSOD2). It can also be observed that proton leak-linked respiration is considerably increased with CKSOD2 cancer cell lines, which can be hypothesized as an increased internal uncoupling activity with CKSOD2 cancer cell lines, as means for ROS scavenging. It has been reported earlier that increased ROS levels can result in mitochondrial dysfunction, which can manifest as impaired respiratory reserve capacity [88] and also our group has previously reported about an increase in ROS levels with

CKSOD2 cancer cell lines [77]. These findings suggest that the impaired respiratory reserve capacity observed with CKSOD2 cancer cell lines point in the direction of impaired mitochondrial bioenergetics associated with chronic *Sod2* deficiency. We also observe an increase in ECAR rates with CKSOD2 cancer cell lines, suggesting increased glycolysis dependence due to impaired mitochondrial bioenergetics. However, the same does not hold true for acute *Sod2* deficient cancer cell lines (CKΔSOD2). In fact, we see a slight increase in maximal respiration with CKΔSOD2 cancer cell lines, suggesting a convenient switch or reliance on electron transport chain activity and hence, a convenient reliance on oxidative phosphorylation. We also report a slight increase in ATP-linked respiration in CKΔSOD2 cancer cell lines (relative to CK and CKSOD2 cancer cell lines), further corroborating the theory of reliance or a convenient switch to oxidative phosphorylation with *Sod2* (acute) deficiency.

To investigate further into mitochondrial bioenergetics differences with control (CK), acute *Sod2* deficient (CKΔSOD2), and chronic *Sod2* deficient (CKSOD2) cancer cell lines. ATP turnover/production from glycolysis, mitochondria (oxidative phosphorylation), and total ATP turnover were evaluated from OCR and ECAR data. We report that there are not significant differences in the total ATP produced across the 3 genotypes. However, there is a significant increase in ATP produced through oxidative phosphorylation (OXPHOS) with acute *Sod2* deficient (CKΔSOD2) cancer cell lines (relative to CK cancer cell lines). Also, a significant amount of ATP contribution from glycolysis with chronic *Sod2* deficient (CKSOD2) cancer cell lines can be observed. This supports the theory that *Sod2* deletion results in an increased reliance on oxidative phosphorylation (OXPHOS) but chronic *Sod2* deficiency results in enhanced glycolytic dependency, possibly a result of an insult to mitochondrial bioenergetics. Comparable levels of total ATP produced across genotypes also suggests that the AMPK activation observed with *Sod2* deficiency could be independent of energy balance (ATP:ADP) but a result of oxidative signaling (ROS) in *Sod2* deleted cancer cell lines. This theory is further supported by the reversal of AMPK activation upon transient complementation of SOD activity with MnTBAP in *Sod2* absent cancer cell lines.

IV.1.5. Acute *Sod2* deficiency results in an increased dependence on oxidative phosphorylation but chronic Sod2 deletion enhances glycolytic dependency.

To better understand the shift in energy production of cancer cell lines upon *Sod2* deletion, we observed the sensitivity and tolerance levels of cancer cell lines to glycolysis suppression. Glycolysis inhibition/ suppression was achieved through treatment of cancer cell lines with a selective inhibitor of glucose transporter 1 (GLUT1) called WZB117. Efficiency of WZB117 in selectively repressing GLUT1 and hence, glycolysis is well established [89]. It has also been established in cancer cell line models that the inhibition of glycolysis forces the cells to shift towards oxidative phosphorylation in a mitochondrial metabolism-dependent fashion [90]. CK and CKSOD cancer cell lines display comparable levels of sensitivity or tolerance to glycolysis inhibition/GLUT1 inhibition. Interestingly, CKΔSOD2 (acute *Sod2* deficiency) cancer cell lines showed increased tolerance to glycolysis inhibition. This finding serves as a direct evidence for the theory that *Sod2* deletion results in a metabolic switch by increasing their reliance on mitochondrial oxidative phosphorylation. Potential dysfunction of mitochondrial bioenergetics in chronic *Sod2* deficient cancer cell lines (CKSOD2) could explain the absence of tolerance to GLUT1 inhibition with CKSOD2 cell lines and the increased contribution from glycolysis reported earlier.

Myc expression and regulation is reported to be an important factor in controlling metabolic pathways in a variety of cancers and is reported as one of the most frequently altered oncoproteins, despite almost never found to be mutated, that regulates a plethora of energy (ATP) related activities such as glycolysis, glutaminolysis, and oxidative phosphorylation. Thus, it is commonly considered that Myc-mediated metabolic differences are commonly a result of quantitative differences in Myc expression [91, 92, 93, 94, 95, 96]. We observed Myc (c-Myc) expression level differences in control CK, acute *Sod2* deficient (CKΔSOD2), and chronic *Sod2* deficient (CKSOD2) cancer cell lines. CKΔSOD2 cancer cell lines show increased expression levels of the c-Myc protein and contrastingly in CKSOD2 cancer cell lines, c-Myc expression levels are decreased drastically. This contrasting expression

patterns in c-Myc between CKΔSOD2 and CKSOD2 cancer cell lines becomes relevant in the context of the different metabolic profiles observed between the two different types of *Sod2* deleted cancer cell lines (acute and chronic). c-Myc, a transcription factor, is also reported to influence and regulate mitochondrial biogenesis and mitochondrial structural integrity [97]. This makes us consider that the contrasting Myc expression patterns between CKΔSOD2 and CKSOD2 cancer cell lines might be the key difference in mediating the vastly different metabolic pathways observed between the acute and chronic *Sod2* deletion. This supports the theory that even though *Sod2* deficiency favours oxidative phosphorylation (as observed in CKΔSOD2 cancer cell lines), deregulated Myc expression with chronic *Sod2* deficiency could result in defective mitochondrial bioenergetics causing a switch to glycolysis in CKSOD2 cancer cell lines. It has also been reported that c-Myc suppression leads to activation of AMPK in leukemia cells [98]. This finding is consistent with the observation of high levels of phosphorylated AMPK in chronic *Sod2* deficient (CKSOD2) cancer cell lines. However, it does not explain the AMPK activation observed with acute *Sod2* deficient (CKΔSOD2) cancer cell lines. AMPK activation observed in CKΔSOD2 cancer cell lines supports our hypothesis of AMPK activation as an immediate effect of *Sod2* loss and potentially serving as an upstream regulator of Myc-mediated regulation of metabolism and bioenergetics. All these findings indicate a strong and an intricate relationship between SOD2 and c-Myc, with the possibility of Myc being an important regulator of *Sod2* deficient phenotype.

IV.1.6. Complex II/ Succinate dehydrogenase (SDH), a key player responsible for impaired mitochondrial bioenergetics observed with Chronic *Sod2* deficiency.

Electron transport chain (ETC) in the mitochondria comprises of 5 complexes: complex I, complex II, complex III, complex IV, and complex V (ATP synthase). It also includes ubiquinone and cytochrome C as electron carriers/transporters. Two electron transport pathways are reported with the ETC. Complex I/III/IV, with NADH as substrate and complex II/III/IV, with succinic acid as the substrate and $FADH_2$ as cofactor. Complex V acts as the ATP synthase which produces energy (ATP) by using the energy accumulated in the proton gradient across the inner membrane,

which is formed as a result of coupling the electron transfer with proton shuttling (across the inner membrane). During this process, some electrons are directly transported to oxygen (O_2) yielding superoxide (O_2^-) and other reactive oxygen species (ROS). This makes mitochondria as the main source of cellular ROS. A total of 11 sites in the mitochondria (ETC pathway) have been reported to be involved in the generation of superoxide (O_2^-) [99, 100, 101, 102]. Considering the relevance of oxidative phosphorylation and mitochondrial bioenergetics in *Sod2* proficient and deficient pancreatic cancer cell lines, functionality of electron transport chain (ETC) complexes and mitochondria becomes crucial. We observe a significant, but a transient, decrease in the expression levels of complex II with chronic *Sod2* deficient cancer cell lines (CKSOD2). Complementation of SOD activity with MnTBAP results in a time-dependent restoration of complex II expression in CKSOD2 cancer cell lines. This MnTBAP-mediated restoration of complex II expression parallels with the effect of MnTBAP in rescuing CKSOD2 cancer cell lines in galactose (as means to enhance their mitochondrial bioenergetics). Complex II expression restoration also suggests that the loss of complex II expression is transient and reversible. Indicating that the loss of complex II expression is more of an activity loss than a genetic deficiency. It also opens the possibility of the role of complex II in mediating the proposed impaired mitochondrial functionality with chronic *Sod2* deficient (CKSOD2) cancer cell lines.

Complex II, which includes, succinate dehydrogenase (SDH) is involved in both the tricarboxylic acid (TCA) cycle and the electron transport chain (ETC). Thus, serving as a crucial nexus between metabolism and oxidative phosphorylation (OXPHOS) [102, 103]. As a part of the TCA cycle, enzymatic activity of succinate dehydrogenase in complex II catalyzes the conversion of succinate to fumarate (an oxidation reaction). In the electron transport chain, complex II serves as an entry point to incoming electrons and transfers them from succinate to ubiquinone. This electron donation happens is mediated by the iron-sulfur (FeS) clusters present in complex II. Complex II is comprised of four subunits: 2 subunits responsible for anchoring the complex to the inner membrane and containing the ubiquinone binding site. The other two subunits are present in the mitochondrial matrix and contain the binding sites for succinate, three FeS clusters, and FAD bound flavoprotein [102,

103, 104, 105]. The presence of FeS clusters in complex II is what we consider to be the determining factor in complex II expression differences and complex II affecting mitochondrial functionality. Iron-sulfur (FeS) clusters are versatile groups reported to be present in a variety of enzymes. It can function as electron transfer groups as observed in complex II and as enzymatic activity determining factors in enzymes by regulating substrate binding. It has also been proposed that FeS clusters are vulnerable and sensitive to oxidation by reactive oxygen species (ROS) such as superoxide (O_2^-). Hence, cellular systems that have increased levels of ROS can target enzymes containing FeS clusters resulting in damage and disaasembly of FeS clusters, rendenring the enzyme/protein inactive [106].

In chronic *Sod2* deficient (CKSOD2) cancer cell lines, we have previously reported elevated levels of reactive oxygen species (ROS) and superoxide (O_2^-) [77]. Hence, we propose that in the case of CKSOD2 cancer cell lines, ROS-mediated damage of FeS clusters results in rendering succinate dehydrogenase (complex II) inactive. The loss of expression in succinate dehydrogenase could be a result of degradation of the enzyme due to disassembly of FeS clusters and loss of functionality. This also explains the restoration of complex II expression by MnTBAP because MnTBAP shares the same mechanism of action in superoxide scavenging as SOD. Malonate/Malonic acid competes with succinate in binding to succinate dehydrogenase and once bound, blocks the enzymatic conversion of succinate to fumarate [107]. We observed that treatment of control cancer cell lines (CK) and acute *Sod2* deficient (CKΔSOD2) with malonate results in an impaired survival in galactose of both CK and CKΔSOD2 cancer cell lines, similar to galactose survival phenotype of chronic *Sod2* deficient (CKSOD2) cancer cell lines (data not shown). This further validates the enzymatic function of complex II/succinate dehydrogenase in influencing mitochondrial functionality and the lack of it in CKSOD2 cancer cell lines.

IV.1.7. CHRONIC *SOD2* LOSS RESULTS IN DAMAGED MITOCHONDRIA.

Transmission electron microscopy (TEM) is a well-established technique that helps in visualizing the structure of mitochondria and the dynamic alterations mitochondria undergo [108]. Mitochondria are double membrane-bound dynamic organelles, which are involved in energy (ATP) production and coordinate a variety of cellular functions. The outer mitochondrial membrane is involved in sensing and importing nuclear-encoded proteins and mediates communication with other cytoplasmic organelles. The inner mitochondrial membrane encompasses a region called mitochondrial matrix, which comprises of mitochondrial DNA and a huge range of enzymes that are crucial to mitochondrial function, bioenergetics, and biogenesis [109, 110]. The topology of mitochondria is primarily mediated by the dynamic alterations to the inner mitochondrial membrane. The outer mitochondrial membrane is not commonly known to display such dynamic alterations except providing a boundary to the organelle. The most reported aspect of mitochondrial dynamics is the change in size of the organelle, presenting either as a spherical giant (also referred to as "mitochondrial swelling") or fragmented/small mitochondria. Such mitochondrial dynamics are controlled and regulated by processes known as mitochondrial fission and fusion [111, 112, 113]. A "normal" or "text-book" mitochondrial structure visualized through electron microscopy includes a limiting membrane, mitochondrial matrix, and cristae structures (appear as internal ridges) that occur in series within which they appear to be parallel to each other at regular intervals [114]. Alterations to mitochondrial structure that result in "mitochondrial swelling" and fragmented mitochondria represent damaged or dysfunctional mitochondria. Mitochondrial damage in cells is seen in physiological disease states such as tissue injury, infection, aging, neurodegenration, carcinogenesis, and oxidative damage. Physiologic disease states mentioned have been reported to disrupt mitochondrial integrity through the damaging effects of reactive oxygen species (ROS) [115, 116, 117].

From visualizing the ultrastructure of mitochondria of CK, CKΔSOD2, and CKSOD2 cancer cell lines using electron microscopy, it can be seen that control (CK) cancer cell lines contain mitochondrial structures with well-defined boundaries and intact cristae structures, that could be categorized as "normal" mitochondrial structures. In

the case of acute *Sod2* deficient (CKΔSOD2) cancer cell lines, we observe a slight increase in size of mitochondria ("Partial swelling") and partial loss of cristae structures ("cristaelysis"). However, it could not be categorised as damaged or dysfunctional mitochondria as some structural features are still comparable to mitochondrial features observed with control CK cancer cell lines. In chronic *Sod2* deficient (CKSOD2) cancer cell lines, we report damaged and dysfunctional mitochondria. The damage to mitochondria is observed as "swollen mitochondria" and through complete loss or absence of cristae structures ("cristaelysis") in CKSOD2 cancer cell lines. These observations provide conclusive evidence to support the theory of mitochondrial damage associated with chronic *Sod2* deficiency. This reported dysfunctional mitochondria correlates with the loss of complex II in CKSOD2 cancer cell lines. This also explains the enhanced glycolysis rates, in CKSOD2 cancer cell lines, despite *Sod2* deficiency pushing cancer cell lines towards oxidative phosphorylation (as theorized from observations in CKΔSOD2 cancer cell lines).

IV.2. UNDERSTANDING THE ROLE OF *REG3B* HELPS ILLUMINATING THE INFLUENCE OF ANIMICROBIAL PROTEINS IN PDAC CARCINOGENESIS.

IV.2.1. *REG3B* DEFICIENT MICE HAVE INCREASED PRECANCEROUS ADM LESION, DESPITE AN UNCHANGED *IN VITRO* ADM FORMING CAPACITY OF *REG3B* DEFICIENT ACINAR CELLS.

Studying acinar-to-ductal metaplasia (ADM) is reported to serve as a good approach in understanding PDAC initiation and carcinogenesis. ADM is commonly reported in pancreatitis and pancreatic regeneration after tissue injury [118, 119]. Exogenous addition of TGFa to collagen-embedded acinar explants is a well-established approach to study *in vitro* ADM and hence, PDAC initiation [120]. To understand the *Reg3b*-mediated changes during ADM, acinar explants from *Reg3b* deleted (Reg3b-/-) and wild-type (WT) mice were used. Acinar explants were treated with TGFa to induce *in vitro* ADM and additionally, recombinant Reg3b protein was added to study effects of Reg3b complementation in *Reg3b* deleted acini. We observed that the basal transdifferentiation potential and TGFa-induced transdifferentiation are comparable between control (WT) and knockout acini (Reg3b-/-). Addition of recombinant Reg3b protein also had comparable effects on WT and *Reg3b* deficient acinar explants. This suggests that *Reg3b* deletion does not have any cell-autonomous effects in modulating *in vitro* ADM. As a next step, *Reg3b* deleted (Whole-body deletion) mice were combined with an oncogenic pancreas ($Kras^{G12D/+}$) mouse model to understand the function of *Reg3b* in the context of PDAC carcinogenesis. This approach yielded us $Kras^{G12D/+}$ (CK) and $Kras^{G12D/+}$; Reg3b-/- (CKReg3b) mice. To study *in vivo* ADM, histological features of pancreata of 12-week-old CK and CKReg3b mice were observed. Contrary to *in vitro* ADM findings between WT and Reg3b-/- mice, there was a significant increase of *in vivo* ADM lesions observed with 12-week-old Reg3b deficient (CKReg3b) mice.

Macrophage infiltration is a good indicator for inflammation in experimental pancreatitis models [121]. F4/80 is an established marker for macrophages and helps in identifying populations of tissue-resident and infiltrated macrophages [122]. Inflammatory state of the pancreas because of tissue injury, pancreatitis, and an

oncogenic pancreas is often characterized by the presence of ADM lesions. Since, we report increased presence of ADM lesions in 12-week-old CKReg3b mice, we wanted to evaluate the inflammatory status of the pancreas by tracking the number of infiltrated macrophages. To this end, immunohistochemistry (IHC) technique was employed to monitor the differences in F4/80 expression differences, which we used to quantify the differences in abundance of macrophage populations between 12-week-old CK and CKReg3b mice. We observed that there is an increased trend in the number of F4/80 positve cells in 12-week-old CKReg3b pancreas (relative to CK). This indicates an inflamed pancreas observed with 12-week-old CKReg3b mice. Considering that *Reg3b* deleted acini do not display cell-autonomous effects in *in vitro* ADM and the increase of *in vivo* ADM in 12-week-old *Reg3b* deleted mice, we hypothesize that *Reg3b* deletion causes external (non-cell-autonomous) factors are involved in exacerbating precancerous ADM in an oncogenic pancreas.

IV.2.2. Antimicrobial Reg3b appears to regulate other Reg-family antimicrobial proteins.

Reg3b is often associated and reported to be elevated during pancreatitis, hence the other name pancreatitis-associated protein 1 (PAP1). It has also been found to function as an antimicrobial protein in conjunction with other Reg family proteins with bactericidal functions [123, 124]. Reg proteins were initially discovered in regenerating islets and categorized into the family of C-type lectins Reg family members have been discovered independently and grouped into 4 categories (Reg1, Reg2, Reg3, and Reg4) based on the structures of their sequence homology [64, 66, 125, 126, 127, 128]. The Reg3 family has been given the attention considering its varied roles (in multiple organs) including participation during pancreatic regeneration after injury, elevated levels of Reg3 proteins during pancreatitis, and the role as an antimicrobial protein in the intestine with bactericidal properties [129, 130]. Reg3 proteins, Reg3b and Reg3g particularly, have been implicated to play a crucial role in maintaining the integrity of the intestinal membrane and inhibiting bacterial translocation from the gut to distal organs. It has been reported that chronic alcohol (ethanol) administration results in specific inhibition of Reg3b and Reg3g. Loss of antimicrobial Reg3 activity as a result of chronic alcohol administration has been

reported to exacerbate alcohol induced steatohepatitis and also result in a state of enteric dysbiosis [131, 132]. This illuminates the importance of Reg3 family proteins in maintaining intestinal membrane integrity and inhibiting bacterial translocation from intestine to other organs. From 12-week-old *Reg3b* deficient oncogenic pancreas (CKReg3b), we observed that mRNA expression levels of other *Reg* family genes (*Reg2, Reg3a, Reg3g, Reg3d*, and *Reg4*) are significantly downregulated relative to control (CK) pancreas. This hints towards the possibility of *Reg3b* being a central regulator of other *Reg* family genes, which has not been previously reported.

IV.2.3. *REG3B* MEDIATED BACTERIAL TRANSLOCATION TO THE PANCREAS ACCELERATES THE FORMATION OF PRECANCEROUS ADM LESIONS.

On comparing the findings from the literature and the observations with CKReg3b mice, we hypothesized that whole body deletion of *Reg3b* results in disruption of intestinal barriers to bacterial translocation and as a result, we observe increased ADM formation aided by the translocated microbial load in *Reg3b* deificient pancreas. As an intial step to validate presence of microbes in the pancreas due to translocation from the intestine, we evaluated the total pancreatic microbial load (measured as concentration of total 16S rRNA). We observed a slight increase in total 16S rRNA concentration in *Reg3b* deficient non-oncogenic pancreas (Reg3b-/- or Reg3bΔ/Δ). However, this increased total 16S load does not translate to *Reg3b* deficient oncogenic pancreas (CKReg3b). We also confirmed the presence of bacteria in the pancreas of *Reg3b* proficient and *Reg3b* deficient mice by inoculating pancreatic homogenates in blood agar plates and detected growth of bacterial colonies in plates containing pancreatic homogenates (data not shown). Since, estimation of total 16S rRNA concentration from the pancreas can only confirm the presence of bacteria but not information about diversity of the species present. We wanted to understand the differences in the diversity of species between *Reg3b* proficient and *Reg3b* deficient intenstine and pancreas. To this end, we performed 16S rRNA sequencing from the faeces and pancreas of 12-week-old *Reg3b* proficient (WT, CK) and *Reg3b* deficient (Reg3b-/-, CKReg3b) mice. Estimation of alpha diversity is a good approach to look at the diversity of species within a microbial ecosystem [133]. As an exploratory approach, we estimated the alpha diversity (Observed_Species) within faeces and pancreas samples from 12-week-old *Reg3b*

proficient and *Reg3b* deficient mice, we report a significant increase in diversity of observed species in faecal samples of *Reg3b* deficient (Reg3b-/-, CKReg3b) mice. However, the diversity of observed species from pancreas samples shows no considerable difference between *Reg3b* proficient and deficient mice. Further analysis about the microbiome of *Reg3b* proficient and deficient mice is needed to understand microbe-mediated exacerbation of precancerous ADM upon *Reg3b* deficiency. The overall increase in alpha diversity in faecal samples upon *Reg3b* deficiency indicates that absence of antimicrobial Reg3 family proteins results in an increased microbial diversity. However, the increased alpha diversity is not observed in *Reg3b* deficient pancreas. Hence, this warrants further investigation into testing the hypothesis of increased bacterial bacterial translocation from intestine to pancreas, as a result of loss of *Reg3b*.

IV.2.4. Future implications of *Reg3b*-mediated control of microbial translocation and the influence of translocated microbes on PDAC carcinogenesis.

We have now obtained preliminary information about microbiota (such as alpha diversity) from faecal and pancreas samples of 12-week-old *Reg3b* proficient and deficient mice. As a next step, we will further analyse the 16S rRNA sequencing results to obtain information about the microbial composition differences upon *Reg3b* deletion. It has been reported that Reg3b can exhibit bactericidal properties specifically on gram-negative bacteria [130]. Hence, as a next step we will use a more targeted approach to estimate the differences in abundance of gram-negative bacterial species between *Reg3b* proficient and deficient mice.

As the understanding about the protective function of *Reg3b* during PDAC initiation is still limited, it can be seen here that the continuation of research into the role of *Reg3b* during carcinogenesis is of increasing importance, especially regarding its early protective role and how it translates to tumour incidence. It must also be noted here that we have provided evidence only for the presence of microbes in the pancreas and not direct evidence for translocation of microbes from gut to pancreas. Hence, the next step involves testing the proposed bacterial translocation hypothesis

(from intestine to pancreas). To this end, we have initiated a novel mouse model exhibiting *Reg3b* deletion specific to intestine and/or oncogenic pancreas (floxed alleles of *Reg3b*). This would help us elucidate the relationship between intestinal microbial defense system and PDAC initiation.

V. Conclusion

We have established a novel approach in understanding the role of oxidative signaling and intestinal antimicrobial peptides in PDAC biology, and initiation. Studying acute and chronic *Sod2* deficient cancer cell lines has now been shown to be an elegant system in understanding the dynamic nature of oxidative signaling in modulating pancreatic cancer biology. Correlating our study of *Sod2* modulated cancer cell lines and the low tumour incidence observed with *Sod2* deficient oncogenic pancreas, we prove that oxidative signaling-mediated changes in mitochondrial bioenergetics determine the progression of PDAC and tumourigenicity of PDAC cancer cell lines.

Previous studies have reported that *Reg3b* deletion can suppress the formation of precancerous ADM in an oncogenic pancreas. Here, we report that non-pancreatic effects mediated by whole body *Reg3b* deletion accelerates ADM formation in an oncogenic pancreas. Our proposal of the influence of gut microbial population on distal organ carcinogenesis is a relatively new concept with very little insight. The present thesis reports a critical role that *Reg3b* might have in maintaining gut microbial homeostasis. Our study also shows that *Reg3b* could be a determining factor in controlling the expression of other antimicrobial *Reg* family genes. However, it must be noted with caution that we have provided evidence only for the presence of microbes in the pancreas and further investigation is needed to provide any proof that *Reg3b* regulates gut microbial homeostasis and is involved in the regulation of microbial translocation from gut to the pancreas.

VI. References

1. Daniel S. Longnecker. (1982) Pathology and Pathogenesis of Diseases of the Pancreas, TEACHING MONOGRAPH, From the Department of Pathology, Dartmouth Medical School, Hanover, New Hampshire, The American Journal of Pathology.

2. OpenStax College. Anatomy & Physiology, Chapter 17.9 The Endocrine Pancreas, Figure 1 2016 [17.9 The Endocrine Pancreas]. Available from: https://legacy.cnx.org/content/col11496/1.8/.

3. Cruickshank, A.H. and Benbow, E.W. (1995) Pathology of the Pancreas, Springer London, London.

4. Rovasio, R.A. (2010) Development and Structure of the Pancreas, in Pancreatic cancer (eds J. Neoptolemos, R. Urrutia, J.L. Abbruzzese, M.W. Büchler), Springer, New York, London, pp. 27-38.

5. American Diabetes Association (2011). Diagnosis and classification of diabetes mellitus. Diabetes care, 34 Suppl 1(Suppl 1), S62–S69. https://doi.org/10.2337/dc11-S062

6. Sarner M and Cotton PB (1984). Classification of pancreatitis. Gut, 25, 756-759. http://gut.bmj.com/ .

7. Pishvaian MJ, Brody JR (2017). Therapeutic Implications of Molecular Subtyping for Pancreatic Cancer. Oncology (Williston Park). 31 (3): 159–66, 168.

8. Anirban Maitra and Ralph H. Hruban (2008). Pancreatic Cancer. Annu. Rev. Pathol. Mech. Dis. 2008.3:157-188. Downloaded from www.annualreviews.org.

9. Ester Royenblum, Mieke Schutte, Michael Goggins, Stephan A. Hahn, Shawn Panzer, Marianna Zahurak, Steven N. Goodman, Taylor A. Sohn, Ralph H. Hruban, Charles J. Yeo and Scott E. Kern (1997). Cancer Research. (57) (9) 1731-1734.

10. Klimstra, D. S. and Longnecker, D. S (1994). K-ras mutations in pancreatic ductal proliferative lesions. The American Journal of Pathology. 145, 1547–1550.

11. Shields, J. M., Pruitt, K., McFall, A., Shaub, A. and Der, C. J. (2000). Understanding Ras: 'it ain't over 'til it's over'. Trends Cell Biology. 10, 147–154.

12. Maitra A, Kern SE, Hruban RH. (2006). Molecular pathogenesis of pancreatic cancer. Best Pract. Res. Clin. Gastroenterol. 20:211–26.

13. Maitra A, Fukushima N, Takaori K, Hruban RH. (2005). Precursors to invasive pancreatic cancer. Adv. Anat. Pathol. 12:81–91.

14. Giulio Riva, Antonio Pea, Camilla Pilati, Giulia Fiadone, Rita Teresa Lawlor, Aldo Scarpa, Claudio Luchini (2018). Histo-molecular oncogenesis of pancreatic cancer: From precancerous lesions to invasive ductal adenocarcinoma. World J Gastrointest Oncol. 10(10): 317-327.

15. Hruban RH, Adsay NV, Albores-Saavedra J, Compton C, Garrett ES, Goodman SN, Kern SE, Klimstra DS, Klöppel G, Longnecker DS, Lüttges J, Offerhaus GJ (2001). Pancreatic intraepithelial neoplasia: a new nomenclature and classification system for pancreatic duct lesions. Am J Surg Pathol. 25: 579-586.

16. Basturk O, Hong SM, Wood LD, Adsay NV, Albores-Saavedra J, Biankin AV, Brosens LA, Fukushima N, Goggins M, Hruban RH, Kato Y, Klimstra DS, Klöppel G, Krasinskas A, Longnecker DS, Matthaei H, Offerhaus GJ, Shimizu M, Takaori K, Terris B, Yachida S, Esposito I, Furukawa T (2015). Baltimore Consensus Meeting. A Revised Classification System and Recommendations from the Baltimore Consensus Meeting for Neoplastic Precursor Lesions in the Pancreas. Am J Surg Pathol. 39:1730-1741.

17. Klimstra DS, Longnecker DS (1994). K-ras mutations in pancreatic ductal proliferative lesions. Am J Pathol. 45: 1547-1550.

18. Lemoine NR, Jain S, Hughes CM, Staddon SL, Maillet B, Hall PA, Klöppel G (1992). K-ras oncogene activation in preinvasive pancreatic cancer. Gastroenterology.102: 230-236.

19. Wu J, Jiao Y, Dal Molin M, Maitra A, de Wilde RF, Wood LD, Eshleman JR, Goggins MG, Wolfgang CL, Canto MI, Schulick RD, Edil BH, Choti MA, Adsay V, Klimstra DS, Offerhaus GJ, Klein AP, Kopelovich L, Carter H, Karchin R, Allen PJ, Schmidt CM, Naito Y, Diaz LA Jr, Kinzler KW, Papadopoulos N, Hruban RH, Vogelstein B (2011). Whole-exome sequencing of neoplastic cysts of the pancreas reveals recurrent mutations in components of ubiquitin-dependent pathways. Proc Natl Acad Sci USA. 108: 21188-21193.

20. Yamaguchi J, Yokoyama Y, Kokuryo T, Ebata T, Nagino M. Cells of origin of pancreatic neoplasms (2018). Surg Today. 48: 9-17.

21. Yamaguchi J, Mino-Kenudson M, Liss AS, Chowdhury S, Wang TC, Fernández-Del Castillo C, Lillemoe KD, Warshaw AL, Thayer SP (2016). Loss of Trefoil Factor 2 From Pancreatic Duct Glands Promotes Formation of Intraductal Papillary Mucinous Neoplasms in Mice. Gastroenterology. 151: 1232-1244.e10.

22. Nicolas Chuvin, David F. Vincent, Roxane M. Pommier, Lindsay B. Alcaraz, Johann Gout, Cassandre Caligaris, Karam Yacoub, Victoire Cardot, Elodie Roger, Bastien Kaniewski, Sylvie Martel, Celia Cintas, Sophie Goddard-Léon, Amélie Colombe, Julie Valantin, Nicolas Gadot, Emilie Servoz, Jennifer Morton, Isabelle Goddard, Anne Couvelard, Vinciane Rebours, Julie Guillermet, Owen J. Sansom, Isabelle Treilleux, Ulrich Valcourt, Stéphanie Sentis, Pierre Dubus, and Laurent Bartholin (2017). Acinar-to-Ductal Metaplasia Induced by Transforming Growth Factor Beta Facilitates $KRAS^{G12D}$-driven Pancreatic Tumorigenesis. Cellular and Molecular Gastroenterology and Hepatology Vol. 4, No. 2.

23. Lowenfels, A.B.; Maisonneuve, P.; Cavallini, G.; Ammann, R.W.; Lankisch, P.G.; Andersen, J.R.; Dimagno, E.P.; Andren-Sandberg, A.; Domellof, L (1993). Pancreatitis and the risk of pancreatic cancer. International Pancreatitis Study Group. N. Engl. J. Med. 328, 1433–1437.

24. Chari, S.T.; Leibson, C.L.; Rabe, K.G.; Timmons, L.J.; Ransom, J.; de Andrade, M.; Petersen, G.M (2008). Pancreatic cancer-associated diabetes mellitus: Prevalence and temporal association with diagnosis of cancer. Gastroenterology 134, 95–101.

25. Maisonneuve, P.; Lowenfels, A.B (2015). Risk factors for pancreatic cancer: A summary review of meta-analytical studies. Int. J. Epidemiol. 44, 186–198. J. Clin. Med. 6, 29 11 of 16.

26. Yeo, T.P (2015). Demographics, epidemiology, and inheritance of pancreatic ductal adenocarcinoma. Semin. Oncol. 42, 8–18.

27. F. Ann Ran, Patrick D. Hsu, Chie-Yu Lin, Jonathan S. Gootenberg, Silvana Konermann, Alexandro Trevino, David A. Scott, Azusa Inoue, Shogo Matoba, Yi Zhang, Feng Zhang (2013). Double nicking by RNA-guided CRISPR Cas9 for enhanced genome editing specificity. Cell. 154(6): 1380–1389.

28. Frezza C, Cipolat S, Scorrano L (2007). Organelle isolation: functional mitochondria from mouse liver, muscle and cultured fibroblasts. Nat Protoc. 2(2):287□295. doi:10.1038/nprot.2006.478.

29. T. Finkel (2011). Signal transduction by reactive oxygen species. J. Cell Biol. 194: 7-15.

30. Z.A. Wood, L.B. Poole, P.A. Karplus (2003). Peroxiredoxin evolution and the regulation of hydrogen peroxide signaling. Science. 300: 650-653.

31. P.J. Kiley, G. Storz (2004). Exploiting thiol modifications. PLoS Biol. 2 : 400.

32. Nathan, C (2003). Specificity of a third kind: reactive oxygen and nitrogen intermediates in cell signaling. J. Clin. Invest. 111: 769–778.

33. Winterbourn, C. C. & Metodiewa, D (1999). Reactivity of biologically important thiol compounds with superoxide and hydrogen peroxide. Free Radic. Biol. Med. 27: 322–328.

34. Imlay, J. A (2003). Pathways of oxidative damage. Annu. Rev. Microbiol. 57: 395–418.

35. Dizdaroglu M and Jaruga P (2012). Mechanisms of free radical-induced damage to DNA. Free Radic. Res. 46: 382-419.

36. Jixiang Zhang, Xiaoli Wang, Vikash Vikash, Qing Ye, Dandan Wu, Yulan Liu, and Weiguo Dong (2016). ROS and ROS-Mediated Cellular Signaling. Oxidative Medicine and Cellular Longevity. http://dx.doi.org/10.1155/2016/4350965.

37. Ratnam DV, Ankola DD, Bhardwaj V, Sahana DK, Kumar MN (2006). Role of antioxidants in prophylaxis and therapy: A pharmaceutical perspective. J Control Release. 113: 189-207.

38. He L, He T, Farrar S, Ji L, Liu T, Ma X (2017). Antioxidants Maintain Cellular Redox Homeostasis by Elimination of Reactive Oxygen Species. Cell Physiol Biochem . 44:532-553.

39. Christofidou-Solomidou M, Muzykantov VR (2006). Antioxidant strategies in respiratory medicine. Treat Respir Med. 5: 47-78.

40. He L, Eslamfam S, Ma X, Li D (2016). Autophagy and the nutritional signaling pathway. Front Agr Sci Eng. 3: 222-230.

41. Ma X, He P, Sun P, Han P (2010). Lipoic acid: an immunomodulator that attenuates glycinin-induced anaphylactic reactions in a rat model. J Agric Food Chem 2010. 58: 5086-5092.

42. Brigelius-Flohe R, Maiorino M (2013). Glutathione peroxidases. Biochim Biophys Acta. 1830: 3289-3303.

43. Margis R, Dunand C, Teixeira FK, Margis-Pinheiro M (2008). Glutathione peroxidase family- an evolutionary overview. FEBS J. 275: 3959-3970.

44. Han P, Ma X, Yin J (2010). The effects of lipoic acid on soybean beta-conglycinin-induced anaphylactic reactions in a rat model. Arch Anim Nutr. 64: 254-264.

45. Liu H, Zhang J, Zhang S, Yang F, Thacker PA, Zhang G, Qiao S, Ma X (2014). Oral administration of Lactobacillus fermentum I5007 favors intestinal development and alters the intestinal microbiota in formula-fed piglets. J Agric Food Chem. 62: 860-866.

46. Lu J, Holmgren A (2014). The thioredoxin antioxidant system. Free Radic Biol Med. 66: 75-87.

47. Argyrou A, Blanchard JS (2004). Flavoprotein disulfide reductases: advances in chemistry and function. Prog Nucleic Acid Res Mol Biol. 78: 89-142.

48. Holmgren A: Thioredoxin and glutaredoxin systems (1989). J Biol Chem 1989. 264: 13963-13966.

49. Sullivan LB, Chandel NS (2014). Mitochondrial reactive oxygen species and cancer. Cancer Metab. 2:17.

50. Chen Y, Zhang H, Zhou H, Ji W, Min W (2016). Mitochondrial Redox Signaling and Tumor Progression. Cancers (Basel). 8:40.

51. Han D, Canali R, Rettori D, Kaplowitz N (2003). Effect of glutathione depletion on sites and topology of superoxide and hydrogen peroxide production in mitochondria. Mol. Pharmacol. 64:1136–1144.

52. Miwa S, St-Pierre J, Partridge L, Brand MD (2003). Superoxide and hydrogen peroxide production by Drosophila mitochondria. Free Rad. Biol. Med. 35:938–948.

53. Lebovitz RM, Zhang H, Vogel H, Cartwright J Jr, Dionne L, Lu N, Huang S, Matzuk MM (1996). Neurodegeneration, myocardial injury, and perinatal death in mitochondrial superoxide dismutase deficient mice. Proc. Nat. Acad. Sci. USA. 93: 9782–9787.

54. Cullen J.J, Weydert C, Hinkhouse M.M, Ritchie J, Domann F.E, Spitz D, Oberley L.W (2003). The role of manganese superoxide dismutase in the growth of pancreatic adenocarcinoma. Cancer Res. 63: 1297–1303.

55. Weydert C, Roling B, Liu J, Hinkhouse M.M, Ritchie J.M, Oberley L.W, Cullen J.J (2003). Suppression of the malignant phenotype in human pancreatic cancer cells by the overexpression of manganese superoxide dismutase. Mol. Cancer Ther. 2: 361–369.

56. Zhou J, Du Y (2012). Acquisition of resistance of pancreatic cancer cells to 2-methoxyestradiol is associated with the upregulation of manganese superoxide dismutase. Mol. Cancer Res. 10: 768–777.

57. Fisher C.J, Goswami P.C (2008). Mitochondria-targeted antioxidant enzyme activity regulates radioresistance in human pancreatic cancer cells. Cancer Biol. Ther. 7: 1271–1279.

58. Patel G.K, Khan M.A, Bhardwaj A, Srivastava S.K, Zubair H, Patton M.C, Singh S, Khushman M, Singh A.P (2017). Exosomes confer chemoresistance to pancreatic cancer cells by promoting ROS detoxification and miR-155-mediated suppression of key gemcitabine-metabolising enzyme, DCK. Br. J. Cancer. 116: 609–619.

59. Kong X, Sun T, Kong F, Du Y, Li Z (2014). Chronic pancreatitis and pancreatic cancer. Gastrointest Tumors. 1: 123–134.

60. Carmen Guerra, Alberto J. Schuhmacher, Marta Canamero, Paul J. Grippo, Lena Verdaguer, Lucıa Perez-Gallego, Pierre Dubus, Eric P. Sandgren, Mariano Barbacid (2007). Chronic Pancreatitis Is Essential for Induction of Pancreatic Ductal Adenocarcinoma by K-Ras Oncogenes in Adult Mice. Cancer Cell. 11: 291–302.

61. Carmen Guerra, Manuel Collado, Carolina Navas, Alberto J. Schuhmacher, Isabel Hernandez-Porras, Marta Canamero, Manuel Rodriguez-Justo, Manuel Serrano, Mariano Barbacid (2011). Pancreatitis-Induced Inflammation Contributes to Pancreatic Cancer by Inhibiting Oncogene-Induced Senescence. Cancer Cell. 19: 728–739.

62. Sarles H, Dagorn JC, Giorgi D, Bernard JP (1990). Renaming pancreatic stone protein as 'lithostathine'. Gastroenterology. 99(3):900–901.

63. Bimmler D, Graf R, Scheele GA, Frick TW (1997). Pancreatic stone protein (lithostathine), a physiologically relevant pancreatic calcium carbonate crystal inhibitor? The Journal of biological chemistry. 272(5):3073–3082.

64. Terazono K, Yamamoto H, Takasawa S, Shiga K, Yonemura Y, Tochino Y, Okamoto H (1988). A novel gene activated in regenerating islets. The Journal of biological chemistry. 263(5):2111–2114.

65. Wu M, Neilson A, Swift AL, Moran R, Tamagnine J, et al. (2007). Multiparameter metabolic analysis reveals a close link between attenuated mitochondrial bioenergetic function and enhanced glycolysis dependency in human tumor cells. Am J Physiol Cell Physiol 292: C125–136.

66. Unno M, Yonekura H, Nakagawara K, Watanabe T, Miyashita H, Moriizumi S, Okamoto H, Itoh T, Teraoka H (1993). Structure, chromosomal localization, and expression of mouse reg genes, reg I and reg II. A novel type of reg gene, reg II exists in the mouse genome. The Journal of biological chemistry. 268(21):15974–15982.

67. Rafaeloff R, Pittenger GL, Barlow SW, Qin XF, Yan B, Rosenberg L, Duguid WP, Vinik AI (1997). Cloning and sequencing of the pancreatic islet neogenesis associated protein (INGAP) gene and its expression in islet neogenesis in hamsters. The Journal of clinical investigation. 99(9):2100– 2109.

68. Iovanna JL, Dagorn JC (2005). The multifunctional family of secreted proteins containing a C-type lectin like domain linked to a short N-terminal peptide. Biochimica et biophysica acta. 1723(1–3): 8–18.

69. Watanabe T, Yonekura H, Terazono K, Yamamoto H, Okamoto H (1990). Complete nucleotide sequence of human reg gene and its expression in normal and tumoral tissues. The reg protein, pancreatic stone protein, and pancreatic thread protein are one and the same product of the gene. The Journal of biological chemistry. 265(13):7432–7439.

70. Violette S, Festor E, Pandrea-Vasile I, Mitchell V, Adida C, Dussaulx E, Lacorte JM, Chambaz J, Lacasa M, Lesuffleur T (2003). Reg IV, a new member of the regenerating gene family, is overexpressed in colorectal carcinomas. Int J Cancer. 103(2):185–193.

71. Kimura N, Yonekura H, Okamoto H, Nagura H (1992). Expression of human regenerating gene mRNA and its product in normal and neoplastic human pancreas. Cancer. 70(7):1857–1863.

72. Bimmler D, Schiesser M, Perren A, Scheele G, Angst E, Meili S, Ammann R, Graf R (2004). Coordinate regulation of PSP/reg and PAP isoforms as a family of secretory stress proteins in an animal model of chronic pancreatitis. J Surg Res. 118(2):122–135.

73. Graf R, Schiesser M, Lussi A, Went P, Scheele GA, Bimmler D (2002). Coordinate regulation of secretory stress proteins (PSP/reg, PAP I, PAP II, PAP III) in the rat exocrine pancreas during experimental acute pancreatitis. J Surg Res. 105(2):136–144.

74. Cash HL, Whitham CV, Behrendt CL, Hooper LV (2006). Symbiotic bacteria direct expression of an intestinal bactericidal lectin. Science 313:1126–1130.

75. Lehotzky RE, Partch CL, Mukherjee S, Cash HL, Goldman WE, Gardner KH, Hooper LV (2010). Molecular basis for peptidoglycan recognition by a bactericidal lectin. Proc. Natl. Acad. Sci. U. S. A. **107**:7722–7727.

76. Hanh-Tu Lieu, Marie-Ther´ ese Simon, Thao Nguyen-Khoa, Messeret Kebede, Alexandre Cortes, Luis Tebar, Andrew J. H. Smith, Rosemary Bayne, Stephen P. Hunt, Christian Brechot, and Laurence Christa (2006). Reg2 Inactivation Increases Sensitivity to Fas Hepatotoxicity and Delays Liver Regeneration Post-hepatectomy in Mice. HEPATOLOGY, Vol. 44, No. 6: 1452-1464.

77. Ruoff C (2015). Role of Sod2 in Pancreatic Carcinogenesis. PhD thesis. TUM. Munich.

78. Weisiger RA, Fridovich I (1973). Mitochondrial superoxide dismutase. Journal of Biological Chemistry. 248(13): 4793–4796.

79. Marroquin LD, Hynes J, Dykens JA, Jamieson JD, Will Y (2007). Circumventing the Crabtree effect: replacing media glucose with galactose increases Galactose Effects on susceptibility of HepG2 cells to mitochondrial toxicants. Toxicol Sci 97: 539–547.

80. Auciello, F. R., Ross, F. A., Ikematsu, N., and Hardie, D. G (2014). Oxidative stress activates AMPK in cultured cells primarily by increasing cellular AMP and/or ADP. FEBS Lett. 588, 3361–3366.

81. Hudson ER, et al (2003). A novel domain in AMP-activated protein kinase causes glycogen storage bodies similar to those seen in hereditary cardiac arrhythmias. Curr Biol.13:861–866.

82. Zong H, et al (2002). AMP kinase is required for mitochondrial biogenesis in skeletal muscle in response to chronic energy deprivation. Proc Natl Acad Sci USA. 99:15983–15987.

83. Kishton et al. (2016). AMPK is essential to balance glycolysis and mitochondrial metabolism to control T-ALL cell stress and survival. Cell Metab. 23(4): 649–662. doi:10.1016/j.cmet.2016.03.008.

84. Zhang et al (2018). AMPK activation serves a critical role in mitochondria quality control via modulating mitophagy in the heart under chronic hypoxia. international journal of molecular medicine 41: 69-76.

85. Chen, Z. et al (2019). Global phosphoproteomic analysis reveals ARMC10 as an AMPK substrate that regulates mitochondrial dynamics. NATURE COMMUNICATIONS. https://doi.org/10.1038/s41467-018-08004-0.

86. Murphy, P.M. et al (2018). Mitochondria-derived ROS activate AMP-activated protein kinase (AMPK) indirectly. J. Biol. Chem. doi: 10.1074/jbc.RA118.002579.

87. B. Tan et al (2015). The profiles of mitochondrial respiration and glycolysis using extracellularflux analysis in porcine enterocyte IPEC-J2. Animal Nutrition 1. 239–243240.

88. E.A. Resseguie et al (2015). Hyperoxia activates ATM independent from mitochondrial ROS anddysfunction. Redox Biology. 5 176–185.

89. Yi Liu, Yanyan Cao, Weihe Zhang, Stephen Bergmeier, Yanrong Qian, Huzoor Akbar, Robert Colvin, Juan Ding, Lingying Tong, Shiyong Wu, Jennifer Hines and Xiaozhuo Chen (2012). A Small-Molecule Inhibitor of Glucose Transporter 1 Downregulates Glycolysis, Induces Cell-Cycle Arrest, and Inhibits Cancer Cell Growth *In Vitro* and *In Vivo*. Mol Cancer Ther. 1672-1682; DOI: 10.1158/1535-7163.MCT-12-0131.

90. Shiratori, R., Furuichi, K., Yamaguchi, M. et al (2019). Glycolytic suppression dramatically changes the intracellular metabolic profile of multiple cancer cell lines in a mitochondrial metabolism-dependent manner. Sci Rep 9, 18699. https://doi.org/10.1038/s41598-019-55296-3.

91. Dang CV (2012). Links between metabolism and cancer. Genes Dev. 26:877–90. doi:10.1101/gad.189365.112.

92. Kalkat M, De Melo J, Hickman KA, Lourenco C, Redel C, Resetca D, et al (2017). MYC deregulation in primary human cancers. Genes (Basel) 8:E151. doi:10.3390/genes8060151.

93. Nesbit CE, Tersak JM, Prochownik EV (1999). MYC oncogenes and human neoplas- tic disease. Oncogene 18:3004–16. doi:10.1038/sj.onc.1202746.

94. Meyer N, Penn LZ (2008). Re ecting on 25 years with MYC. Nat Rev Cancer 8:976–90. doi:10.1038/nrc2231.

95. Sabnis HS, Somasagara RR, Bunting KD (2017). Targeting MYC dependence by metabolic inhibitors in cancer. Genes (Basel) 8:E114. doi:10.3390/ genes8040114.

96. Zaytseva O, Quinn LM (2017). Controlling the master: chromatin dynamics at the MYC promoter integrate developmental signaling. Genes (Basel) 8:E118. doi:10.3390/genes8040118.

97. LI ET AL. (2005). Myc Stimulates Nuclearly Encoded Mitochondrial Genes and Mitochondrial Biogenesis. MOLECULAR AND CELLULAR BIOLOGY p. 6225–6234.

98. Jae-Moon Shin, Yun-Jeong Jeong, Hyun-Ji Cho, Junji Magae, Young-Seuk Bae, Young-Chae Chang (2016). Suppression of c-Myc induces apoptosis via an AMPK/mTORdependent pathway by 4-O-methyl-ascochlorin in leukemia cells. Apoptosis. 21:657–668 DOI 10.1007/s10495-016-1228-3.

99. Turrens JF (2003). Mitochondrial formation of reactive oxygen species. J Physiol 552: 335-344.

100. Cadenas E and Davies KJ (2000). Mitochondria free radical generation, oxidative stress, and aging. Free Radic Biol Med 29: 222-230.

101. Brand Md (2016). Mitochondrial generation of superoxide and hydrogen peroxide as the source of mitochondrial redox signaling. Free Radic Biol Med 100: 14-31.

102. ZHAO et al (2019). MITOCHONDRIAL ETC, ROS GENERATION AND UNCOUPLING. INTERNATIONAL JOURNAL OF MOLECULAR MEDICINE. 44: 3-15.

103. Cecchini G (2003). Function and structure of complex II of the respira- tory chain. Annu Rev Biochem 72: 77-109.

104. Sun F, Huo X, Zhai Y, Wang A, Xu J, Su d, Bartlam M and Rao Z (2005). Crystal structure of mitochondrial respiratory membrane protein complex II. cell 121: 1043-1057.

105. Bezawork-Geleta A, Rohlena J, dong L, Pacak K and Neuzil J (2017). Mitochondrial complex II: At the crossroads. Trends Biochem Sci 42: 312-325.

106. Popović-Bijelić A, Mojović M, Stamenković S, et al (2016). Iron-sulfur cluster damage by the superoxide radical in neural tissues of the SOD1 (G93A) ALS rat model. Free Radic Biol Med. 96:313-322. doi:10.1016/j.freeradbiomed.2016.04.028.

107. Laura Valls-Lacalle, Ignasi Barba, Elisabet Miró-Casas, Juan José Alburquerque-Béjar, Marisol Ruiz-Meana, Marina Fuertes-Agudo, Antonio Rodríguez-Sinovas, David García-Dorado (2016). Succinate dehydrogenase inhibition with malonate during reperfusion reduces infarct size by preventing mitochondrial permeability transition, Cardiovascular Research, Volume 109, Issue 3, Pages 374–384, https://doi.org/10.1093/cvr/cvv279.

108. Cho YM, Kwon S, Pak YK, et al (2006). Dynamic changes in mitochondrial biogenesis and antioxidant enzymes during the spontaneous differentiation of human embryonic stem cells. Biochem Biophys Res Commun. 348(4):1472-1478. doi:10.1016/j.bbrc.2006.08.020.

109. Straub, S. P., Stiller, S. B., Wiedemann, N., & Pfanner, N (2016). Dynamic organization of the mitochondrial protein import machinery, Biological Chemistry, 397(11), 1097-1114. doi: https://doi.org/10.1515/hsz-2016-0145.

110. Frey, T. G., & Mannella, C. A (2000). The internalstructure of mitochondria. Trends in Biochemi-cal Sciences, 0004, 1–6.

111. Westermann, B (2010). Mitochondrial fusion and fission in cell life and death. Nat. Rev. Mol. Cell Biol. 11, 872– 884.

112. Chan, D. C (2006). Mitochondria: dynamic organelles in disease, aging, and development. Cell 125, 1241–1252.

113. Ricci, J. E., Waterhouse, N., and Green, D. R.(2003). Mitochondrial func- tions during cell death, a complex (I-V) dilemma. Cell Death Differ. 10, 488 – 492.

114. PALADE, G. E (1953). AN ELECTRON MICROSCOPE STUDY OF THE MITOCHONDRIAL STRUCTURE. Journal of Histochemistry & Cytochemistry, 1(4), 188-211. https://doi.org/10.1177/1.4.188.

115. Lemasters, J. J.(2005). Selective mitochondrial autophagy, or mitophagy, as a targeted defense against oxidative stress, mitochondrial dysfunction, and aging. Rejuvenation Res. 8, 3–5.

116. Green, D. R., Galluzzi, L., and Kroemer, G (2011). Mitochondria and the autophagy-inflammation-cell death axis in organismal aging. Science 333, 1109 –1112.

117. Youle, R. J., and Narendra, D. P (2011). Mechanisms of mitophagy. Nat. Rev. Mol. Cell. Biol. 12, 9 –14.

118. Kopp JL, von Figura G, Mayes E, et al (2012). Identification of Sox9-Dependent Acinar-to-Ductal Reprogramming as the Principal Mechanism for Initiation of Pancreatic Ductal Adenocarcinoma. Cancer Cell. 22:737–750.

119. Xie VK, Maitra A (2017). Krüppel-Like Factor 4 Promotes Pancreatic Acinar-to-Ductal

Metaplasia and Tumor Initiation. Pancreas. 46:139–142.

120. Ardito et al (2012). EGF Receptor is Required for KRAS-induced Pancreatic Tumorigenesis. Cancer Cell. 22(3): 304–317. doi:10.1016/j.ccr.2012.07.024.

121. Deng X, Wang L, Elm MS, Gabazadeh D, Diorio GJ, Eagon PK, et al (2005). Chronic alcohol consumption accelerates fibrosis in response to cerulein-induced pancreatitis in rats. Am J Pathol 166(1): 93-106,2005.

122. Xue J, Sharma V, Hsieh MH, Chawla A, Murali R, Pandol SJ, et al (2015). Alternatively activated macrophages promote pancreatic fibrosis in chronic pancreatitis. Nat Commun6: 7158,2015.

123. Mukherjee S, Partch CL, Lehotzky RE, Whitham CV, Chu H, Bevins CL, Gardner KH, Hooper LV (2009). Regulation of C-type lectin antimicrobial activity by a flexible N-terminal prosegment. J Biol Chem. 284(8): 4881–4888.

124. Mukherjee S, Zheng H, Derebe MG, Callenberg KM, Partch CL, Rollins D, Propheter DC, Rizo J, Grabe M, Jiang QX, Hooper LV (2014). Antibacterial membrane attack by a pore-forming intestinal C-type lectin. Nature. 505(7481): 103–107.

125. Hartupee JC, Zhang H, Bonaldo MF, Soares MB, Dieckgraefe BK (2001). Isolation and characterization of a cDNA encoding a novel member of the human regenerating protein family: Reg IV. Biochim Biophys Acta. 1518(3): 287–293.

126. Iovanna J, Orelle B, Keim V, Dagorn JC. (1991). Messenger RNA sequence and expression of rat pancreatitis-associated protein, a lectin-related protein overexpressed during acute experimental pancreatitis.JBiolChem. 266(36):24664–24669.

127. Abe M, Nata K, Akiyama T, Shervani NJ, Kobayashi S, Tomioka- Kumagai T, Ito S,

Takasawa S, Okamoto H (2000). Identification of a novel Reg family gene, RegIII delta, and mapping of all three types of Reg family gene in a 75 kilobase mouse genomic region.Gene. 246(1-2):111–122.

128. Suzuki Y, Yonekura H, Watanabe T, Unno M, Moriizumi S, Miyashita H, Okamoto H (1994). Structure and expression of a novel rat RegIII gene. Gene. 144(2):315–316.

129. Gironella M, Folch-Puy E, LeGoffic A, Garcia S, Christa L, Smith A, Tebar L, Hunt SP, Bayne R, Smith AJ, Dagorn JC, Closa D, Iovanna JL (2007). Experimental acute pancreatitis in PAP/HIP knock- out mice. Gut. 56(8):1091–1097.

130. Van Ampting et al (2012). Intestinally Secreted C-Type Lectin Reg3b Attenuates Salmonellosis but Not Listeriosis in Mice. Infection and Immunity. 80 (3): 1115–1120.

131. Yan AW, Fouts DE, Brand lJ, Stärkel P, Torralba M, Schott E, Tsukamoto H, Nelson KE, Brenner DA, Schnabl B (2011). Enteric dysbiosis associated with a mouse model of alcoholic liver disease. Hepatology. 53(1): 96–105.

132. Wang L, Fouts DE, Sta¨rkel P, Hartmann P, Chen P, Llorente C, DePew J, Moncera K, Ho SB, Brenner DA, Hooper LV, Schnabl B (2016). Intestinal REG3 lectins protect against alcoholic steatohepatitis by reducing mucosa-associated microbiota and preventing bacterial translocation. Cell Host Microbe. 19(2): 227–239.

133. Prehn-Kristensen A, Zimmermann A, Tittmann L, Lieb W, Schreiber S, Baving L, et al (2018). Reduced microbiome alpha diversity in young patients with ADHD. PLoS ONE 13(7): e0200728. https://doi.org/10.1371/journal.pone.0200728.

134. Auciello Romana F, Ross A Fiona, Ikematsu Naoko, and Hardie D Grahame (2014). Oxidative stress activates AMPK in cultured cells primarily by increasing cellular AMP and/or ADP. FEBS Lett. 588(18): 3361-3366.

135. Staffas A, Burgos da Silva M, Slingerland AE, Lazrak A, Bare CJ, Holman CD, Docampo MD, Shono Y, Durham B, Pickard AJ, Cross JR, Stein-Thoeringer C, Velardi E, Tsai JJ, Jahn L, Jay H, Lieberman S, Smith OM, Pamer EG, Peled JU, Cohen DE, Jenq RR, van den Brink MRM (2018). Nutritional Support from the Intestinal Microbiota Improves Hematopoietic Reconstitution after Bone Marrow Transplantation in Mice. Cell Host Microbe. 23(4):447-457.e4. doi: 10.1016/j.chom.2018.03.002.

ACKNOWLEDGEMENTS

Firstly, I would like to thank my supervisor and main scientific advisor Dr. Henrik Einwächter for his constant guidance and support. Thank you for all the ideas, valuable inputs, improving my research presentation skills, corrections and also for encouraging scientific discussions throughout the entire duration. This was truly motivating and inspiring.

I would also like to thank my supervisor Prof. Dr. Roland M. Schmid for accepting me as a doctoral researcher at Gastolabor II. Your guidance, support, all the valuable inputs and ideas in helping me were truly inspiring. Thank you also for enabling many events such as rock climbing, retreat and the Christmas parties. Also, I would like to thank you for those valuable comments as a part of my Thesis Advisory Committee (TAC).

I would like to express my deepest gratitude to Prof. Dr. Martin Klingenspor and Dr. Günter Schneider for agreeing to be a part of my Thesis Advisory Committee (TAC). Their active participation, comments and valuable inputs during the 3 TAC meetings helped a lot in developing my research and thesis manuscript.

Furthermore, I would like to thank all fellow lab mates of AG Einwächter (Mathilde, Thorsten, Melanie, Anja, Anke, Leanne, Chao, and Bailing) for their methodological advice, inputs and help. I would like to thank Thorsten and Leanne especially for taking time to proofread my thesis manuscript. Your comments have been extremely valuable and informative. I would also like to thank Thorsten for all the kicker games, constant help and for all the interesting scientific discussions. I would also like to thank Melanie for helping me with mouse room work, german translation of the abstract and for all the kicker games that I won. I would also like to thank fellow lab mates Kivanc and Ezgi from AG Algül for providing me with inputs regarding thesis submisison to the medical graduate centre.

I would also like to thank Prof. Dr. Hans Zischka and Frau Carola Eberhagen for helping us with obtaining EM pictures and I would also like to thank Dr. Christoph Stein-Thoeringer for 16S rRNA analysis of our samples.

Finally, I would like to thank Frau Raphaela Blum, Frau Bettina Kratzer and Frau Desislava Zlatanova from the medical graduate centre for keeping me informed about the PhD program requirements.